2023
October

Academic Studies in **SCIENCE AND MATHEMATICS**

EDITORS
Prof. Dr. E. Nihal ERCAN
Prof. Dr. Hasan AKGÜL

gece kitaplığı

İmtiyaz Sahibi • Yaşar Hız
Genel Yayın Yönetmeni • Eda Altunel
Yayına Hazırlayan • Gece Kitaplığı
Editörler • Prof. Dr. E. Nihal ERCAN
Prof. Dr. Hasan AKGÜL

Birinci Basım • Ekim 2023 / ANKARA

ISBN • 978-625-425-225-9

Gece Kitaplığı
Adres: Kızılay Mah. Fevzi Çakmak 1. Sokak Ümit Apt
No: 22/A Çankaya/ANKARA Tel: 0312 384 80 40

www.gecekitapligi.com
gecekitapligi@gmail.com

Baskı & Cilt
Bizim Buro
Sertifika No: 42488

Academic Studies in Science and Mathematics

October 2023

Editors

Prof. Dr. E. Nihal ERCAN
Prof. Dr. Hasan AKGÜL

İÇİNDEKİLER

CHAPTER 1

LIFE IN SOLAR SYSTEM

E. Nihal ERCAN[1]

1 Prof.Dr., Physics Dept. of Boğaziçi University, ercan@boun.edu.tr

Introduction

Life outside of the Earth is an intriguing concept; seeking life in space is a fascinating topic for scientific research throughout history. This concept has taken our attention from ancient myths to modern science fiction. In the dawn of humanity, we were busy discovering our planet and did not worry about the out of it. With technological developments and increasing possibilities of advanced research methods, our knowledge about our planet increased exponentially. Then we started to question what outside of the planet is like and discover the universe. After discovering exoplanets, stars, and galaxies, searching for life in our solar system has become a pressing scientific endeavor.

History of Searching Life in the Solar System

The search for life in the solar system can be traced back to Galileo and Cassini's observations about planets and moons. Galileo, the father of observational astronomy [1], discovered the most significant four of Jupiter's moons (Ganymede, Io, Europa, and Callisto). Cassini discovered Saturn's four moons (Rhea, Tethys, Dione, and Lapetus) [3]. These discoveries show that not all celestial bodies orbited around the Earth [2] and the possibility of life exists around the Solar System because it was seen that other worlds that might support life beyond Earth.

Speculations emerged about the possible life potentials on Mars and Venus at the beginning of the 19th and 20th centuries. Scientists made these speculations based on their apparent similarities to Earth [4]. In the middle of the 20th century, with the first successful missions to the Moon, Mars, and Venus, a new era for discovering and exploring the solar system started. These missions are:

1) Mission Luna 1: the first spacecraft that attained Moon and flew by it in 1959. The Soviet Union launched it. [6]

2) Mission Venera 3: Venera 3 landed on Venus in 1965. It was the first spacecraft that succeeded this. The mission was unsuccessful due to the failure to transmit data back to Earth. However, this mission is still considered a milestone in exploring the solar system. The Soviet Union also launches Venera 3. [7]

3) Mission Mariner 4, 1964, the first spacecraft-Mariner four flown by Mars. Moreover, Mariner 4 was able to transmit images back to Earth. NASA launched it. [8]

Nevertheless, space missions' main objective was the search for life in the solar system in the 1970s. Since the launch of the Viking missions to Mars [5], many experiments and missions that aim to find traces of life

in the solar system have been conducted. These experiments and missions included Mars, Europa, Enceladus, and Titan.

Nowadays, investigating traces of life in the solar system is still an ongoing process, leaving question marks in scientists' heads. Moreover, the possibility of life outside of Earth (both for humans and aliens) is an exciting concept for science and popular culture, movies, and comic books. Scientific inquiry and exploration history have helped us better understand this subject and prepared the groundwork which enables simpler exploration and discovery processes in the future.

Theoretical Aspects of Life in the Solar System

Theoretically, the possibility of life outside our Earth can be explained by life in extreme conditions. For example, life exists in a variety of extreme environments such as deep ocean vents (temperature can rise about 400 degrees Celsius), deserts (extreme temperature changes and drought), areas near to south and north poles (temperature can decline to -60, -70 degree Celsius) and even in the presence of radiation (hazardous for any life form known by now). Theoretically, these examples of life in extreme conditions encourage the possibility of life existing on other planets. Also, they provide a method to evaluate the possibility of the existence of life on other planets and moons by helping to set boundaries existence of life [9].

According to theoretical models, the most essential criteria for the sustainability and existence of life are the presence of liquid water, organic compounds, and energy sources [10]. The existence of these three is necessary, but more is needed to prove that life exists. Liquid water is the primary solvent of all living organisms we have ever known. Although it is theoretically possible that a living organism can use a different primary solvent, such as liquid methane, there is no instance such that life form is observed. Moreover, the rock-liquid water interactions are known to be essential for abiogenesis (origin of life). Even if there is no observation of living organisms on some planet/moon at some point, it is theoretically possible that this rock-liquid water interaction caused abiogenesis, and hence life exists. Therefore, liquid water is one essential determinant in evaluating a planet or Moon's life support potential. The existence of organic compounds is also an important concept. All living organisms use organic compounds and produce. Therefore, if a life form exists on some planet or Moon, it must contain organic matter. However, it is also important to emphasize that some inorganic processes produce some organic compounds, so a planet or Moon that includes organic matter but does not support life can exist. The energy source is another essential thing for living organisms. Since living organisms need energy to maintain their metabolic activities, an energy source must exist for the survival of living

organisms. Some possible energy sources are: Sun (for living organisms that make photosynthesis), Oxygen (for aerobic respiration), methane (for anaerobic respiration), Sulfur dioxide (for anaerobic respiration)

In addition to these three, many other factors are essential to evaluate the possibility of life in the solar system. These factors are related to the main three factors' existence and also affect the maintenance of life rather than existence. Such factors are temperature, pressure and atmospheric conditions, terrestrial or gas environment, and distance from the Sun. Temperature and pressure are essential for liquid water and affect organisms' metabolism. A terrestrial planet generally offers a more stable environment for living organisms to survive and evolve than gas giants, given that other conditions are the same. When this theoretical information is combined with observational information, it is seen that many candidates support life in the solar system. A more detailed discussion about these candidates is made in the next part.

Observational Aspects & Discussion about Life in Solar System

In this part, some celestial bodies in the solar system are evaluated based on their support of life, providing some observational aspects that are related to the possibility of the existence of life on these planets and moons.

a) Planets

1. Mercury

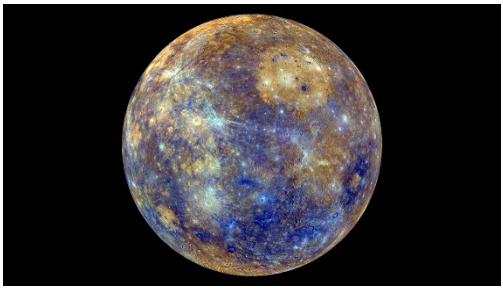

Mercury is a rocky planet with extreme temperature changes due to its slow rotation around its axis and thin atmosphere. The days' temperature in Mercury can reach 426 °C and -179 °C on the nights despite its proximity to the Sun. According to the current information, life is impossible in mercury [11]. Although some water ice exists in the craters of Mercury, which is detected by MESSENGER, and this may support microbial life, there is no strong evidence about it [12].

2. Venus

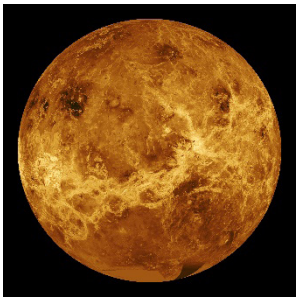

Venus is a terrestrial planet whose surface temperature is about 464 °C [13]. Although Venus is the second closest planet to the Sun, it is the hottest planet in the solar system due to the greenhouse effect of its thick cloudy atmosphere. The surface of Venus is highly hostile to any potential life because of the extreme temperature, high pressure due to the thick atmosphere, and intense volcanic activity. Despite the hostile surface, the upper atmosphere of Venus (50-70 km above the surface) has a temperature of about 0-50 °C, and atmospheric pressure is much lower.

These more friendly conditions convinced some scientists that thermoacidophile extremophile microorganisms may exist in this region [14]. The fact that Venus' atmosphere contains mostly carbon dioxide and contains water which enables photosynthesis supports this idea. Moreover, there are some recent observations have made supports microorganisms' existence in this region. Astronomers reported significant long-term absorbance and albedo changes observed, which seemed almost identical to the light absorbance of microorganisms in Earth's clouds in Venus' atmosphere in 2019 [15] [16]. Some phosphine gas was also detected in the same region (50-70 km above the surface). According to the current knowledge about Venus, no chemical process produces phosphine in Venus [17]. Therefore, the discovery of phosphine is excellent evidence that supports life because this gas is the output of some organic chemical processes.

Nowadays, the investigation of life on Venus continues rapidly. To sum up, life on Venus is only limited to microorganisms that live in clouds 50-70 km above the surface.

3. Mars

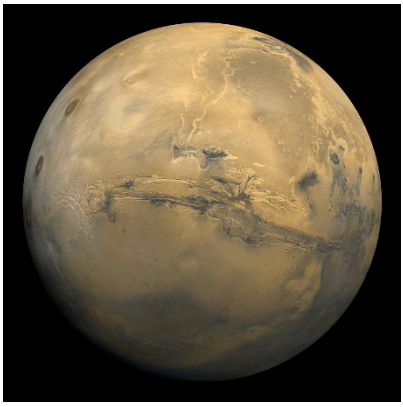

Mars and Venus are the closest planets to the Earth. Mars is a rocky planet with a thin atmosphere similar to the Earth in terms of composition, size, and location in the solar system (proximity to the Sun). These analogies between Earth and Mars significantly encourage scientists to investigate whether life exists and the habitability potential of humans in the Red Planet and caused many speculations about life on Mars (like Venus) [4].

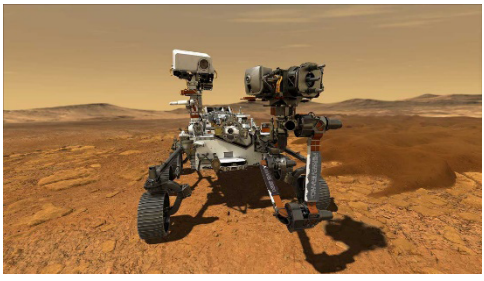

The surface conditions of Mars are hostile. Temperature varies from -110 °C to 35 °C (in the equator at Mars summer) [18]. Moreover, dust storms occur often, which are the most significant dust storms and are harmful to potential living organisms. Although the surface conditions are harsh on Red Planet, there is a strong possibility, supported by evidence, that liquid water may exist underground and, at earlier times, may have existed on its surface. It is known that water ice exists on Mars, which was observed and reported by NASA in 2016 [19]. Unfortunately, liquid cannot exist on the surface due to low atmospheric pressure. However, the geographic conditions on Mars suggested that liquid water existed on the surface. The canals on Mars show a similar pattern to the rivers on Earth. So, these structures can be created by the liquid water flowing in the past. Moreover, some organic compounds and methane were discovered on the Red Planet recently, further encouraging the speculations about life possibility on Mars [20]. Nevertheless, these findings are necessary but not suf-

ficient to say that life exists on the Red Planet because some non-biological processes can be responsible for creating those compounds.

Studies and discovery missions have been continuing to uncover mysteries about Mars' potential for life. Multiple Missions were made for this objective. For example, in February 2021, the Mars 2020 Perseverance rover landed on the Red Planet's surface. The rover's main objective is to investigate the signs of microorganisms and collect samples to make further analysis on Earth [21]. Additionally, there are some plans for the ExoMars mission made by the European Space Agency, sending a rover that contains a drill that is able to dig up to 2 meters beneath the surface to investigate traces of potential life on Mars [22].

Furthermore, despite the harsh conditions on the Red Planet, Mars should be the first candidate for the Moon. For human colonization considering its proximity to Earth and conditions are more suitable compared with other planets/moons in the solar system. There are many ongoing plans and projects about the terraforming and colonizing of Mars. One example of such a project is Elon Musk's SpaceX Mission to Mars, which is the most popular Mars project recently [23].

In conclusion, although there are significant ongoing efforts made, considering the hostility of Mars' surface conditions, high levels of radiation due to the lack of a global magnetic field that protects the planet from cosmic and solar radiation, extreme temperature changes, and a thin atmosphere that fails to protect from cosmic rays; Survival of complex life forms on the surface is improbable. Nevertheless, no hard evidence that prevents microbial life may exist in subsurface environments, such as underground aquifers or hydrothermal vents.

4. Jupiter

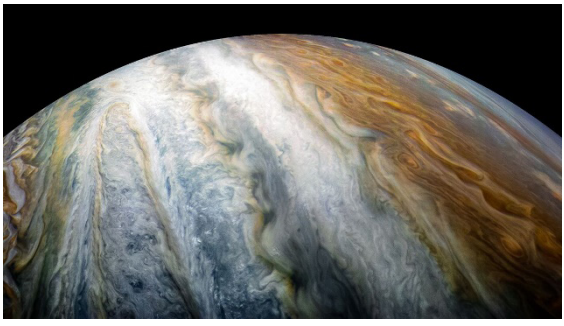

Jupiter is the most giant planet in the solar system. The fact that Jupiter has no solid surface significantly discourages potential life. Jupiter's upper atmosphere is around -145°C and the extreme atmospheric conditions even further make potential life difficult. Moreover, the atmosphere of Jupiter

is composed primarily of hydrogen and helium, and organic molecules do not exist. The pressure is approximately above 100 atmospheric pressure of Earth.

Although conditions on the surface are incredibly hostile, there is the possibility that life could exist in the upper clouds of the atmosphere of Jupiter, similar to Venus, according to some scientists. For example, one theory suggests that if a living organism could utilize the chemical energy from hydrogen-like some bacteria on Earth and methane, it would survive in the upper regions of the atmosphere of Jupiter. Moreover, potential living organisms use Sun as an energy source; Jupiter is the fifth closest planet to the Sun, and it is still close enough to use Sun as an energy source for potential living organisms. Nevertheless, the possible life on Jupiter is only on a speculation level; no concrete evidence (organic molecules, energy source, liquid water) implies possible life on Jupiter. The extreme conditions also create an extremely hostile environment for any possible life forms.

In summary, since there is no hard evidence and enough missions and research about life on Jupiter, the possibility of life is just about scientists' speculation. More detailed exploration operations are needed to make comments or discuss the probability of life on Jupiter.

5. Saturn

Saturn is the second planet in the solar system, a gas giant without a solid surface. Saturn's surface temperature is about -176°C and the pressure near the surface and upper atmosphere is significantly high but slightly lower than Jupiter's [49]. Saturn's atmosphere is also similar to Jupiter's, mainly consisting of hydrogen, but it also includes small amounts of organic molecules such as acetylene, ethane, propane, phosphine, and methane [51].

Because conditions on Saturn are much similar to Jupiter, if life exists there, it would be the same as the life possibilities in Jupiter. Therefore, there are similar theories for Saturn that there is the possibility of life in the upper clouds of the atmosphere for potential living organisms which utilize chemical energy from methane and hydrogen or use the Sun as an

energy source. Although conditions in Jupiter and Saturn are analogous, the chance of Saturn's support of potential life is higher than Jupiter's because of the detection of organic molecules, which implies some organic activities and reactions.

In short, as with Jupiter, the extreme conditions of Saturn's atmosphere make any potential life form's survival difficult. Moreover, the fact that there is no solid surface considerably deteriorates the development process of potentially complex life forms. The possibility of life in Saturn is also at only a speculative level. The only research about the potential life on Saturn can be the detection of organic materials in the atmosphere by the Cassini Spacecraft. However, this spacecraft was sent to something other than Saturn for this specific purpose [50]. More detailed research processes and more space missions on Saturn are required to make more solid statements about life on Saturn.

6. Uranus

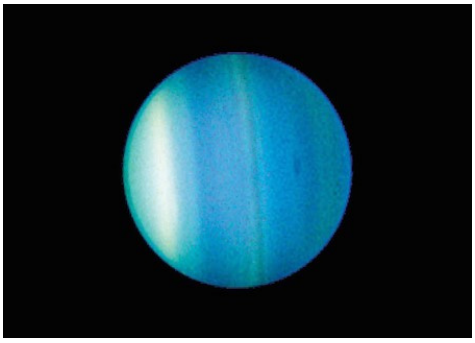

Uranus is another gas giant in the solar system. The atmosphere of Uranus is mainly composed of hydrogen and helium but also includes littler amounts of methane and ammonia which are very similar to Saturn's atmosphere. The surface temperature is about -197°C and the upper atmosphere is even colder, which is about -224°C [52]. In addition, the pressure is exceptionally high Similar to other gas giants in the solar system. Given the extreme conditions in Uranus' atmosphere, it is not very likely that complex life forms as we know them could survive. Although conditions are even more unfriendly for potential life than Jupiter and Saturn, there are still some speculations about potential life in Uranus. Some theories suggest that similar to the theories about Jupiter and Saturn, some microorganisms are utilized to use hydrogen and methane as an energy source for the Sun. However, the possibility of these ideas is even lower compared the Saturn and Jupiter because Uranus is far more distant than Sun. Moreover, the thick clouds in Uranus' atmosphere make it even more difficult for photons to penetrate and make the environment colder, which makes it

far more unfriendly.

In conclusion, there is no concrete evidence of life in Uranus or its atmosphere. The lack of a solid surface and extreme atmospheric conditions (winds, rapid pressure changes) deteriorate the survival and evolving potential of possible living organisms. There currently needs to be a planned mission for researching the possible traces of life in Uranus. More research and exploration processes in detail are needed to obtain a precise evaluation of the situation in Uranus. However, it is also important to emphasize that the possibility of life is far lower than in Jupiter and Saturn. Therefore, according to current knowledge, exploring these two gas giants makes more sense.

7. Neptune

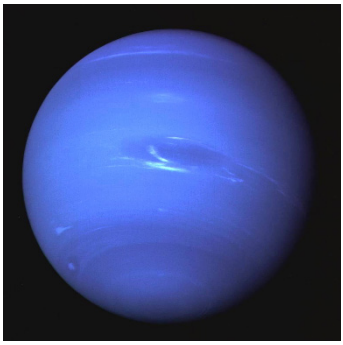

Neptune is a gas giant whose atmosphere is composed primarily of hydrogen and helium with little traces of methane, similar to the other three gas giants. The surface temperature is about -201, and the upper atmosphere can be as low as -218 with an extremely high pressure analogous to the other three gas giants in the solar system [53].

Given these extreme conditions, the possibility of complex life forms could survive in Neptune's atmosphere, according to today's knowledge. Nevertheless, like the case of the other three gas giants, some researchers have theorized that microorganisms can use hydrogen and methane as energy sources or directly use the Sun. could survive within the atmosphere of Neptune. However, Neptune is even more distant from Sun than Uranus and receives meagre sunlight. Moreover, similar to the case in other gas giants, lacking solid surface and extreme atmospheric conditions (winds and rapid pressure changes) make the environment more hostile. There are no missions to search for potential life in Neptune; more information is needed to analyze possible life here. However, examining Saturn and Jupiter first is more favourable because Neptune's conditions are similar to these 2. However, it is a much even more unfriendly version of them.

b) Moons

8. The Moon (Luna)

The Moon is the Earth's natural satellite. Luna is a rocky world with extreme temperatures (ranging from 140 °C to −171 °C). Due to its low gravitational force, the Moon has no atmosphere, so the temperature change between day and night is high. The Moon is not a good candidate for life as we know it.

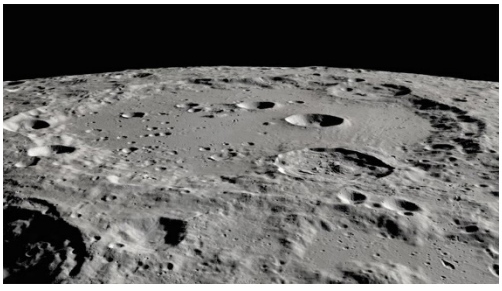

The detection of water ice [54] in some of the Moon's craters encouraged life possibility in our only Moon. However, the lack of air (any gas) and organic compounds makes this possibility unlikely. Moreover, there is much research about the Moon, and they need help finding evidence of traces of life.

On the other hand, this water can serve as a potential resource for future human colonization. Additionally, there are many plans for colonising the Moon, and many options are developed to protect humans from the harsh environment and radiation with underground bases in some craters. Although the Moon may not have the conditions for life to exist naturally, it may still be a good candidate for human colonization to explore the solar system.

9. Ganymede

Ganymede is the largest Moon of Jupiter and the solar system, even more significant than Mercury. It has a thin atmosphere compared to mostly Oxygen and includes more water than all of Earth's oceans combined, which makes it one of the strong potential candidates for the existence of life. It has its magnetic fields apart from other Galilean moons. It is the only Moon that contains global liquid water ocean in the solar system [24] despite the surface temperature of -163 °C [25].

The subsurface ocean of Ganymede is placed about 150 km below the surface (primarily crusts of ice) and is estimated to be 100 km deep. The reason that water stays as liquid can be explained by the heat generated by tidal forces from Jupiter's gravitational pull and the ice crust layer above the ocean, which isolates the ocean from the -163°C surface. An energy source that potentially supports life can be generated by the interaction of the ocean and the Moon's rocky mantle, according to scientists [25].

The subsurface ocean may also have a layer of ice which separates the ocean and the rocky seafloor, like Europa's ice crusts. Nutrients and organic compounds may be trapped and accumulate in this layer, creating an environment that enables microbial life and even more complex fish/amphibia-like life forms.

In addition, the Oxygen in Ganymede's atmosphere, produced by the breakdown of water molecules by solar radiation, offers a resource utilization option for human colonization. However, the atmosphere is thin and hence cannot protect any life form from the radiation, but below the surface is safe.

There are many missions planned/made to explore Ganymede. For example, the Galileo mission in the 1990s [26] and the upcoming Europa Clipper and JUICE (Jupiter et al.) missions [27]. These missions reveal significant details about the Ganymede's geology, composition, and potential for life.

10. Europa

Europa is another moon of Jupiter that has the potential to support life. Europa is similar to Ganymede. It is a much smaller, smoother surface containing mostly ice crust with a temperature of about −160 °C [28] and a subsurface ocean containing liquid water. The reason water stays liquid is the same as the Ganymede [29]. Europa has a geologically active surface which contains geysers. Some organic compounds are detected on Europa's surface that may come from an asteroid or geyser [30]. Also, there is a significantly high probability that the ocean floor contains hydrothermal vents, an energy source supporting living organisms like deep-ocean hydrothermal vents on Earth [31].

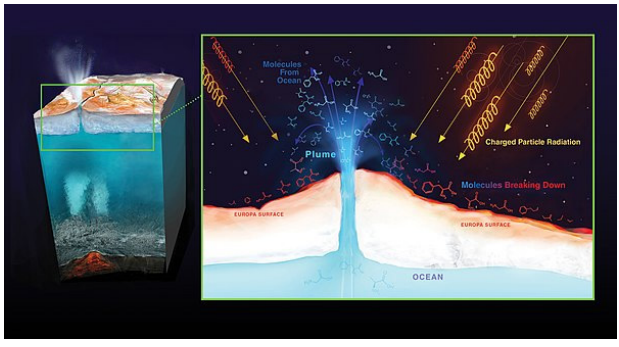

There were several missions to investigate potential Life on Europa, and new missions are planned. The most critical development is Europa Clipper Mission [32]. This mission conducts a detailed reconnaissance of Europa to study its ice shell, subsurface ocean, and geology and search for traces of life.

Compared to Ganymede, Europa's possibility to support life is more remarkable because of a much thinner ice crust that allows easier access to subsurface oceans, more geologically active surface may enable that dynamic and potentially habitable environment and is thought to have more chemical energy sources.

11.Callisto

Callisto is another of 4 biggest Jupiter moons similar to Europa and Ganymede. The surface is covered by craters and contains mainly ice and rock. There are no geological activities in Callisto compared to Ganymede and Europa [33]. Callisto can also have a subsurface ocean, but currently, there is no direct evidence for it. Because tidal forces are lower in Callisto than Europa and Ganymede, there are fewer energy sources for heating [34]. In short, if Callisto supports life, it would be like life in Ganymede and Europa. However, the possibility of supporting life is significantly lesser than in Ganymede and Europa [35]. There is no planned mission for searching for possible life in Callisto.

12. Enceladus

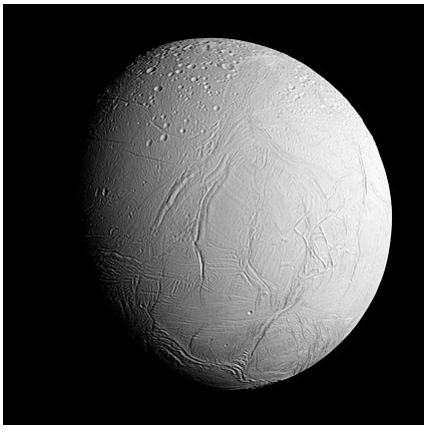

Enceladus is a moon of Saturn. It is much smaller than Ganymede and Europa, with its 500 km diameter [36]. Enceladus' surface is mainly covered with cleaner, fresher ice than Ganymede and Europa, and Enceladus consists of mostly ice and rock similar to Ganymede and Europa. Its surface temperature is about −198 °C far colder than Jupiter's moons

because of the reflective ice-covered surface, and it has lots of geysers like Europa [38]

There is hard evidence about a subsurface ocean about 10 km deep that contains liquid water discovered by NASA in 2014 [37]. In addition, there are observations about the geysers which eject salted water and some organic compounds [39]. Some examples of these organic compounds are methane (CH4), propane (C3H8), acetylene (C2H2) and formaldehyde (CH2O). These discoveries imply a great possibility of an energy source for hydrothermal activities in Enceladus' subsurface ocean [40].

If current information about Enceladus is evaluated, considering the existence of complex organic compounds that are interacting with the Moon's rocky core, the existence of a source of energy and patterns of ocean circulation [41], it could be said that Enceladus is a great candidate for extraterrestrial life, especially for microorganisms that metabolize molecular hydrogen to methane (like methanogen bacteria) [42].

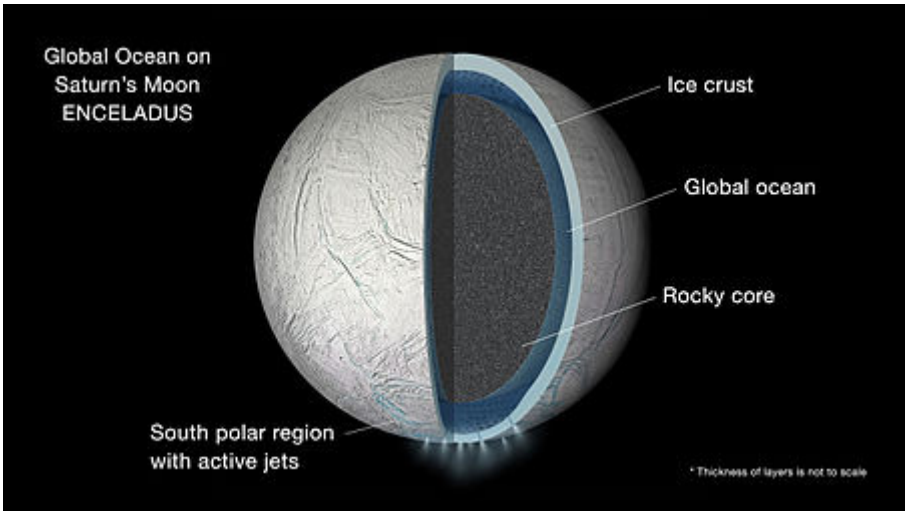

Enceladus and Europa are more likely to support life compared to Ganymede due to their more active surface features, which indicates a more dynamic process like an ecosystem and enables us to discover more evidence like ejaculated materials from geysers that enables us to gain information about inner layers of moons. Therefore, the research and space missions are focused on these two moons compared to others.

Life Investigation For Enceladus, Journey to Enceladus and Titan, Enceladus Explorer, Enceladus Life Finder, and Enceladus Life Signatures and Habitability are some of the examples of proposed missions that aim to explore habitability and the possibility of potential life in Enceladus.

13. Titan

Titan is the largest Moon of Saturn and the second-largest Moon of the solar system after Ganymede. Titan is the only Moon with a dense atmosphere in the solar system. Its atmosphere mainly includes nitrogen and a surface temperature of about -179 °C. Titan mainly consists of rock and water ice like Ganymede, Europa, and Enceladus. It includes liquid hydrocarbon rivers and lakes (predominantly methane and ethane), observed in the Cassini-Huygens mission in 2004 [46].

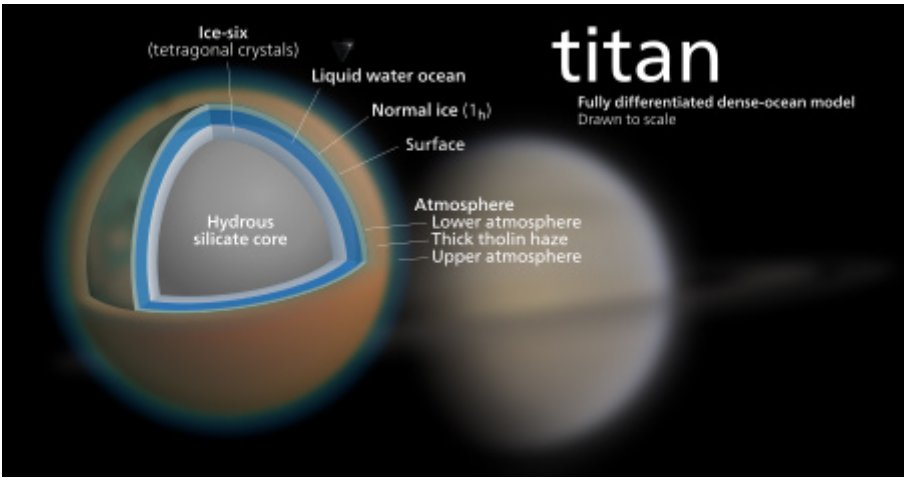

Titan is an exciting candidate for extraterrestrial life because of its rich organic chemistry, complex atmosphere, and hydrocarbon lakes and seas. Although there is no direct evidence of the existence of liquid water, there is a high possibility that the subsurface ocean contains liquid water [43]. Moreover, Titan is extremely rich in complex organic compounds different from Ganymede, Europa, and Enceladus [44]. This rich environment is considered suitable for abiogenesis, allowing exotic life forms to exist. For example, suppose a life form uses a hydrocarbon as a primary solvent instead of water. In that case, Titan is an appropriate environment for creating more complex organic molecules and hence such living organisms' existence [45]. Because such a life form does not depend on water, the lack of direct evidence of liquid water on Titan is no longer a problem for the existence of life.

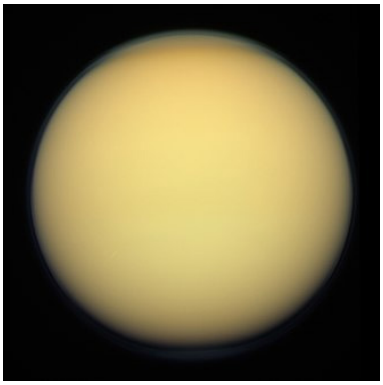

Titan is in a unique position in the possibility of life compared to other planets and moons in the solar system. Because Titan includes the most complex organic molecules in the solar system (excluding Earth) without the existence of liquid water is proven. If the existence of liquid water were somehow proven in Titan (like a subsurface ocean), then Titan would become the first candidate to support possible life (but not habitability of humans due to distance, atmospheric conditions and harsher surface conditions).

14. Ceres

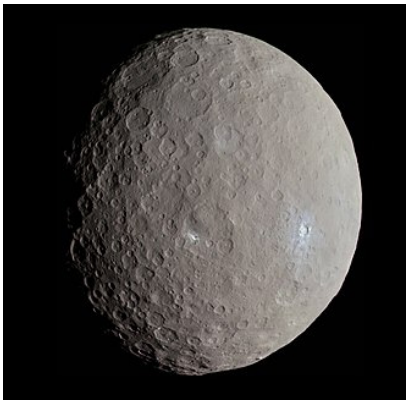

Ceres is the largest object in the asteroid belt between Mars and Jupiter. Ceres have a surface temperature of about -105 and a diameter of about 940 km [47]. Organic compounds and water are observed in Ceres, and the conditions are suitable for some organic reactions [48]. A subsurface ocean possibly exists in Ceres, but no direct evidence exists.

Ceres is not mentioned in the context of potential extraterrestrial life candidates such as Europa, Enceladus, Titan and Mars. It is a reasonably good candidate to explore. However, the lack of atmosphere and hence high radiation levels significantly discourage potential life. Further re-

search may reveal more information about Ceres, but currently, Ceres is behind the possibility of supporting life compared to other alternatives. Lastly, Ceres is a good alternative for human colonization because it contains lots of water and is close to Earth.

Conclusion

The solar system is not about the eight planets. It includes many dwarf planets and hundreds of moons. Although there is no concrete evidence implying the existence of a life form in the solar system, many planets and moons have the potential to support life or, in the future, become convenient for life. Moreover, the fact that a planet/moon does not support life does not mean that the planet/moon is not suitable for potential human colonization in the future. The habitability of these planets/moons can be advantageous for humans to explore the universe and utilize resources such as finding alternative energy sources or water. Even though detecting complex life forms like us is more accessible, many microorganisms can hide in the solar system. To sum up, further research and explorations are needed to understand the solar system's potential life better. It would not be surprising to find exotic fishes or amphibians in Europa or Enceladus someday.

All figures are taken from NASA-related web pages, so their credit belongs to NASA.

NASA Photojournal (https://photojournal.jpl.nasa.gov/

I would like to thank one of my undergraduate students, Mert Nardal, for his help in preparing the manuscript.

References:

1) Singer, C. (1941). "A Short History of Science to the Nineteenth Century". Clarendon Press: 217.

2) Galileo's Observations of the Moon, Jupiter, Venus, and the Sun – NASA Solar System Exploration (2009)

https://solarsystem.nasa.gov/news/307/galileos-observations-of-the-moon-jupiter-venus-and-the-sun/

3) Van Helden, Albert (2009). "The beginnings, from Lipperhey to Huygens and Cassini". Experimental Astronomy. 25 (1–3)

4) Proctor P.A. Other Worlds than Ours: The Plurality of Worlds Studied under the Light of Recent Scientific Researches. Hill, and Co.; New York, NY, USA: 1870. p. 94.

5) Schulze-Makuch, Dirk, and Louis N. Irwin. Life in the Universe: Expectations and Constraints, 3rd ed., Springer, 2018.

6) Luna 1 Mission

https://nssdc.gsfc.nasa.gov/nmc/spacecraft/display.action?id=1959-012A

7) Venera 3 Mission

https://nssdc.gsfc.nasa.gov/nmc/spacecraft/display.action?id=1965-092A

8) Mariner 4 Mission

https://solarsystem.nasa.gov/missions/mariner-04/in-depth/

9) Christopher P. McKay (2014) "Requirements and limits for life in the context of exoplanets" https://www.pnas.org/doi/abs/10.1073/pnas.1304212111

10) Wanda L. Davis & Christopher P. McKay (1996) "Origins of life: A comparison of theories and application to Mars" https://link.springer.com/article/10.1007/BF01808160

11) Mercury - NASA. October 19, 2021. Retrieved July 4, 2022.

https://solarsystem.nasa.gov/planets/mercury/in-depth/

12) Ingersoll, Andrew P.; Svitek, Tomas; Murray, Bruce C. (1992). "Stability of polar frosts in spherical bowl-shaped craters on the Moon, Mercury, and Mars"

13) NASA. Archived from the original on September 29 2006. Retrieved April 12 2007. https://web.archive.org/web/20060929003116/http://sse.jpl.nasa.gov/planets/profile.cfm?Object=Venus&Display=Facts&System=Metric

14) Dartnell, Lewis R.; Nordheim, Tom Andre; Patel, Manish R.; Mason, Jonathon P.; Coates, Andrew J.; Jones, Geraint H. (September 2015). "Constraints on a potential aerial biosphere on Venus: I. Cosmic rays".

15) Lee, Yeon Joo; Jessup, Kandis-Lea; Perez-Hoyos, Santiago; Titov, Dmitrij V.; Lebonnois, Sebastien; Peralta, Javier; Horinouchi, Takeshi; Imamura,

Takeshi; Limaye, Sanjay; Marcq, Emmanuel; Takagi, Masahiro; Yamazaki, Atsushi; Yamada, Manabu; Watanabe, Shigeto; Murakami, Shin-ya; Ogohara, Kazunori; McClintock, William M.; Holsclaw, Gregory; Roman, Anthony (26 August 2019). "Long-term Variations of Venus's 365 nm Albedo Observed by Venus Express, Akatsuki, MESSENGER, and the Hubble Space Telescope"

16) Anderson, Paul (September 3 2019). "Could microbes be affecting Venus' climate?"

17) Seager, Sara; Petkowski, Janusz J.; Gao, Peter; Bains, William; Bryan, Noelle C.; Ranjan, Sukrit; Greaves, Jane (14 September 2020). "The Venusian Lower Atmosphere Haze as a Depot for Desiccated Microbial Life: A Proposed Life Cycle for Persistence of the Venusian Aerial Biosphere".

18) "Mars Exploration Rover Mission: Spotlight" Marsrover.nasa.gov

19) https://www.jpl.nasa.gov/news/mars-ice-deposit-holds-as-much-water-as-lake-superior

20) https://www.nasa.gov/press-release/nasa-finds-ancient-organic-material-mysterious-methane-on-mars

21) National Aeronautics and Space Administration. "Mars 2020 Perseverance Rover." NASA, 2021, https://mars.nasa.gov/mars2020/

22) https://www.esa.int/Science_Exploration/Human_and_Robotic_Exploration/Exploration/ExoMars

23) https://www.spacex.com/human-spaceflight/mars/

24) Chang, Kenneth (March 12, 2015). "Suddenly, It Seems, Water Is Everywhere in Solar System"

25) Delitsky, Mona L.; Lane, Arthur L. (1998). "Ice chemistry of Galilean satellites"

26) https://solarsystem.nasa.gov/missions/galileo/in-depth/

27) https://europa.nasa.gov/mission/history/#europa-discovered

28) McFadden, Lucy-Ann; Weissman, Paul; Johnson, Torrence (2007). The Encyclopedia of the Solar System

29) Greenberg, Richard (2005). Europa: The Ocean Moon: Search for an Alien Biosphere. Springer

30) McFadden, Lucy-Ann; Weissman, Paul; Johnson, Torrence (2007). The Encyclopedia of the Solar System

31) Chandler, David L. (October 20 2002). "Thin ice opens lead for life on Europa."

32) https://europa.nasa.gov/

33) Greeley, R.; Klemaszewski, J. E.; Wagner, L.; et al. (2000). "Galileo views of the geology of Callisto".

34) Musotto, Susanna; Varadi, Ferenc; Moore, William; Schubert, Gerald (2002). "Numerical Simulations of the Orbits of the Galilean Satellites".

35) Lipps, Jere H.; Delory, Gregory; Pitman, Joe; et al. (2004). Hoover, Richard B; Levin, Gilbert V; Rozanov, Alexei Y (eds.). "Astrobiology of Jupiter's Icy Moons"

36) https://web.archive.org/web/20131016093801/http://solarsystem.nasa.gov/planets/profile.cfm?Object=Sat_Enceladus&Display=Facts

37) https://www.jpl.nasa.gov/news/nasa-space-assets-detect-ocean-inside-saturn-moon

38) Dyches, Preston; Brown, Dwayne; et al. (July 28, 2014). "Cassini Spacecraft Reveals 101 Geysers and More on Icy Saturn Moon"

39) Wall, Mike (May 7, 2015). "Ocean on Saturn Moon Enceladus May Have Potential Energy Source to Support Life"

40) O' Neill, Ian (March 12, 2015). "Enceladus Has Potentially Life-Giving Hydrothermal Activity"

41) Spotts, Peter (September 16, 2015). "Proposed NASA mission to Saturn moon: If there is life, we will find it."

42) Sample, Ian (April 3, 2014). "Ocean discovered on Enceladus may be the best place to look for alien life."

43) Robert Brown; Jean Pierre Lebreton; Hunter Waite, eds. (2009). Titan from Cassini-Huygens

44) https://phys.org/news/2013-04-nasa-team-complex-chemistry-titan.html

45) https://nap.nationalacademies.org/read/11919/chapter/8

46) https://science.nasa.gov/solar-system/programs/outer-planets-flagship

47) Ermakov, A. I.; Fu, R. R.; Castillo-Rogez, J. C.; Raymond, C. A.; Park, R. S.; Preusker, F.; Russell, C. T.; Smith, D. E.; Zuber, M. T. (November 2017). "Constraints on Ceres' Internal Structure and Evolution From Its Shape and Gravity Measured by the Dawn Spacecraft"

48) Marchi, S.; Raponi, A.; Prettyman, T. H.; De Sanctis, M. C.; Castillo-Rogez, J.; Raymond, C. A.; Ammannito, E.; Bowling, T.; Ciarniello, M.; Kaplan, H.; Palomba, E.; Russell, C. T.; Vinogradoff, V.; Yamashita, N. (2018). "An aqueously altered carbon-rich Ceres".

49) https://www.weather.gov/fsd/saturn

50) Guerlet, S.; Fouchet, T.; Bézard, B. (November 2008). Charbonnel, C.; Combes, F.; Samadi, R. (eds.). "Ethane, acetylene and propane distribution in Saturn's stratosphere from Cassini/CIRS limb observations".

51) Cain, Fraser (January 22 2009). "Atmosphere of Saturn"

52) Podolak, M.; Weizman, A.; Marley, M. (December 1995). "Comparative models of Uranus and Neptune". Planetary and Space Science.

53) https://nssdc.gsfc.nasa.gov/planetary/factsheet/neptunefact.html

54) Pieters, C. M.; Goswami, J. N.; Clark, R. N.; Annadurai, M.; Boardman, J.; Buratti, B.; Combe, J.-P.; Dyar, M. D.; Green, R.; Head, J. W.; Hibbitts, C.; Hicks, M.; Isaacson, P.; Klima, R.; Kramer, G.; Kumar, S.; Livo, E.; Lundeen, S.; Malaret, E.; McCord, T.; Mustard, J.; Nettles, J.; Petro, N.; Runyon, C.; Staid, M.; Sunshine, J.; Taylor, L.A.; Tompkins, S.; Varanasi, P. (2009). "Character and Spatial Distribution of OH/H2O on the Surface of the Moon Seen by M3 on Chandrayaan-1"

CHAPTER 2

THE EFFECTS OF DIFFERENT SALT CONCENTRATIONS ON SEEDLING DEVELOPMENT OF HYSSOPUS OFFICINALIS L. (HYSSOP)

Tuba DEMİRKAYA[1], Sibel ULCAY[2]

1 Doktora Öğrencisi, Ahi Evran Üniversitesi, Ziraat Fakültesi, Tarla Bitkileri Bölümü, Kırşehir, https://orcid.org/0000-0002-8892-4456
2 Dr. Öğr. Üyesi, Ahi Evran Üniversitesi, Ziraat Fakültesi, Tarla Bitkileri Bölümü, Kırşehir, https://orcid.org/0000-0002-2878-1721

INTRODUCTION

Hyssopus officinalis L. is a plant species belonging to the Lamiaceae family (Güner et al., 2012). It is popularly known as "hyssop grass, hyssop grass, hyssop grass" (Özer et al., 2006). The extract of thyme is used in the beverage and food industry. (Akgül, 1993). In Gümüşhane and Erzurum regions, mint is added to soups and dishes to add flavor. (Baytop, 1991). It has an antiviral effect due to the tannin contained in its extract, and an antioxidant property due to rosmarinic acid.. It is consumed in the form of tea or mouthwash for throat infections, cough, lung, digestive and chest disorders, intestinal diseases and menstrual irregularities. Externally diaphoretic, it is used for skin irritations, crushes, frostbite and also for the treatment of tumors. (Leung and Foster, 1996).

Salinity, along with population growth, is one of the environmental factors that threatens productive agriculture worldwide and severely limits food production. (Botella et al., 2005). Salinity can be divided into two groups as primary and secondary salinity according to the reasons for its formation. The weathering of bedrock, climatic factors and the oceans are the causes of primary salinity (Munns and Tester, 2008). The causes of secondary salinity are; the rise of groundwater rich in various salts to the soil surface, overgrazing, intensive irrigation in agricultural areas, opening of agricultural lands by destroying the natural vegetation of a region and contamination of soils with various chemicals (Pessarakli and Szabolcs, 1999; Demir, 2018). Most of the salty soils in the world are salty soils caused by Na2SO4 and NaCl. (Pessarakli and Szabolcs, 1999).

Salinity shows its direct effect on plants by creating osmotic and ion stress, while its indirect effect is manifested by the structural deterioration of the plant as a result of these stress factors and the synthesis of toxic compounds (Botella et al., 2005; Hong et al., 2009; Demir 2021).

In this study, it was aimed to contribute to the salt stress that hyssop faced in our soils with increasing salinity, to determine the physiological responses of the seedling development stage, based on limited opportunities and limited criteria. In the study, root length (cm), shoot length (cm), root dry and fresh weight (g), shoot dry and fresh weight (g), number of branches (number of leaves (number/plant) and leaf diameter (mm) were determined, and it was tried to reveal the salt stress mechanism in the material based on the interactions between these criteria.

MATERIAL AND METHOD

The experiment was carried out in the greenhouse of Kırşehir Ahi Evran University, Faculty of Agriculture, Department of Field Crops in the spring-summer period of 2022. In the research, hyssop (*Hyssopus officina-*

lis L.) seeds were used as plant seedling material. The salt dose was used in the form of sodium chloride (NaCl) in the study. The research was carried out as a three replication pot experiment at 4 different dose salt concentrations (0 mM, 50 mM, 100 mM, 150mM, and 200 mMNaCl), according to a single factor randomized plot design.

In the study, hyssop grass was planted in 3-liter plastic pots filled with a mixture of 1/3 peat, 1/3 perlite and 1/3 soil (sand, burnt barn manure, garden soil) during the seedling period when they had 4-5 real leaves. The soil used in the experiment was obtained from the field crops of Ahi Evran University, and some of the physical and chemical properties of the soil used are as follows; pH (8.01), lime (12%), total soluble salt (0.01%), organic matter (0.34%), useful P (kg/da) (1.95ppm), useful K (kg/da) (105.9 ppm). The soil used in the experiment does not have a feature that restricts the cultivation of the plant materials in question. In the study, soil was placed in 3-liter pots and the seedlings were planted at the end of May with one plant in each pot. 14.61 g of NaCl to 50 mM, 29.22 g of NaCl to 100mM, 43.83 g of NaCl to 150 mM and 58.44 g of NaCl to 200 mM were added to each 5-liter water scale. The plants were watered every day from October, and irrigation was carried out every other day with salt application. When the plants reached a certain maturity (10th day), salt stress applications were started with 250 ml of solution per plant. Plants were collected for necessary analyzes 40 days after planting and the experiment was stopped. In order to determine root, seedling and leaf yields in the experiment, 10 randomly selected plants from each salt dose application were harvested during flowering. Root length (cm), shoot length (cm), root dry and fresh weight (g), shoot dry and fresh weight (g), number of branches, number of leaves and leaf diameter (mm) were measured at the end of the experiment. Measurement of the length of plant roots and seedlings; after the harvest, the plants were washed and cleaned with tap water and the root lengths and seedling lengths of the plants were measured and recorded. Root length is determined by the distance from the bottom of the soil structure to the root collar, where it meets the soil and the part from the root collar to the apex was recorded as the seedling length of the plant. Fresh weights were determined by weighing the root and seedling parts of the plants separately. To determine the dry weight, it was dried in an oven at 70°C for 48 hours until it reached a constant weight and its dry weight was measured. (Açıkgöz et al., 2004; Demir 2022).

Data Analysis: The research was carried out in 3 repetitions in accordance with the "factorial trial" trial design. The data obtained from the research were evaluated with the statistical package program SPSS (version 16.0). The LSD test, which is one of the multiple comparison tests, was used to determine the differences between applications. $p<0.05$ was con-

sidered statistically significant in the analysis. In addition, the mean and standard errors of 3 replications are given in the tables (Table1- Table 10).

RESULTS AND DISCUSSION

Salt (NaCl) applied at different concentrations, root length (cm), shoot length (cm), root dry and fresh weight (g), shoot dry and fresh weight (g), number of branches, number of leaves and leaf diameter (mm) of hyssop) are given in Table 1. There were statistically significant differences between salt concentrations at the 5% probability level in terms of all investigated properties (Table 1). Images of hyssop seedlings, shoots and roots at different salt concentrations are given in Figure 2., Figure 3. and Figure 4.

Table 1. Root length (cm), shoot length (cm), root dry and fresh weight (g), shoot dry and fresh weight (g), number of branches (number/plant), number of leaves (number/plant) in hyssop of different salt doses) and leaf diameter (mm) values

NaCI Rates (mM)	Root Length (cm)	Root Fresh Weight (g)	Shoot Length (cm)	Shoot Fresh Weight (g)	Root Dry Weight (g)	Shoot Dry Weight (g)	Number of Branches (Adet/ bitki)	Number of Leaves (adet/ bitki)	Leaf Diameter (mm)
0 mM	31.2 [a]	0.0365[a]	60.8 [a]	0.0175	5.27 [a]	3.83 [a]	24 [a]	252 [a]	9.91 [a]
50 mM	27.7 [a]	0.0295[a]	46.4 [b]	0.016	2.83 [b]	1.79 [b]	12 [b]	127 [b]	8.32 [b]
100 mM	18.2 [b]	0.012 [b]	32.7 [c]	0.022	1.30 [c]	0.91 [c]	8 [b]	65 [c]	6.64 [c]
150 mM	0	0	0	0	0	0	0	0	0
200 mM	0	0	0	0	0	0	0	0	0
Ort.	25.7	0.026	46.63	0.0185	3.13	2.18	14	148	8.29
Significant Degree	*	*	*		*	*	*	*	*

* Correlation is significant at the 0.05 level ($p<0.05$) The difference between the averages denoted by the same letters is insignificant.

The variance analysis values of the effects of different salt doses on the root length of hyssop (*H.officinalis*) is given in Table 2. The effect of different salt doses on the root length of the was found to be statistically significant at the rate of 5%.

Table 2. Variance analysis results for root length

VS	df	Sum of Squares	Mean Square	F
Salt Doses	2	905	452.5	28.32
Error	27	431.3	15.97	-
Total	29	1336.3	-	-

VS: Variation Sources

The averages of different salt doses over the root length of the hyssop plant are shown in Table 1. The average root length value determined by the study is 25.7 cm. Root length values in the study varied between 31.2-18.2 cm. The effect of different salt dosage applications on the root length of the plant was found to be statistically significant at the $p<0.05$ level. The lowest root length was obtained with 18.2 cm from the salt dose of 100 mM, and the highest root length as 31.2 cm was obtained from the 0 mM salt dose.

The variance analysis values of the effects of different salt doses on the root fresh weight of the hyssop (*H.officinalis*) is given in Table 3. The effect of different salt doses on root fresh weight was found to be statistically significant at the rate 5%.

Table 3. Variance analysis results regarding root wet weight

VS	df	Sum of Squares	Mean Square	F
Salt Doses	2	0.003	0.002	8.136
Error	27	0.005	0	-
Total	29	0.008	-	-

VS: Variation Sources

The average values of different salt doses over the root fresh weight of the hyssop plant are shown in Table 1. The average root fresh weight value determined by the study is 0.026 gr. Root fresh weight values in the study varied between 0.0365-0.012 g. The effect of different salt dosage applications on the fresh weight of the plant was found to be statistically significant at the $p<0.05$ level. The lowest root fresh weight was obtained with 0.012 gr from the salt dose of 100 mM, and the highest root fresh weight as 0.0365 gr was obtained from the 0 mM salt dose.

The variance analysis values of the effects of different salt doses on the shoot length of the hyssop (*H.officinalis*) is given in Table 4. The effect of different salt doses on shoot length was found to be statistically significant at the rate 5%.

Table 4. Variance analysis results on shoot length

VS	df	Sum of Squares	Mean Square	F
Salt Doses	2	3948.86	1974.43	38.29
Error	27	1392.1	51.55	-
Total	29	5340.96	-	-

VS: Variation Sources

The averages of different salt doses over the shoot length of the hyssop plant are shown in Table 1. The average shoot length value determined by the study is 46.63 cm. In the study, shoot length values varied between 60.8-32.7 cm. The effect of different salt dosage applications on the shoot length of the plant was found to be statistically significant at the $p<0.05$ level. The lowest shoot length was obtained with 32.7 cm from the salt dose of 100 mM, and the highest shoot length as 60.8 cm was obtained from the 0 mM salt dose.

The variance analysis values of the effects of different salt doses on the shoot fresh weight of the hyssop (*H.officinalis*) is given in Table 5. The effect of different salt doses on the shoot fresh weight was not found to be statistically significant.

Table 5. Variance analysis results on shoot fresh weight

VS	df	Sum of Squares	Mean Square	F
Salt Doses	2	0.000195	0.0000975	0.672
Error	27	0.003913	0.000145	-
Total	29	0.004108	-	-

VS: Variation Sources

The averages of different salt doses over the shoot fresh weight of the hyssop plant are shown in Table 1. The average shoot fresh weight value determined by the study is 0.0185 gr. In the study, shoot fresh weight values ranged from 0.0175 to 0.022 g. The effect of different salt dosage applications on the shoot fresh weight was not found to be statistically significant. The lowest shoot fresh weight was obtained with 0.022 gr from the salt dose of 100 mM, and .the highest shoot fresh weight as 0.0175 gr was obtained from the 0 mM salt dose.

The variance analysis values of the effects of different salt doses on root dry weight in hyssop (*H.officinalis*) is given in Table 6. The effect of different salt doses on root dry weight was found to be statistically significant at the rate 5%.

Table 6. Variance analysis results for root dry weight

VS	df	Sum of Squares	Mean Square	F
Salt Doses	2	80.52	40.26	11.52
Error	27	94.29	3.49	-
Total	29	174.81	-	-

VS: Variation Sources

The averages of different salt doses over the root dry weight of the hyssop plant are shown in Table 1. The average root dry weight value determined by the study is 3.13 gr. Root dry weight values in the study varied between 5.27-1.30 g. The effect of different salt dosage applications on the root dry weight of the plant was found to be statistically significant at the $p<0.05$ level. The lowest root dry weight was obtained with 1.30 g from the salt dose of 100 mM, and the highest root dry weight as 5.27 g was obtained from the 0 mM salt dose.

The variance analysis values of the effects of different salt doses on shoot dry weight in hyssop (*H.officinalis*) is given in Table 7. The effect of different salt doses on shoot dry weight was found to be statistically significant at the rate 5%.

Table 7. Variance analysis results for shoot dry weight

VS	df	Sum of Squares	Mean Square	F
Salt Doses	2	44.64	22.32	31.24
Error	27	19.28	0.71	-
Total	29	63.92	-	-

VS: Variation Sources

The averages of different salt doses over the shoot dry weight of the hyssop plant are shown in Table 1The average shoot dry weight value determined by the study is 2.18 gr. In the study, shoot dry weight values varied between 3.83-0.91 g. The effect of different salt dosage applications on the shoot dry weight of the plant was found to be statistically significant at the $p<0.05$ level The lowest shoot dry weight was obtained with 0.91 gr from the salt dose of 100 mM, and the highest shoot dry weight as 3.83 gr was obtained from the 0 mM salt dose.

The variance analysis values of the effects of different salt doses on the number of branches in the hyssop (H.officinalis) is given in Table 8. The effect of different salt doses on the number of branches was found to be statistically significant at the rate 5%.

Table 8. Variance analysis results regarding the number of branches

VS	df	Sum of Squares	Mean Square	F
Salt Doses	2	1233.8	616.9	29.79
Error	27	559	20.70	-
Total	29	1792.8	-	-

VS: Variation Sources

The averages of different salt doses over the the number of branches of the hyssop plant are shown in Table 1. The average number of branches value determined by the study is 14. The number of branches in the study varied between 24 and 8. The effect of different salt dosage applications on the the number of branches of the plant was found to be statistically significant at the $p<0.05$ level. The lowest number of branches was obtained with 8 from the salt dose of 100 mM, and the highest number of branches as 24 was obtained from the 0 mM salt dose.

The variance analysis values of the effects of different salt doses on the number of leaves in the hyssop (*H.officinalis*) is given in Table 9. The effect of different salt doses on the number of leaves was found to be statistically significant at the rate 5%.

Table 9. Variance analysis results regarding the number of leaves

VS	df	Sum of Squares	Mean Square	F
Salt Doses	2	181543.5	90771.73	73.04
Error	27	33553.2	1242.71	-
Total	29	215096.7	-	-

VS: Variation Sources

The averages of different salt doses over the the number of leaves of the hyssop plant are shown in Table 1. The average number of leaves value determined by the study is 148. The number of leaves in the study ranged from 252 to 65. The effect of different salt dosage applications on the the number of leaves of the plant was found to be statistically significant at the $p<0.05$ level. The lowest leaf number was obtained with 65 from the salt dose of 100 mM, and the highest leaf number as 252 was obtained from the 0 mM salt dose.

The variance analysis values of the effects of different salt doses on leaf diameter in hyssop (H.officinalis) is given in Table 10. The effect of different salt doses on leaf diameter was found to be statistically significant at the rate 5%.

Table 10. Variance analysis results for leaf diameter

VS	df	Sum of Squares	Mean Square	F
Salt Doses	2	53.51	26.75	24.04
Error	27	30.04	1.11	-
Total	29	83.55	-	-

VS: Variation Sources

The averages of different salt doses over the leaf diameter of the hyssop plant are shown in Table 1. The average leaf diameter value determined by the study is 8.29 mm. Leaf diameter values in the study ranged between 9.91-6.64 mm (Table 1). The effect of different salt dosage applications on the leaf diameter of the plant was found to be statistically significant at the $p<0.05$ level. The lowest leaf diameter was obtained with 6.64 mm from the salt dose of 100 mM, and the highest leaf diameter as 9.91 mm was obtained from the 0 mM salt dose.

Öztürk et al. (2004) investigated the effects of 4 different salt doses (0.25, 1.00, 2.00, 4.00 and 6.00 dSm-1) on lemongrass (*Melissa officinalis* L.) and with the increase in salt doses, plant height, root length and root dry weight decreased. reported to have arrived. It was observed that the dry and fresh weights of the plants and the number of branches increased by 1.00 dSm-1, and a decrease was observed as the salt doses increased. As a result of the study, it was reported that the maximum root length was obtained from the dose of 0.25 dSm-1 with 56.53 cm, and minimum value was obtained from the dose of 38.93 cm with 6.00 dSm-1. The average root length value is 49.96 cm, and it has been determined by us that it is considerably higher than the root length value obtained from the study.

Shalan et al. (2006) applied 3 different salt doses (0 ppm, 2000 ppm, 4000 ppm and 6000 ppm) to marjoram (*Majorana hortensis* L.) plant in their research. As a result of the application, it was stated that there were serious decreases in plant length, the number of branches, and plant dry weights and fresh weights due to increasing salt doses.

Khorasaninejad et al. (2010) in their study to determine the effect of 3 different salt doses (0, 50, 100 and 150 mM NaCl) on the mint component (*Mentha piperita* L.), they found that increasing salt dose caused decreases in root length, shoot dry weight, root fresh weight they detected. As a result of the study, it was observed that the highest shoot dry weight occurred at the dose of 11.86 g and 0 mM, and the lowest value was observed at the dose of 0.8 g and 100 mM. The decrease caused by increasing salt doses in the calculated values is consistent with our study. Shoot dry weight was found to be 4.76 g on average, and it was revealed that the data was higher than the shoot dry weight value obtained from the study.

Mohammadzadeh et al. (2013) investigated the effects of 3 different salt doses (0, 50, 100 and 150 mM) on 4 masses of native basil (Ocimum basilcum L.) and it was stated that with increasing salt doses, the number of branches, root fresh weight, root dry weight and shoot dry weight, decreased. The decrease caused by increasing salt doses in the calculated values is consistent with our study. It was reported that the highest fresh root weight in plants was 10.62 g at the dose of 0 mM, and the lowest value was at the dose of 4.58 g and 150 mM. Root fresh weight was determined as 7.58 g on average. It has been determined by us that these results are considerably higher than the root wet weight value obtained from the study.

Kaya and İnan (2014) investigated the effect of 2 different salt doses (25 and 50 mM NaCl) on basil (Ocimum basilicum L.) plant in their study. As a result of the application, it was observed that fresh and dry herb weights, number of branches, plant height decreased significantly with the increase in salt doses. As the salt concentrations increased, less branch formation was observed in the plants. The highest number of branches in the plants was measured as 7.33 units/plant and 8.41 units/plant, respectively, in the control groups (0 mM), while the lowest number of branches was measured as 5.00 units/plant and 7.83 units/plant, respectively, at 50 mM doses. The average number of branches was determined as 6 and 7 pieces/plant, respectively, and it was observed that the data were less than the number of branches obtained from the study.

CONCLUSION

Soil or water salinity is one of the important abiotic stress factors that negatively affect plant growth and productivity. When the salinity in the soil exceeds a critical level, water intake becomes very difficult and the plant may die.

Reclamation of soils that are or may be affected by salinity is time consuming and costly, so it is necessary to use species and cultivars with high salinity tolerance in order to achieve efficient and successful production in such areas. Determining the salt tolerance levels of plants will not only provide benefits in terms of economy and time, but also will provide the opportunity to have the desired chemical content.

In this study, it was determined that the increase in salt concentration during the seedling development stage of hyssop root length (cm), shoot length (cm), root fresh and dry weight (g), shoot fresh and dry weight (g), number of branches (number/plant), leaf It has been shown that the number (pieces/plant) and leaf diameter (mm) significantly decrease. In all data, the lowest values were found at 100 mM NaCl dose, and the lowest value

was obtained from 50 mM NaCl dose only in shoot wet weight. The lowest values were obtained at a dose of 100 mM NaCl, and seedling growth did not occur in 150 mM and 200 mM NaCl applications. As a result, there is not much research on the hyssop plant, which has an important potential for our country's agriculture. As a result of this study carried out under controlled conditions, it was determined that the tolerance of the examined hyssop to different doses of chlorine salts varies, and it is recommended that more comprehensive studies be conducted to examine the physiological mechanism of salt tolerance.

ACKNOWLEDGMENT

This study was supported by Kırşehir Ahi Evran University Scientific Research Projects Unit with Project Number: ZRT.A4.22.022.

REFERENCES

Açıkgöz, N. İlker, E. Gökçöl, A. (2004). Biyolojik araştırmaların bilgisayarda değerlendirilmesi. Ege Üniversitesi Tohum Teknolojisi Uygulama ve Araştırma Merkezi, Yayın No:2, s.236.

Akgül, A. (1993). Baharat ve bilim teknolojisi. Selçuk Üniversitesi, Gıda Bilimi ve Teknolojisi Bölümü, Gıda Teknolojisi Derneği Yayınları No:15, S:180-181.

Baytop, T. (1991). Türkçe bitki adları sözlüğü, Atatürk Kültür ve Dil ve Tarih Kurumu, Türk Dil Kurumu Yayınları, 578: 294 S.

Botella, M.A. Rosado, A. Bressan, R.A. Hasegawa, P.M. (2005). Plant adaptive responses to salinity stress. Plant Abiotic Stress, Blackwell Publishing Ltd., 270p.

Bulut, N., (2019). Yabani asma *(V. vinifera*ssp*. silvestris)* ve bazı Amerikan asma anaçlarında tuz stresi toleransının değerlendirilmesi. Yüksek Lisans Tezi, Dicle Üniversitesi, Fen Bilimleri Enstitüsü, Bahçe Bitkileri Anabilim Dalı, Diyarbakır.

Demir, İ., Karaca, K. (2018). The Effect of Different Nitrogen and Phosphor Doses on Yield and Yield Parameters of Safflower (Carthamus tinctorius L.) in Arid Conditions. Turkish Journal of Agriculture-Food Science and Technology, 6(8), 971-976.

Demir, I. (2021). The effect of sowing dates on growth and yield parameters of black cumin (Nigella sativa L.) cultivars in Kırşehir semi-arid conditions. Medicinal and aromatic plants: economics production, agricultural utilization and other aspects, (419-444), Iksad Publications.

Demir, I. (2022), The effects of nitrogen doses on yield and yield components of linseed (Linum usitatissimum L.) in semi-arid ecological conditions. Industrial plants: economics, production, agricultural, utilization and other aspects, (67-82) Iksad Publications.

Güner, A. Aslan, S. Ekim, T. Vural, M. Babaç, M.T. (2012). Türkiye bitkileri listesi (Damarlı Bitkiler). Nezahat Gökyiğit Botanik Bahçesi ve Flora Araştırmaları Derneği Yayını. İstanbul.

Hong, C-Y.Chao, Y-Y. Yang, M-Y.Cho, S-C. Kao, C.H. (2009). Na+ but not Clorosmotic stress is ın volved in NaCl ınduced expression of glutathionereductase in roots of rice seedlings. Journal of Plant Physiology, 166, 1598-1606.

Kaya, A. İnan, M. (2017). Tuz (NaCl) stresine maruz kalan reyhan (*Ocimum basilicum* L.*)* bitkisinde bazı morfolojik, fizyolojik ve biyokimyasal parametreler üzerine salisilik asidin etkileri. Harran Tarım ve Gıda Bilimleri Dergisi, 2017, 21(3): 332-342

Khorasaninejad, S. Mousavi, A. Soltanloo, H. Hemmati, K. Khalighi, A. (2010). The effect of salinity stress on growth parameters, essential oil yield and

constituent of peppermint (*Mentha piperita* L.).World Applied Sciences Journal,11(11), 1403-1407.

Kiyas, Ü. (2020). Farklı leonardit ve tuz seviyelerinin fasulyenin *(Phaseolus vulgaris* L.*)* fide gelişimi üzerine etkisi. Yüksek Lisans Tezi, Bingöl Üniversitesi, Fen Bilimleri Enstitüsü, Tarla Bitkileri Anabilim Dalı, 2020, Bingöl.

Leung, A. Foster, S. (1996). Encyclopedia of common natural ın gredients used in food, drugs, and cosmetics, ISBN: 978047508267.

Mohammadzadeh, M. Arouee, H. Neamati, S.H.Shoor, M. (2013). Effect of different levels of salt stress and salicylic acid on morphological characteristics of four mass native basils (*Ocimum basilcum*). International Journal of Agronomy and Plant Production,4 (Special Issue), 3590-3596.

Munns, R. Tester, M. (2008). Mechanisms of salinity tolerance. Annual Review of Plant Biology, 59, 651-681.

Özer, H. Sökmen, M. Güllüce, M. (2006). In vitro antimicrobial and antioxidant activities of the essential oils and methanol extracts of *Hyssopus officinalis* L. Ssp angustifolius. *Ital. J. Food Sci*., 18: 73–83.

Öztürk, A. Ünlükara, A. İpek, A. Gürbüzi, B. (2004). Effects of salt stress and water deficit on plant growth and essential oil content of lemonbalm (*Melissa officinalis* L.). Farm Structures and Irrigation Department, Faculty of Agriculture, University of Ankara, 06110, Turkey, Pak. J. Bot., 36(4): 787-792, 2004.

Pessarakli, M. Szabolcs, I. (1999). Soilsalinityandsodicity as particular plant/crop stress factors. Handbook of Plant Crop Stress, ISBN 0-8247-1948-4, New York, 1198 p.

Razmjoo, K., Heydarizadeh, P.,Sabzalian, M. R.,(2008). Effect of salinityanddroughtstresses on growthparametersandessentialoilcontent of Matricariachamomile. Int. J. Agric. Biol,10(4), 451-454.

Shalan, M.N. Abdel-Latif, T.A, El-Ghadban, E.M.A. (2006). Effect of water salinity and some nutritional compounds on the growth and production of sweet marjoramplants (*Majorana Hortensis* L.). Egyptian Journal of Agricultural Research,84(3), 959-975.

Ulas, F. (2021). Effects of grafting on growth, root morphology and leaf physiology of pepino (*Solanum muricatum* Ait.) as affectedby salt stressunder hydroponic conditions. International Journal of Agriculture, Environment and Food Sciences**.**

CHAPTER 3

BIOCHEMICAL BIOMARKERS USED IN THE ECOTOXICOLOGIAL RISK ASSESSMENT

Numan YILDIRIM[1],

Nuran CIKICKOGLU YILDIRIM[2], Osman SERDAR[3]

1 Munzur University, Tunceli Vocational School, Department of Plant and Animal Production, Organic Agriculture Programme, TR62000 Tunceli, Turkey e-mail:numanyildirim44@gmail.com, ORCID: 0000-0003-1109-8106

2 Munzur University, Pertek Sakine Genç Vocational School, Department of Veterinary Medicine, Laboratorian and Veterinarian Health Programme, TR62000 Tunceli, Turkey e-mail:nurancyildirim@gmail.com, ORCID: 0000-0003-3975-6705

3 Munzur University, Fisheries Faculty, TR62000 Tunceli, Turkey e-mail:osmserdar@gmail.com ORCID: 0000-0003-1744-8883

1. Introduction

Ecotoxicology is a scientific discipline that focuses on studying the effects of pollutants, contaminants, and environmental stressors on ecosystems, organisms, and populations. It involves assessing the potential risks that these stressors pose to the environment, wildlife, and human health. Ecotoxicology combines principles from ecology, toxicology, chemistry, and other scientific fields to understand the complex interactions between living organisms and their environment in the context of pollution and contamination (Harborne, 1993; Paixao et al. 2008).

1.1. Environmental Contaminants

Ecotoxicology investigates a wide range of environmental contaminants, including pollutants from industrial activities, agricultural runoff, urban development, and various human-made chemicals. These contaminants can be present in air, water, soil, and sediments, and they can have diverse effects on different components of ecosystems (Zhou et al., 2020).

1.2. Biological Responses

Ecotoxicologists study the biological responses of organisms to environmental stressors. This includes understanding how pollutants can affect organisms at various levels, such as individual health, reproduction, growth, behavior, and survival. The effects of contaminants can cascade through food chains and impact entire ecosystems (Bauer and Herrmann, 1997).

1.3. Toxicology and Mechanisms of Action

Understanding the toxicological mechanisms through which contaminants affect organisms is a central component of ecotoxicology. This involves investigating how pollutants interact with biological systems at the molecular and cellular levels, leading to adverse effects on physiological processes (Brandts et al., 2018; Batel et al., 2016).

1.4. Biomarkers and Bioindicators

Ecotoxicologists often use biomarkers and bioindicators to assess the impact of contaminants on organisms. Biomarkers are measurable indicators of physiological or biochemical changes that can reveal the presence of stress or toxicity. Bioindicators are species or groups of organisms that are particularly sensitive to environmental changes and can serve as indicators of ecosystem health (Browne et al., 2013; O'Donovan et al., 2018).

1.5. Risk Assessment and Management

Ecotoxicology contributes to risk assessment and management strat-

egies for pollutants. By understanding the potential impacts of contaminants on ecosystems and human health, ecotoxicologists help guide decisions about pollution control, environmental regulations, and conservation efforts. Beyond individual organisms, ecotoxicology also considers the broader impacts of contaminants on ecosystems. This includes investigating how contamination can alter community dynamics, disrupt ecosystem services, and influence overall biodiversity (Aylward et al. 2005; Pham et al. 2019).

1.6. Environmental Monitoring and Modeling

Ecotoxicological studies often involve environmental monitoring to assess the presence and concentration of contaminants in different environmental compartments. Long-term monitoring helps track trends, identify emerging issues, and evaluate the effectiveness of mitigation measures (Mkandawire et al. 2014).

Ecotoxicologists use computer models to simulate the behavior of contaminants in the environment and predict their potential impacts. These models can help researchers and policymakers make informed decisions about pollution prevention and control (Blinova 2004; Gubbins et al. 2011).

Given the complexity of environmental systems, ecotoxicology requires collaboration across disciplines. Ecologists, toxicologists, chemists, statisticians, and other experts work together to gather data, analyze results, and provide holistic insights into the effects of contaminants (Lam and Gray, 2003).

In summary, ecotoxicology is a multidisciplinary field that seeks to understand the effects of pollutants and contaminants on ecosystems and organisms. By investigating the interactions between environmental stressors and living organisms, ecotoxicologists contribute to environmental protection, conservation efforts, and the sustainable management of our natural resources.

2. Biomarkers

Biomarkers are measurable indicators that reflect biological, biochemical, or physiological changes occurring in organisms exposed to environmental stressors, such as pollutants or contaminants. They can be used to detect, quantify, and monitor the effects of these stressors on organisms. Biomarkers play a crucial role in ecotoxicological evaluations of wastewater treatment efficiencies by providing a quantitative assessment of the impact of treated wastewater on aquatic organisms. These biomarkers can indicate sublethal effects, physiological responses, and potential risks to ecosystems (Aksmann and Tukaj, 2004).

Biochemical biomarkers are crucial indicators used to assess the toxic effects of wastewater on organisms. These biomarkers are derived from changes in the biochemical and enzymatic processes within organisms when exposed to pollutants present in wastewater (Lewis et al., 2001)

Here is detailed information about some common biochemical biomarkers used to determine the toxic effects of wastewater:

2.1. Acetylcholinesterase (AChE)

An enzyme that plays a crucial role in the nervous system is AChE, which breaks down the neurotransmitter acetylcholine (ACh) at synapses. ACh is a chemical messenger that transmits signals between nerve cells and from nerve cells to muscles, leading to muscle contractions and other physiological responses. AChE's primary function is to rapidly terminate the action of ACh, allowing for precise control of nerve signals and preventing overstimulation of target cells (Getman et al., 1992; Daniels 2007).

AChE acts on the neurotransmitter acetylcholine by catalyzing its hydrolysis into choline and acetate. This breakdown of acetylcholine into its components is essential for terminating nerve impulses and ensuring proper functioning of the nervous system. AChE is found at cholinergic synapses, which are connections between nerve cells that use acetylcholine as their neurotransmitter (Daniels 2007).

After a nerve impulse triggers the release of acetylcholine into the synapse, it binds to receptors on the postsynaptic cell, transmitting the signal. AChE quickly degrades the acetylcholine in the synaptic cleft, preventing continuous stimulation of the postsynaptic cell. This degradation allows for the termination of the nerve signal and the subsequent relaxation of the muscle or cessation of nerve cell communication. AChE is particularly important at neuromuscular junctions, which are synapses between motor neurons and muscle cells. Here, acetylcholine released from motor neurons triggers muscle contractions. AChE ensures that acetylcholine is rapidly removed from the synapse, preventing continuous muscle contraction and allowing muscles to relax between signals (Moriarity, 1999).

AChE is used as a biomarker in ecotoxicological and environmental studies due to its sensitivity to certain classes of chemicals, particularly organophosphate and carbamate pesticides. These chemicals inhibit AChE activity by binding to the enzyme's active site, resulting in the accumulation of acetylcholine and prolonged nerve signal transmission. This can lead to toxic effects in organisms, including neurological and behavioral disturbances (Fuentes and Bouchot 2004; Lionetto et al., 2013).

As mentioned earlier, AChE inhibition can occur due to exposure to certain pesticides. Symptoms such as muscle twitching, tremors, convul-

sions, and, in severe cases, paralysis and death occur due to a buildup of acetylcholine caused by this inhibition. Organophosphate and carbamate pesticides, as well as nerve agents, are potent AChE inhibitors. AChE's role in terminating nerve signals and its sensitivity to chemical inhibition make it a valuable target for both medical research and environmental monitoring. Studying AChE activity provides insights into the health of nervous systems in various organisms and helps assess potential risks posed by pollutants in the environment (Sultatos and Kaushik 2007).

2.2. Catalase (CAT)

CAT is an antioxidant enzyme that helps convert hydrogen peroxide into water and oxygen, thereby preventing oxidative damage to cells. Changes in CAT activity can indicate oxidative stress caused by wastewater pollutants. An enzyme that plays a crucial role in protecting cells from oxidative damage is catalase, which breaks down hydrogen peroxide (H2O2), a reactive oxygen species (ROS), into water and oxygen. Due to its involvement in antioxidant defense mechanisms, catalase is often used as a biomarker to assess oxidative stress and the impact of various stressors, including pollutants, on organisms (Halliwell and Gutteridge 2015).

Catalase is primarily located in the peroxisomes of eukaryotic cells and in the cytoplasm of prokaryotic cells. Its primary function is to facilitate the breakdown of hydrogen peroxide, which is a byproduct of various cellular processes. Hydrogen peroxide is potentially damaging to cells as it can generate highly reactive hydroxyl radicals that can cause oxidative stress and damage cellular components like proteins, lipids, and DNA. Catalase is a critical component of the cellular antioxidant defense system. Catalase helps prevent the accumulation of reactive oxygen species that can lead to cellular damage by breaking down hydrogen peroxide into water and oxygen. This process helps maintain cellular homeostasis and protect cells from oxidative stress (Mhamdi et al., 2010).

Changes in catalase activity can serve as a biomarker to assess oxidative stress in response to various stressors, including exposure to pollutants, chemicals, and environmental contaminants. Increased catalase activity is often indicative of a cell's attempt to counteract increased levels of ROS due to stressors. Conversely, decreased catalase activity can suggest impaired antioxidant defense mechanisms and increased susceptibility to oxidative damage. Catalase activity is commonly measured in ecotoxicological studies to evaluate the impact of pollutants and contaminants on organisms exposed to adverse environmental conditions. When organisms are exposed to pollutants, oxidative stress can occur due to the generation of ROS. Measuring catalase activity provides insights into the organism's response to this stress and its ability to mitigate oxidative damage (Darabi

et al., 2022; denBesten et al., 2013).

Catalase activity is typically measured by assessing the rate of hydrogen peroxide decomposition over time. The enzyme's activity is often reported in terms of micromoles of hydrogen peroxide broken down per minute per milligram of protein (μmol/min/mg protein) (Aebi 1984; Chance and Maehly 1955).

In summary, catalase is an essential enzyme involved in antioxidant defense mechanisms, and its activity can be used as a biomarker to assess oxidative stress in response to environmental stressors, including pollutants. Measuring catalase activity provides valuable insights into an organism's ability to manage oxidative damage and its overall health in various ecological contexts.

2.3. Superoxide Dismutase (SOD)

SOD is another antioxidant enzyme that neutralizes superoxide radicals, which are highly reactive molecules. An increase in SOD activity can indicate the presence of oxidative stress and the organism's attempt to counteract it. An enzyme that plays a vital role in protecting cells from oxidative damage is SOD, which catalyzes the conversion of superoxide radicals (O2•-) into less harmful molecules, namely hydrogen peroxide (H2O2) and molecular oxygen (O2). SOD is a crucial component of the cellular antioxidant defense system, and its activity can be used as a biomarker to assess oxidative stress and the impact of various stressors on organisms (Fridovich 1995).

Superoxide radicals ($O_2^{\bullet-}$) are highly reactive and can cause oxidative damage to cellular components. SOD accelerates the dismutation of superoxide radicals into hydrogen peroxide and molecular oxygen, which are less reactive and less damaging to cells. There are different forms of SOD found in cells, including copper-zinc SOD (Cu/Zn SOD), manganese SOD (Mn SOD), and extracellular SOD (EC-SOD), each localized in specific cellular compartments (Mishra and Imlay 2012).

SOD is a critical part of the cellular antioxidant defense system. It acts as the first line of defense against superoxide radicals generated during various metabolic processes and stress conditions. By converting superoxide radicals into less harmful molecules, SOD helps prevent oxidative damage and maintains cellular health (McCord and Fridovich 1969).

Changes in SOD activity can serve as a biomarker to assess oxidative stress and the impact of stressors, pollutants, and contaminants on organisms. Increased SOD activity is often indicative of an organism's response to elevated levels of superoxide radicals caused by stress. Higher SOD activity reflects the organism's attempt to mitigate oxidative damage. SOD

activity is frequently measured in ecotoxicological studies to evaluate the impact of pollutants and environmental stressors on organisms. Exposure to pollutants can lead to increased ROS production, including superoxide radicals. Measuring SOD activity provides insights into how organisms respond to oxidative stress and their ability to manage the associated damage (Vlahogianni et al., 2007; Carvalho et al., 2012).

SOD activity is typically measured by assessing its ability to dismutate superoxide radicals, often using colorimetric or spectrophotometric assays. These assays quantify the rate of superoxide radical dismutation and are reported as units of enzyme activity per milligram of protein (U/mg protein) (Beauchamp and Fridovich 1971).

In summary, Superoxide Dismutase is a critical enzyme in the cellular antioxidant defense system, and its activity can be used as a biomarker to assess oxidative stress and the impact of stressors on organisms. Measuring SOD activity provides insights into an organism's ability to manage oxidative damage and its overall health in various ecological contexts.

2.4. Glutathione-S-Transferase (GST)

GST is an enzyme involved in detoxification processes by catalyzing the conjugation of glutathione to reactive compounds. Elevated GST activity suggests exposure to xenobiotics and increased detoxification efforts. Glutathione-S-Transferase (GST) is an enzyme that plays a key role in cellular detoxification processes by catalyzing the conjugation of the tripeptide molecule glutathione (GSH) to various electrophilic compounds. GSTs are a diverse group of enzymes that are involved in the metabolism of endogenous and exogenous compounds, including environmental pollutants, carcinogens, drugs, and toxins. In the context of ecotoxicology and environmental monitoring, GST activity is often used as a biomarker to assess exposure to xenobiotics and the overall health of organisms (Hayes and Pulford 1995).

GSTs comprise multiple isoforms that are classified into different classes based on their structural and functional characteristics. Different GST isoforms have specific substrate preferences, allowing them to metabolize a wide range of compounds. GSTs are found in various tissues and organs, and their distribution can vary depending on the organism and environmental conditions (Hayes et al., 2005).

Increased GST activity is often observed in response to exposure to xenobiotics, including pollutants, chemicals, and environmental contaminants. The upregulation of GST activity is an adaptive response to counteract the potential toxicity of these substances. Measuring GST activity can provide insights into an organism's exposure to xenobiotics and its ability

to metabolize and eliminate them. GST activity is commonly used as a biomarker in ecotoxicological studies to assess the impact of pollutants on organisms. Increased GST activity indicates that organisms are responding to the presence of potentially harmful compounds in their environment. However, it's important to note that the induction of GSTs can vary depending on factors such as the type of pollutant and the species being studied (Dasari et al., 2018; Crane et al., 2002).

GST activity is typically measured using enzyme assays that monitor the formation of glutathione-conjugated products. These assays are often conducted in vitro using tissue or cell homogenates. The activity is reported as micromoles of substrate conjugated to glutathione per minute per milligram of protein (μmol/min/mg protein)(Habig et al., 1974; Habig and Jakoby 1981).

In summary, An enzyme involved in detoxification processes is GST, and its activity serves as a biomarker for exposure to xenobiotics and pollutants. Measuring GST activity provides insights into an organism's response to environmental stressors and its ability to metabolize and eliminate potentially harmful compounds.

2.5. Glutathione peroxidase (GPx)

GPx is a critical component of the cellular antioxidant defense system. It is involved in neutralizing hydrogen peroxide, a reactive molecule that can cause oxidative damage to cellular components, including lipids, proteins, and DNA. One of the primary functions of GPx is to detoxify hydrogen peroxide by converting it into water and oxygen. This process helps prevent the formation of highly reactive hydroxyl radicals, which can cause extensive damage to cell structures. GPx is a selenoprotein, meaning that it contains selenium in its active site. An essential trace element that plays a crucial role in the antioxidant defense system is selenium. The activity of GPx is closely linked to selenium availability (Flohé and Maiorino 2013; Flohé and Günzler 1985).

Changes in GPx activity can serve as a biomarker for oxidative stress. When organisms are exposed to pollutants or environmental stressors that generate ROS, the activity of GPx may be altered as it responds to the increased oxidative load. GPx is commonly used in ecotoxicological studies to assess the impact of pollutants on organisms' antioxidant defense systems. Exposure to pollutants can lead to oxidative stress and alterations in antioxidant enzyme activities, including GPx (Ranjbar et al., 2002; Wang et al., 2003).

GPx activity can be measured using various assays that involve monitoring the rate of hydrogen peroxide reduction. Spectrophotometric methods

are often used to quantify the decrease in absorbance at a specific wavelength over time (Flohé and Günzler 1984; Shalwitz, and Sunde 2009).

In summary, Glutathione peroxidase (GPx) is an essential enzyme that plays a crucial role in cellular antioxidant defense against oxidative stress. It serves as a biomarker in ecotoxicological studies to assess the impact of pollutants and contaminants on organisms' antioxidant defense systems. Measuring GPx activity provides valuable insights into an organism's response to oxidative stress and its potential susceptibility to oxidative damage caused by environmental stressors.

2.6. Cytochrome P450 (CYP450)

A superfamily of heme-containing enzymes that play a key role in the metabolism of a wide range of endogenous and exogenous compounds are CYP450 enzymes. In ecotoxicology, CYP450 enzymes are often used as bioindicators to assess the exposure of organisms to environmental pollutants and contaminants. These enzymes are involved in the detoxification of xenobiotics and play a crucial role in the biotransformation of various chemicals, making them valuable indicators of exposure to contaminants that can be harmful to organisms and ecosystems (Munro et al., 2018).

Exposure to certain chemicals can induce or inhibit the activity of CYP450 enzymes. Induction occurs when the presence of a chemical increases the expression and activity of specific CYP450 enzymes, enhancing the organism's ability to metabolize the chemical. Conversely, inhibition occurs when a chemical suppresses the activity of CYP450 enzymes, potentially leading to the accumulation of toxic compounds. Changes in CYP450 enzyme activity can serve as bioindicators of exposure to environmental contaminants. Increased or decreased enzyme activity can signal the presence of specific pollutants and their potential effects on an organism's metabolism and detoxification processes. CYP450 enzymes are used as bioindicators in ecotoxicological studies to assess the exposure of organisms to pollutants and contaminants in their environment. Monitoring changes in enzyme activity can provide insights into the presence of specific chemicals and their potential impact on organisms' health (Guengerich 2008; Almeida et al., 2022).

CYP450 enzyme activity is typically measured using techniques that involve assessing the rate of metabolism of a known substrate by these enzymes. These assays often use fluorescent probes or specific substrates that are metabolized by CYP450 enzymes. The resulting products are quantified to determine enzyme activity (Guengerich 2001; Omura and Sato 1964).

In summary, Cytochrome P450 (CYP450) enzymes serve as bioindicators of exposure to environmental contaminants, reflecting an organ-

ism's ability to metabolize and detoxify xenobiotics. Monitoring changes in CYP450 enzyme activity provides insights into pollutant exposure and potential effects on an organism's metabolism. Their use in ecotoxicological studies contributes to our understanding of the impact of pollutants on organisms and ecosystems.

2.7. Lipid Peroxidation

A process that involves the oxidative degradation of lipids, particularly unsaturated fatty acids, resulting in the generation of reactive oxygen species (ROS) and the formation of lipid peroxides is lipid peroxidation. This process can cause damage to cell membranes and other cellular components, leading to cell dysfunction and various health issues. Lipid peroxidation is commonly used as a biomarker to assess oxidative stress and the impact of environmental stressors on organisms (Halliwell and Gutteridge 2015; Ayala et al., 2014).

Lipid peroxidation starts with the attack of ROS, such as hydroxyl radicals (•OH), on unsaturated fatty acids in cell membranes. This leads to the abstraction of hydrogen atoms from the lipid molecules, generating lipid radicals. These radicals initiate a chain reaction that results in the formation of lipid peroxides, such as hydroperoxides. Lipid peroxides can further degrade into various reactive aldehydes, such as malondialdehyde (MDA), which is a common marker of lipid peroxidation. Lipid peroxidation can lead to structural and functional damage to cell membranes. Cell membranes are composed of lipids, and when lipid peroxidation occurs, the membrane's integrity can be compromised. This can result in increased permeability, altered membrane fluidity, and impaired cellular functions (Halliwell and Gutteridge 2015).

Lipid peroxidation serves as a biomarker for assessing oxidative stress, which arises from an imbalance between the production of reactive oxygen species (ROS) and the protective antioxidant mechanisms. Elevated levels of lipid peroxidation products, such as MDA, indicate increased oxidative stress and potential damage to cellular components. Lipid peroxidation is commonly used in ecotoxicological studies to assess the impact of pollutants, contaminants, and environmental stressors on organisms. Exposure to pollutants can lead to increased ROS production and subsequent lipid peroxidation. Measuring lipid peroxidation levels provides insights into an organism's response to oxidative stress and the potential damage caused by pollutants (Comporti 1985; Valavanidis et al., 2009).

Lipid peroxidation is typically measured by quantifying the levels of lipid peroxidation products, such as MDA, in tissues or body fluids. Various methods, such as thiobarbituric acid reactive substances (TBARS) as-

say, are used to measure MDA levels, which are often reported in terms of concentration (e.g., nanomoles per milligram of protein) (Ohkawa 1979; Draper and Hadley 1990).

In summary, lipid peroxidation is a process that reflects oxidative damage to lipids in cell membranes and serves as a biomarker for oxidative stress. Measuring lipid peroxidation levels provides valuable insights into an organism's response to environmental stressors and its potential susceptibility to oxidative damage.

2.8. Metabolites and Biochemical Components:

2.8.1. Glutathione (GSH)

GSH is a tripeptide that acts as a major antioxidant and detoxification molecule in cells. Its levels can be used as an indicator of the cellular response to oxidative stress caused by wastewater contaminants. Glutathione (GSH) is a tripeptide molecule composed of three amino acids: cysteine, glycine, and glutamic acid. It is a critical antioxidant and detoxification molecule in cells, playing a central role in maintaining cellular redox balance, protecting against oxidative stress, and participating in various biochemical processes. Glutathione is used as a biomarker to assess the cellular response to oxidative stress, exposure to pollutants, and overall health of organisms (Wu et al., 2004; Townsend et al., 2003)

Glutathione plays a pivotal role in detoxification processes, specifically in the conjugation of electrophilic compounds with glutathione, forming more water-soluble and readily excretable molecules. This process helps neutralize and eliminate various xenobiotics, including pollutants, drugs, and environmental contaminants. Changes in glutathione levels can serve as a biomarker to assess oxidative stress. Under conditions of increased ROS production or exposure to stressors, glutathione levels may be depleted as it is consumed to neutralize ROS. Decreased glutathione levels can indicate oxidative stress and potential damage to cellular components (Hayes and McLellan 1999; Sies 1999).

Glutathione is commonly used as a biomarker in ecotoxicological studies to assess the impact of pollutants, contaminants, and environmental stressors on organisms. Exposure to pollutants can lead to oxidative stress and the depletion of glutathione as it is utilized to neutralize ROS generated by the stressor (Ercal et al., 2001; Pereira et al., 2013).

Glutathione levels can be measured directly in tissues, cells, or body fluids using various assays. Different forms of glutathione, including reduced glutathione (GSH) and oxidized glutathione (GSSG), can be measured individually or in combination to assess the redox state of cells. Assays often involve colorimetric or spectrophotometric methods (Anderson

1985; Griffith 1980).

In summary, Glutathione is a crucial antioxidant and detoxification molecule in cells, and its levels are used as a biomarker to assess oxidative stress, cellular redox balance, and exposure to environmental stressors. Measuring glutathione levels provides insights into an organism's antioxidant defense response and its ability to mitigate oxidative damage.

2.8.2. Endocrine Disruptors

Some wastewater pollutants can mimic or interfere with natural hormones, leading to endocrine disruption. Biomarkers related to reproductive hormones, such as estradiol, testosterone, and vitellogenin, are used to assess the effects of wastewater on the endocrine system of aquatic organisms. Chemicals known as endocrine disruptors have the ability to interfere with the regular operations of the endocrine system, responsible for hormone production and regulation within the body. These chemicals can mimic, block, or alter the actions of hormones, leading to various physiological and developmental effects in organisms. Endocrine disruptors can serve as biomarkers in ecotoxicological studies to assess the impact of environmental contaminants on the endocrine system of organisms (Diamanti-Kandarakis et al., 2009;)

Endocrine disruptors can affect the endocrine system through various mechanisms. They can bind to hormone receptors, leading to inappropriate activation or inhibition of signaling pathways. Some disruptors can interfere with hormone synthesis, secretion, transport, metabolism, and elimination. Endocrine disruptors can impact a wide range of hormones, including estrogen, androgen, thyroid hormones, insulin, and more. They can disrupt various endocrine pathways, leading to effects on growth, reproduction, development, metabolism, and immune function (Gore et al., 2015).

In ecotoxicology, the effects of endocrine disruptors on organisms' endocrine systems can be used as biomarkers to assess exposure to pollutants and contaminants. These effects can include alterations in hormone levels, changes in reproductive behaviors, developmental abnormalities, and disruptions in the balance of sex-specific characteristics. Reproductive hormones such as estradiol, testosterone, and vitellogenin are commonly used as biomarkers of endocrine disruption. For example, altered levels of these hormones can indicate disturbances in reproductive processes and the potential effects of endocrine disruptors on an organism's ability to reproduce. Endocrine disruptors are studied in ecotoxicological research to understand how pollutants and contaminants impact organisms' endocrine systems. These studies can provide insights into potential reproductive and developmental effects, population-level impacts, and the overall health of

ecosystems (Jobling et al., 2006; Beausoleil et al., 2017).

Biomarkers of endocrine disruption can be measured using various methods, including enzyme-linked immunosorbent assays (ELISAs) for hormone quantification and histological examinations to assess changes in gonadal morphology (Sosa-Ferrera et. al., 2013).

In summary, endocrine disruptors are chemicals that interfere with hormone signaling in organisms, leading to a range of effects on development, reproduction, and health. Biomarkers related to reproductive hormones and endocrine pathways serve as valuable tools for assessing the impact of endocrine disruptors on organisms and ecosystems, contributing to our understanding of environmental health and regulatory decisions.

3. Conclusion

In the field of ecotoxicological evaluation, biochemical biomarkers have emerged as invaluable tools for assessing the impact of pollutants, contaminants, and environmental stressors on organisms and ecosystems. These biomarkers provide a window into the intricate biochemical and physiological responses of organisms when exposed to various stressors. By examining changes in enzyme activities, oxidative stress biomarkers, metabolites, and endocrine disruption indicators, researchers gain insights into the health, resilience, and adaptive capacities of organisms in the face of environmental challenges.

Enzyme activities, such as acetylcholinesterase (AChE) inhibition, catalase (CAT) activity, and glutathione-S-transferase (GST) induction, offer crucial information about the effects of pollutants on neurological function, oxidative stress defense, and detoxification processes. Lipid peroxidation and total antioxidant capacity (TAC) serve as biomarkers that shed light on the balance between oxidative damage and antioxidant defense mechanisms, providing a glimpse into cellular health under stress.

Furthermore, endocrine disruptors and their impact on reproductive hormones present a deeper understanding of how pollutants can interfere with hormonal balance and disrupt reproductive processes in organisms. These biomarkers contribute to unraveling the intricate interactions between pollutants and the endocrine system, highlighting potential risks to reproductive success and population sustainability.

The utilization of these biochemical biomarkers is not only confined to the laboratory but extends to ecotoxicological studies in natural environments, enabling researchers to assess the health of ecosystems as a whole. These biomarkers assist in identifying early warning signs of environmental degradation, guiding regulatory measures, and fostering a greater un-

derstanding of the intricate relationships between pollutants, organisms, and the environments they inhabit.

However, it's crucial to acknowledge that the interpretation of biochemical biomarkers requires a holistic approach that considers species-specific variations, physiological responses, and potential interactions between multiple stressors. The use of multiple biomarkers in combination enhances the accuracy and reliability of assessments, offering a comprehensive view of the complex dynamics involved.

In conclusion, biochemical biomarkers play an indispensable role in ecotoxicological evaluations, providing essential insights into the physiological, cellular, and biochemical responses of organisms to environmental stressors. These markers bridge the gap between laboratory research and real-world ecosystems, fostering a deeper comprehension of the intricate connections between pollution, ecological health, and the sustainability of our natural world. As the study of ecotoxicology continues to evolve, biochemical biomarkers stand as crucial allies in safeguarding the delicate balance of life in the face of anthropogenic impacts.

4. References

Aebi, H. (1984). Catalase in vitro. In Methods in enzymology, 105,121-126. Academic press.

Aksmann, A. and Tukaj, Z. (2004). The effect of anthracene and phenanthrene on the growth, photosynthesis, and SOD activity of the green alga Scenedesmus armatus depends on the PAR irradiance and CO 2 level. Archives of Environmental Contamination and Toxicology, 47, 177-184.

Almeida, E.M., Tisserand, F., Faria, M. and Chèvre, N. (2022). Efficiency of Several Cytochrome P450 Biomarkers in Highlighting the Exposure of Daphnia magna to an Organophosphate Pesticide. Toxics, 10(8): 482.

Anderson, M.E. (1985). Determination of Glutathione and Glutathione Disulfide in Biological Samples. Methods in Enzymology, 113, 548-555.

Aylward, B., Bandyopadhyay, J., Belausteguigotia, J., Borkey, P., Cassar, A., Meadors, L. and Voutchkov, N. (2005). Freshwater ecosystem services. In 'Ecosystems and Human Well-being: Policy Responses. 3, 213–255.

Batel, A., Linti, F., Scherer, M., Erdinger, L. and Braunbeck, T. (2016). Transfer of benzo [a] pyrene from microplastics to Artemia nauplii and further to zebrafish via a trophic food web experiment: CYP1A induction and visual tracking of persistent organic pollutants. Environmental Toxicology and Chemistry, 35(7), 1656-1666.

Bauer, M.J. and Herrmann, R. (1997). Estimation of the environmental contamination by phthalic acid esters leaching from household wastes. Science of the Total Environment, 208(1-2), 49-57.

Beauchamp, C. and Fridovich, I. (1971). Superoxide Dismutase: Improved Assays and an Assay Applicable to Acrylamide Gels. Analytical Biochemistry, 44(1), 276-287.

Beausoleil, C., Belzunces, L. P., Desaint, G., et al. (2017). Non-Targeted Effects of Pesticides on Organisms in Freshwater and Terrestrial Habitats: A Review and Meta-Analysis. Science of the Total Environment, 587-588, 111-121.

Blinova, I. (2004). Use of freshwater algae and duckweeds for phytotoxicity testing. Environmental Toxicology: An International Journal, 19(4), 425-428.

Brandts, I., Teles, M., Gonçalves, A. P., Barreto, A., Franco-Martinez, L., Tvarijonaviciute, A. and Oliveira, M. (2018). Effects of nanoplastics on Mytilus galloprovincialis after individual and combined exposure with carbamazepine. Science of The Total Environment, 643, 775-784.

Browne, M. A., Niven, S. J., Galloway, T. S., Rowland, S. J. and Thompson, R.

C. (2013). Microplastic moves pollutants and additives to worms, reducing functions linked to health and biodiversity. Current biology, 23(23), 2388-2392.

Carvalho, C.S., Bernusso, V.A., deAraujo, H.S.S.,Espindola, E.L. and Fernandes, M.N. (2012). Biomarker responses as indication of contaminant effects in Oreochromis niloticus. Chemosphere, 89(1), 60-69.

Chance, B. and Maehly, A.C. (1955). Assay of catalases and peroxidases. Methods in Enzymology, 2,764-775.

Comporti, M. (1985). Lipid Peroxidation and Cellular Damage in Toxic Liver Injury. Laboratory Investigation, 53(6), 599-623.

Crane, M., Sildanchandra, W. and Callaghan, A. (2002). Relationship between biomarker activity and developmental endpoints in Chironomus riparius Meigen exposed to an organophosphate insecticide. Ecotoxicology and Environmental Safety, 53(3), 361-369.

Daniels, G. (2007). Functions of red cell surface proteins. Vox sanguinis, 93(4), 331-340.

Darabi, F., Keshavarzi, M., Abdullah, M.N., Dehghani, F., Khanjani, N., Yousefinejad, S., Khajehnasiri, F. and Zamanian, Z. (2022). Evaluation of oxidative stress and biochemical biomarkers, and psychological parameters in cement plant workers. Toxicology and Industrial Health, 38(1):29-40.

Dasari, S., Ganjayi, M.S. and Meriga, B. (2018). Glutathione S-transferase is a good biomarker in acrylamide induced neurotoxicity and genotoxicity. Interdisciplinary Toxicology, 11(2): 115–121.

DenBesten, H.M.W., Effraimidou, S. and Abee, T. (2013). Catalase Activity as a Biomarker for Mild-Stress-Induced Robustness in Bacillus weihenstephanensis. Applied and Environmental Microbiology, 79(1): 57–62.

Diamanti-Kandarakis, E., Bourguignon, J. P., Giudice, L. C., et al. (2009). Endocrine-Disrupting Chemicals: An Endocrine Society Scientific Statement. Endocrine Reviews, 30(4), 293-342.

Draper, H. H. and Hadley, M. (1990). Malondialdehyde Determination as Index of Lipid Peroxidation. Methods in Enzymology, 186, 421-431.

Ercal, N., Gurer-Orhan, H. and Aykin-Burns, N. (2001). Toxic Metals and Oxidative Stress Part I: Mechanisms Involved in Metal-Induced Oxidative Damage. Current Topics in Medicinal Chemistry, 1(6), 529-539.

Flohé, L. and Günzler, W. A. (1984). Assays of Glutathione Peroxidase. Methods

in Enzymology, 105, 114-120.

Flohé, L. and Günzler, W. A. (1985). The Biophysiology of the Glutathione Peroxidase. Role in Protection against Oxidative Stress. Bulletin et Mémoires de l'Académie Royale de Médecine de Belgique, 140(2-3), 119-138.

Flohé, R.B. and Maiorino, M. (2013). Glutathione Peroxidases. Biochimica et Biophysica Acta (BBA) - General Subjects, 1830(5), 3289-3303.

Fridovich, I. (1995). Superoxide Radical and Superoxide Dismutases. Annual Review of Biochemistry, 64, 97-112.

Getman, D. K., Eubanks, J. H., Camp, S., Evans, G. A. and Taylor, P. (1992). The human gene encoding acetylcholinesterase is located on the long arm of chromosome 7. American journal of human genetics, 51(1), 170-177.

Griffith, O.W. (1980). Determination of Glutathione and Glutathione Disulfide Using Glutathione Reductase and 2-Vinylpyridine. Analytical Biochemistry, 106(1), 207-212.

Gore, A.C., Chappell, V.A., Fenton, S.E., et al. (2015). EDC-2: The Endocrine Society's Second Scientific Statement on Endocrine-Disrupting Chemicals. Endocrine Reviews, 36(6), E1-E150.

Gubbins, E.J., Batty, L.C. and Lead, J.R. (2011). Phytotoxicity of silver nanoparticles to Lemna minor L. Environmental Pollution, 159(6), 1551-1559.

Guengerich, F.P. (2001). Common and Uncommon Cytochrome P450 Reactions Related to Metabolism and Chemical Toxicity. Chemical Research in Toxicology, 14(6), 611-650.

Guengerich, F.P. (2008). Cytochrome P450 and Chemical Toxicology. Chemical Research in Toxicology, 21(1), 70-83.

Habig, W.H., Pabst, M.J. and Jakoby, W.B. (1974). Glutathione S-Transferases. The First Enzymatic Step in Mercapturic Acid Formation. Journal of Biological Chemistry, 249(22), 7130-7139.

Habig, W.H. and Jakoby, W.B. (1981). Assays for Differentiation of Glutathione S-Transferases. Methods in Enzymology, 77, 398-405.

Halliwell, B. and Gutteridge, J.M. (2015). Free radicals in biology and medicine. Oxford university press, USA.

Harborne, J.B. (2014). Introduction to ecological biochemistry. Academic press. 4th ed London.

Hayes, J. D. and McLellan, L.I. (1999). Glutathione and Glutathione-Dependent

Enzymes Represent a Co-ordinately Regulated Defence Against Oxidative Stress. Free Radical Research, 31(4), 273-300.

Hayes, J.D., Flanagan, J.U. and Jowsey, I.R. (2005). Glutathione Transferases. Annual Review of Pharmacology and Toxicology, 45, 51-88.

Hayes, J.D. and Pulford, D.J. (1995). The Glutathione S-Transferase Supergene Family: Regulation of GST and the Contribution of the Isoenzymes to Cancer Chemoprotection and Drug Resistance. Critical Reviews in Biochemistry and Molecular Biology, 30(6), 445-600.

Jobling, S., Nolan, M., Tyler, C. R., Brighty, G. and Sumpter, J. P. (1998). Widespread sexual disruption in wild fish. Environmental Science & Technology, 32(17), 2498-2506.

Lam, P.K. and Gray, J.S. (2003). The use of biomarkers in environmental monitoring programmes. Marine Pollution Bulletin, 46(2), 182-186.

Lewis, S., Donkin, M.E. and Depledge, M.H. (2001). Hsp70 expression in Enteromorpha intestinalis (Chlorophyta) exposed to environmental stressors. Aquatic Toxicology, 51(3), 277-291.

Lionetto, M.G., Caricato, R., Calisi, A., Giordano, M.E. and Schettino, T. (2013). Acetylcholinesterase as a Biomarker in Environmental and Occupational Medicine: New Insights and Future Perspectives. BioMed Research International, 2013: 321213.

McCord, J.M. and Fridovich, I. (1969). Superoxide dismutase: an enzymic function for erythrocuprein (hemocuprein). Journal of Biological chemistry, 244(22), 6049-6055.

Mhamdi A, Queval G, Chaouch S, Vanderauwera S, Van-Breusegem F, et al. (2010) Catalase function in plants: a focus on Arabidopsis mutants as stress-mimic models. Journal of Experimental Botany, 61: 4197–4220

Mishra, S. and Imlay, J. (2012). Why do bacteria use so many enzymes to scavenge hydrogen peroxide?. Archives of biochemistry and biophysics, 525(2), 145-160.

Mkandawire, M., Teixeira da Silva, J. A. and Dudel, E. G. (2014). The Lemna bioassay: Contemporary issues as the most standardized plant bioassay for aquatic ecotoxicology. Critical Reviews in Environmental Science and Technology, 44(2), 154-197.

Moriarty, F. (1999). Ecotoxicology, the study of pollutants in ecosystems (3rd Ed). San Diego, California: Academic Press

Munro, A.W., McLean, K.J., Grant, J.L. and Makris, T.M. (2018). Structure and function of the cytochrome P450 peroxygenase enzymes. Biochem Soc Trans, 46(1): 183–196.

O'Donovan, S., Mestre, N.C., Abel, S., Fonseca, T.G., Carteny, C.C., Cormier, B. and Bebianno, M.J. (2018). Ecotoxicological effects of chemical contaminants adsorbed to microplastics in the clam Scrobicularia plana. Frontiers in Marine Science, 5, 143.

Ohkawa, H., Ohishi, N. and Yagi, K. (1979). Assay for Lipid Peroxides in Animal Tissues by Thiobarbituric Acid Reaction. Analytical Biochemistry, 95(2), 351-358.

Omura, T. and Sato, R. (1964). The Carbon Monoxide-Binding Pigment of Liver Microsomes. I. Evidence for Its Hemoprotein Nature. Journal of Biological Chemistry, 239(7), 2370-2378.

Pereira, S., Pinto, A.L., Cortes, R., Fontaínhas-Fernandes, A. and Coimbra, A.M. (2013). Gill histopathological and oxidative stress evaluation in native fish captured in Portuguese northwestern rivers. Ecotoxicology and Environental Safety, 90,157–166.

Pham, H.V., Torresan, S., Critto, A. and Marcomini, A. (2019). Alteration of freshwater ecosystem services under global change–A review focusing on the Po River basin (Italy) and the Red River basin (Vietnam). Science of the Total Environment, 652, 1347-1365.

Ranjbar, A., Pasalar, P. and Abdollahi, M. (2002). Induction of Oxidative Stress and Acetylcholinesterase Inhibition in Organophosphorous Pesticide Manufacturing Workers. Human & Experimental Toxicology, 21(4), 179-182.

Rodrí guez-Fuentes, G. and Gold-Bouchot, G. (2004). Characterization of cholinesterase activity from different tissues of Nile tilapia (Oreochromis niloticus). Marine Environmental Research, 58(2-5), 505-509.

Sies, H. (1999). Glutathione and Its Role in Cellular Functions. Free Radical Biology and Medicine, 27(9-10), 916-921.

Sosa-Ferrera, Z., Mahugo-Santana, C. and Santana-Rodríguez, J.J. (2013). Analytical methodologies for the determination of endocrine disrupting compounds in biological and environmental samples. BioMed Research International, 2013:674838.

Sultatos, L. G. and Kaushik, R. (2007). Interactions of chlorpyrifos oxon and acetylcholinesterase. FASEB Journal, 21, 883–892

Valavanidis, A., Vlachogianni, T. and Fiotakis, K. (2009). Tobacco Smoke: Involvement of Reactive Oxygen Species and Stable Free Radicals in Mecha-

nisms of Oxidative Damage, Carcinogenesis and Synergistic Effects with Other Respirable Particles. International Journal of Environmental Research and Public Health, 6(2), 445-462.

Vlahogianni, T., Dassenakis, M., Scoullos, M.J. and Valavanidis, A. (2007). Integrated use of biomarkers (superoxide dismutase, catalase and lipid peroxidation) in mussels Mytilus galloprovincialis for assessing heavy metals' pollution in coastal areas from the Saronikos Gulf of Greece. Marine Pollution Bulletin, 54(9):1361-71.

Townsend, D. M., Tew, K. D. and Tapiero, H. (2003). The Importance of Glutathione in Human Disease. Biomedicine & Pharmacotherapy, 57(3-4), 145-155.

Wu, G., Fang, Y. Z., Yang, S., et al. (2004). Glutathione Metabolism and Its Implications for Health. The Journal of Nutrition, 134(3), 489-492.

Zhao, H. J., Xu, J. K., Yan, Z. H., Ren, H. Q. and Zhang, Y. (2020). Microplastics enhance the developmental toxicity of synthetic phenolic antioxidants by disturbing the thyroid function and metabolism in developing zebrafish. Environment International, 140, 105750.

CHAPTER 4

SATURN

E. Nihal ERCAN[1]

1 Prof.Dr., Physics Dept. of Boğaziçi University, ercan@boun.edu.tr

Introduction

Saturn is the 6th and second-largest planet in the Solar System. Like Jupiter, it is also a gas giant that is mainly composed of hydrogen and helium. It also has a complex structure of rings and a lot of moons. Compared to Earth, the mass of Saturn is 95 times greater. However, its density is only one-eighth of the Earth, also it is less dense than water.[1] Also, Saturn's radius is 9.5 times greater than Earth's radius.[2] So, its volume is 755 times greater than that of the Earth. The most known space mission that is studying Saturn is the Cassini-Huygens. With the help of the Cassini-Huygens mission, astronomers hope to find answers to questions about the internal structure of Saturn, its magnetic field, moons, rings, etc. The origin of the name is Roman mythology. It was one of the Roman gods that is known as the god of agriculture and wealth. It was also the father of Jupiter. One of the days' names Saturday is also named for the Roman god (Saturn's day).[3] Also, in astronomy, every planet has a symbol. Saturn's symbol is ♄.

In this short review article, we will study the general aspects of Saturn as well as the observational and possible theoretical scenarios related to it.

General Characteristics

Its Size, Mass, and Distance:

Saturn is the second largest and second most massive planet in our Solar System. Its diameter is almost 120.000 km, almost nine times wider than the Earth. Since it has no solid surface, its diameter is measured at a level where the atmospheric pressure is 1 bar, which corresponds to the pressure measured on Earth at sea level.[4] Saturn's diameter is nine times greater than that of Earth. Its mass is also roughly 95 times greater than Earth's mass.[7] The total mass of Jupiter and Saturn makes up %92 of the total mass of the planets in our Solar System.[9] Saturn's average density is almost equal to 70 percent of the density of water whereas Earth's density is 550 times and Jupiter's is 130 times that of the density of water.[5] Saturn is known to be the only planet in our Solar System that has a smaller density than water.[6]

Saturn is approximately 9.5 astronomical units away from the Sun, which is 9.5 times farther than the Earth. The sunlight travels roughly 80 minutes to arrive at Saturn from the Sun.

Composition:

Saturn is a gas giant and is mainly composed of helium and hydrogen. At the innermost layer, it has a solid core.[8] However, it is entirely composed of gases other than the core. Its core is composed of metals like iron and nickel. These metals are surrounded by a solid compound. This

solidity is because of the extreme pressure and temperature conditions. The core is surrounded by liquid metallic hydrogen. Saturn's core looks like the core of Jupiter, but it is much smaller.

Formation:

Saturn formed from the solar nebula nearly 4.5 billion years ago. Gas and dust turned out to be this gas giant due to the gravitational effects. There are some theories about how Saturn is formed. The most known theories are the core accretion and the disk instability theories.

Almost 4 billion years ago, Saturn was in its current position. It is the sixth planet from the Sun, located in the outer Solar System, after Jupiter.

History:

Saturn can be seen from the Earth using only the naked eye. The name of the planet is given by the Romans, the god of the harvest. Also, it corresponds to the Kronos, in Greek mythology. The ring of the planet is first discovered by Galileo Galilei by using a telescope. He thought that he was observing the moons of the planet. After Galileo, Christian Huygens used a better telescope and realized that they are the rings of the planet, not the moons. He also discovered the largest moon of Saturn, Titan. Then, Jean-Domanique Cassini observed four other moons of Saturn which are Iapetus, Rhea, Tethys, and Dione.

Bigger discoveries about Saturn were made after the spacecraft missions. The first spacecraft that visited Saturn is Pioneer 11. After that, Voyager 1 visited Saturn, and Voyager 2, one year after. Major observations are made after the Cassini spacecraft arrived at Saturn in 2004. Cassini observed mainly the moons of the planet and discovered four new ones. Also, the liquid hydrocarbon seas on the moon Titan are first seen by Cassini.

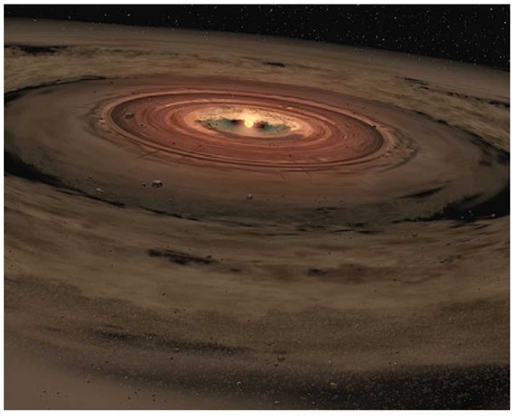

Figure 1. Credit : NASA Photojournal (https://photojournal.jpl.nasa.gov/targetFamily/Saturn)

Potential For Life:

The composition of Saturn is not suitable for organisms to live. There is no water which is essential for known life formations. The atmospheric conditions of Saturn are too extreme. The temperatures and pressures are not convenient for adaptations of the known organisms.

Because of these unfavorable conditions, the environment of Saturn is not suitable for life. However, these conditions are not the same for many of its moons. Titan and Enceladus are the ones that are possibly known as good candidates to support life other than Earth.

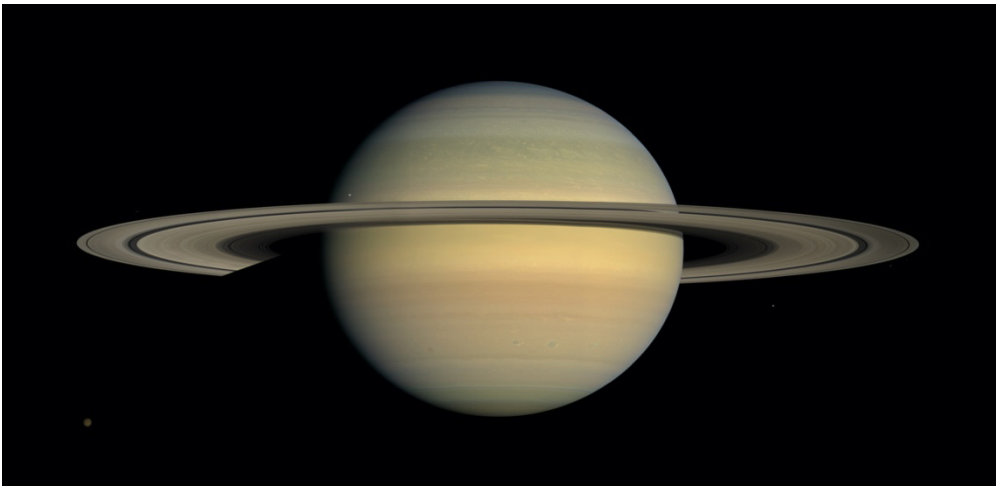

Figure 2. NASA Photojournal (https://photojournal.jpl.nasa.gov/targetFamily/Saturn)

Observational Aspects

The Atmosphere and Cloud Layers:

The outer atmosphere of Saturn is mainly composed of molecular hydrogen and helium. By volume, the atmosphere includes almost %96.3 hydrogen and %3.25 helium, and by mass, approximately %6 helium, %91 hydrogen, and %3 other molecules.[10] Except for hydrogen and helium, Saturn's atmosphere contains small amounts of methane, ammonia, and other gases.[11] Also, it is thought to be lower parts of Saturn's atmosphere including small amounts of hydrogen sulfide and water vapor. With the help of some information on spacecraft missions, one can say that Saturn has the most hydrogen-containing atmosphere in our Solar System.[12]

The surface of Saturn is mainly composed of clouds.[13] The composition of these clouds changes with pressure and depth. The highest layer of the clouds is mostly made of crystals of frozen ammonia. In the deep layers, there are thought to be clouds which are made of ammonia droplets and water ice crystals.[12]

In spacecraft images, Saturn's clouds look golden yellow/brown. However, in 2005 the Cassini spacecraft took images of Saturn's clouds that appeared blue in the northern hemisphere and yellow/brown in the southern hemisphere. These colors are thought to be because of Rayleigh's scattering.[14]

Like Jupiter, Saturn also has brighter and darker bands of clouds that are changing continuously due to winds. They also have swirling storm which appears as red, white, and brown ovals. These storms happen almost every thirty years. Also, at the north and south pole of Saturn, there are huge cyclones. The one at the north pole is also covered by a hexagonal pattern. This was first observed with an image taken by Voyager.[15] Saturn's atmosphere always hosts storms. One of the long-lived storms which is called the Dragon Storm flares up from time to time in Saturn's atmosphere.

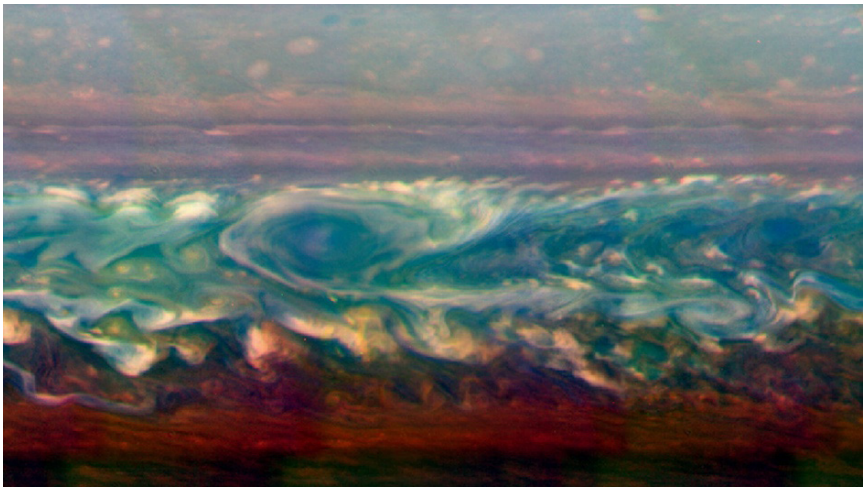

Figure 3. NASA Photojournal (https://photojournal.jpl.nasa.gov/targetFamily/Saturn)

Magnetosphere:

Saturn's magnetic field is much stronger than the Earth's magnetic field, but it is less strong than Jupiter's. Like Jupiter's magnetic field, the orientation of the poles is opposite of Earth, that is if one uses a compass in

Saturn's magnetic field it would point south. The magnetic field of Saturn covers a region in space which is called the magnetosphere. It is roughly 1.200.000 km from the planet which looks like a teardrop.

Like Jupiter, its magnetic polarity is opposite that of the Earth's polarity, that is if one places a compass, it points south pole of Saturn.[17] The magnetic field lines in Saturn pass from the south pole to the north pole. Also, both Saturn's and Jupiter's magnetic fields are dominated by dipole components. Saturn's magnetic field is aligned with its rotation axis, unlike the other planets in our Solar System.[16]

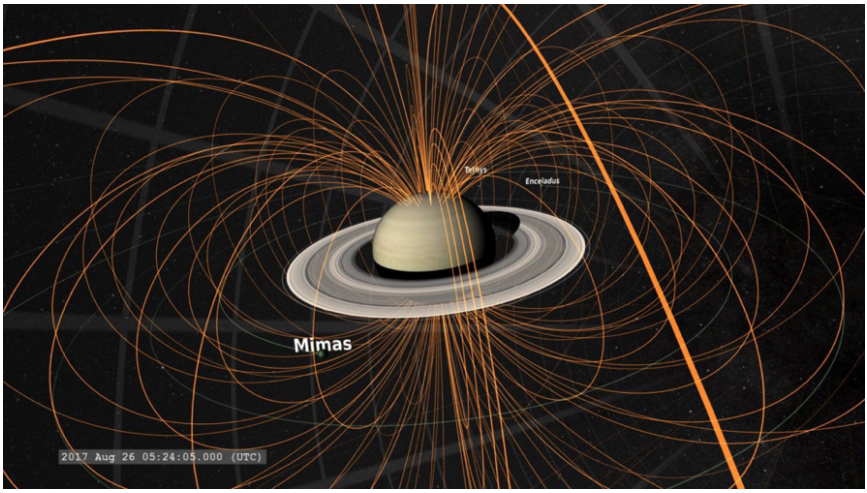

Figure 4. NASA Photojournal (https://photojournal.jpl.nasa.gov/targetFamily/Saturn)

Some of the moons of Saturn orbit in the edges of the magnetosphere of Saturn. One of the most famous moons which is called Titan orbits at the edge of the magnetosphere. It sometimes moves in and sometimes moves out of it depending on its position.

When solar wind ions or ions from the moons follow the magnetic field lines of the planet, they create auroras which are light due to the energy of the accelerated particles. Saturn's aurora is unique in our Solar System. It displays both dark and bright auroras.

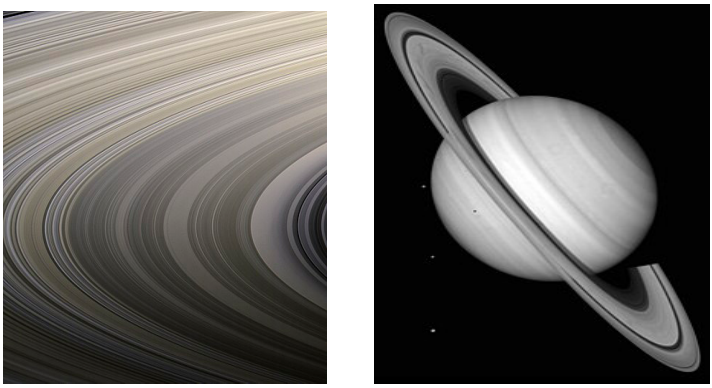

Figure 5.NASA Photojournal (https://photojournal.jpl.nasa.gov/targetFamily/Saturn)

Saturn's Rings:

Saturn's rings are the broadest and brightest ring system in our Solar System. They can be easily seen from Earth, and it is the first discovered ring system. The first observations were made by Galileo in 1610, but he failed to name them as rings. Instead, he thought that he observed the moons of Saturn. He also described them as ''Saturn's ears''. In 1655, Christian Huygens was able to see a ring around the planet with a more developed telescope.[18] In 1857, James Clark Maxwell mathematically proved that the rings cannot be solid, but they are composed of countless small particles, orbiting Saturn.[19]

The diameter of the main rings is roughly 270.000 kilometers. The outer rings may extend farther but they are fainter than the main ring. The rings are thin, but their thickness is almost 100 meters. They consist of small particles, mostly water ice, and dust.[20] They orbit around Saturn like its moons. With the help of radio signals, scientists can determine the distribution of these small particles.The ring system of Saturn consists of three groups. They are called A ring, B ring, and C ring from farthest to closest to the planet, respectively. One can see these three main groups with a telescope from Earth. The broadest, brightest, and thickest ring is the B ring. A and C have lower densities than that of B. After the C ring, there is also the D ring which is closer to Saturn. Also, F, G, and E rings are after the A ring. From A to E, the ring system almost covers 1.000.000 kilometers.

Figure 6. Saturns moons. NASA Photojournal (https://photojournal.jpl.nasa.gov/targetFamily/Saturn)

Also, there are some gaps between the rings. One of the major gaps is called the Cassini division which is located between A and B rings. [21]

By Voyager 1, dark radial structures in the rings are discovered which are called the spokes.[22] They are 8.000 km long and 2.000 km wide. They develop rapidly and then disappeared. The spokes travel with the rotation of the rings. They look dark in reflected light and bright in the scattered light. Since Saturn's rings are very bright one can say that they are composed of fresh material that is geologically young. Since small particles in the rings can move by magnetic forces, one can conclude that the D, E, F, are G rings have short lifetimes.

The Moons:

Saturn has 145 moons.[23] In addition to this number, there are also many moonlets in the rings. The major moons of Saturn are Mimas, Enceladus, Tethys, Dione, Rhea, Titan, Hyperion, Iapetus, and Phoebe, in the order of increasing distance from the planet.[24]

Saturn's inner moons orbit around a nearly circular path. For this reason, they are called regular. Inner moons include all the major moons above except Phoebe. The outer moons have tilted orbits and they are called irregular moons. They are much farther from Saturn.

Titan is the largest moon of Saturn. It is also greater than the planet Mercury. It is the second largest moon in our Solar System after Jupiter's moon Ganymede. Its atmosphere is rich in nitrogen which is similar to that of the Earth. [25] However, its atmosphere is much denser than Earth and its surface pressure is almost 1.5 times greater than Earth's. Titan's atmosphere also contains methane. This gas might play a role like water vapor on Earth.[31]

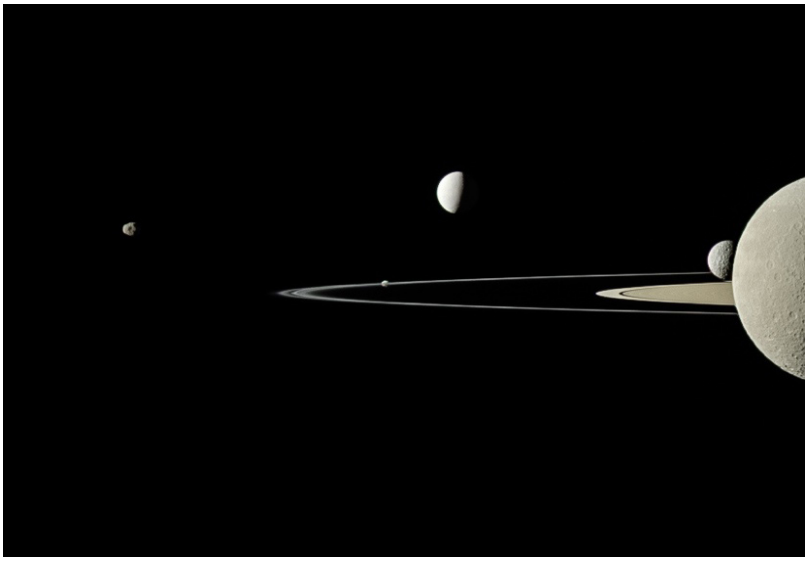

Figure 7. NASA Photojournal (https://photojournal.jpl.nasa.gov/targetFamily/Saturn)

Titan was first discovered by Christian Huygens in 1655.[26] Eight of the moons of the planet were discovered with the help of optical telescopes. After that, Tethys, Dione, Rhea, and Iapetus were discovered by Cassini. In 1789, Mimas and Enceladus were discovered by William Herschel.[27] Later, Hyperion was discovered in 1848.[28]

Later, additional moons were discovered with the help of spacecraft. Voyager discovered three new satellites: Atlas, Prometheus, and Pandora in 1980.[29] Also, the Cassini discovered three more new moons in 2004 and observed other moons but didn't confirm.[30]

Orbit and Rotation:

Saturn orbits around the Sun almost in 10.759 days which is equal to 29.5 Earth years.[32] Its distance from the Sun is almost 9 astronomical units. Also, one day takes only 10.7 hours on Saturn which is the second closest day in our Solar System. It orbits around the Sun roughly at a speed of 9.69 km/s.

Like Earth's tilted axis, Saturn's axis is also tilted at approximately 26.73 degrees. This tilted angle proves that Saturn experiences seasons like Earth.

Parts of the planet have different rotational rates as can be seen from the Earth. These different rates depend on latitude. There are different rotation periods in different regions of the planet.

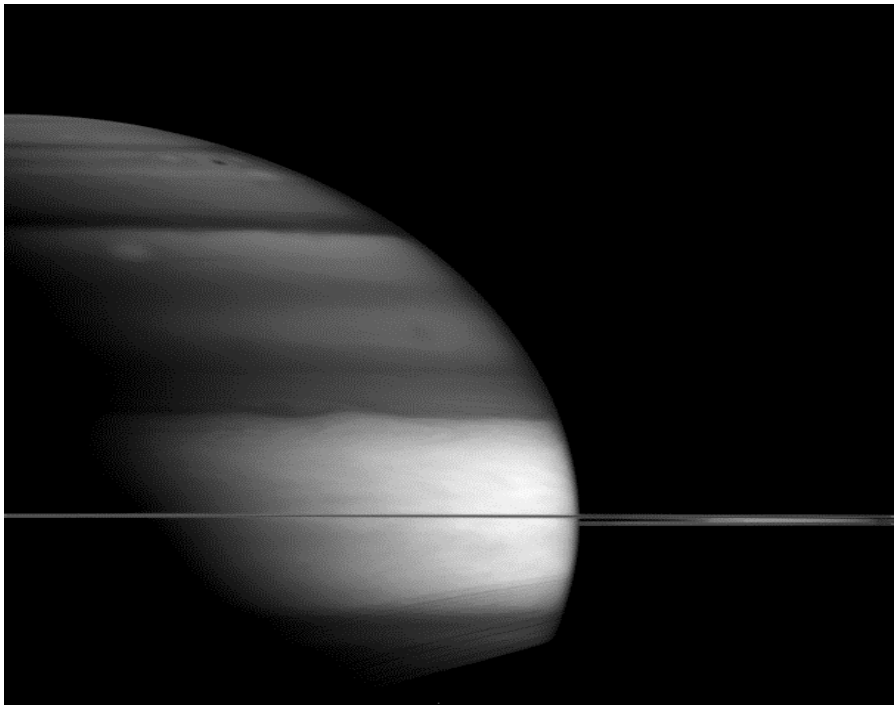

Figure 8. NASA Photojournal (https://photojournal.jpl.nasa.gov/targetFamily/Saturn)

Theoretical Aspects

The Shape of the Globe:

The rotation of the planet causes it to have a flattened appearance. This flattened shape is obvious even with a small telescope. It is flattened at the poles and bulging at the equator.

This was first observed by William Herschel in 1789. He gave the ratio of 11:10 to the equatorial to the polar diameter. Later, he made detailed measurements and concluded that the planet is also flattened at the equator like it is flattened at the poles. This gives a square-shouldered look to Saturn.

He also observed irregularities in the shape of the ring shadow. At that time, it is thought to be the rings were solid. And it was assumed that the shadow irregularities were due to real irregularities in the rings. It would be probably wrong to conclude that the rings are completely uniform, but the irregularities couldn't be observed from the Earth.

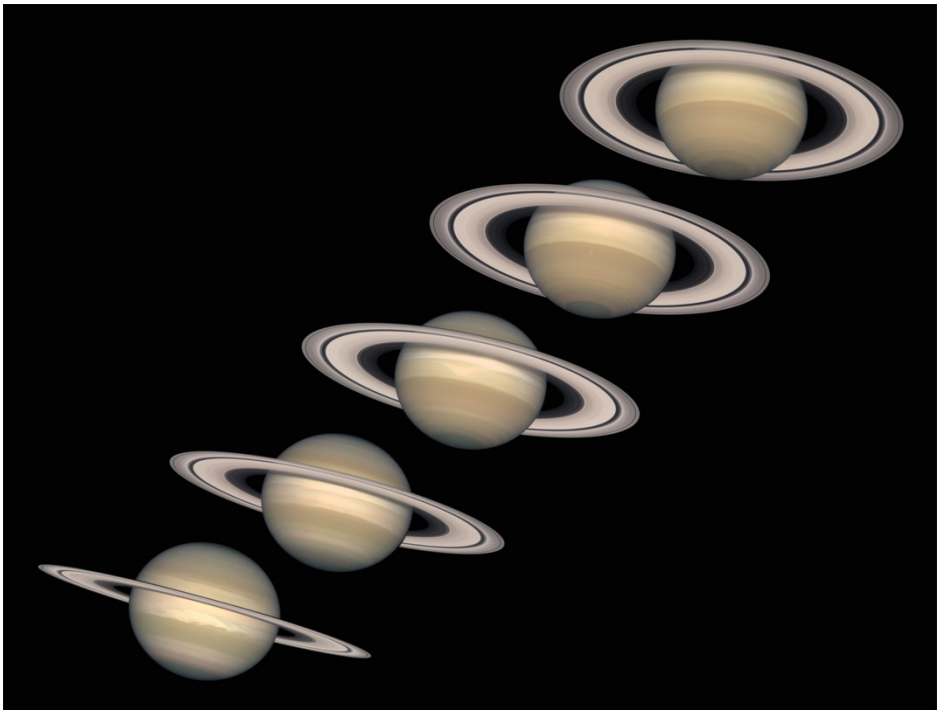

Figure 9. NASA Photojournal (https://photojournal.jpl.nasa.gov/targetFamily/Saturn)

Features of the Disc:

The disc of Saturn is not an easy subject to work on because the features of the disc are not that common. There is also the Great White Spot and known as Great White Oval like Jupiter's Great Red Spot. These spots are continuous storms that can be seen from the Earth by telescope. The white spots on Saturn are observed to have shorter lifetimes than that of Jupiter's. These storms are periodic at 28.5-year intervals.

These seasonal storms on Saturn were first discovered by Cassini. With the help of Cassini, the composition and temperature of the planet's atmosphere were studied. Cassini also provided information about plasma and radio waves to the scientists. Almost every 28 years, mega-storms occur on the surface of Saturn. Cassini detected flashes in a giant storm in 2011.

Saturn's rotational axis around the Sun is tilted like the Earth. This effect causes the seasons to form almost each of the seasons is seven Earth years long. Also, a 28-year storm is an annual fact for Saturn.

The Nature of Saturn:

Early observations showed that outer planets are not like the Earth. They are much bigger, and they don't have a solid surface. With their gaseous surfaces and great size, they are thought to be miniature stars. The low surface temperatures are thought to be explained by the miniature-sun theory.[34]

Since Hydrogen is the most abundant element in the universe, it is reasonable to expect that Saturn must contain a huge amount of it. Later, it is observed that it is true. Besides the great amount of Hydrogen, it also contains methane and some ammonia which are also compounds of Hydrogen. [35] In addition, in the miniature-sun theory, the essential characteristics are provided: the rocky core, the ice layer, and the hydrogen-rich atmosphere.

Later another theory was proposed that the planet contains a huge amount of Hydrogen, but it is most likely to be in liquid form. Also, even if the core of Saturn is extremely hot, its outer layers are extremely cold.

Changing Aspects of the Rings:

The reason why the giant planets have rings is first proposed by Eduard Roche. The planet and its moons are under the effect of gravitational force. Our moon causes ocean tides by pulling opposite sides of the Earth. These forces also affect the moon. If the moon comes so close to the planet, these tidal forces may overcome the gravitational forces between the moon and the planet, and the moon may form a ring. The minimum distance between the planet and its moon is called the Roche limit which is roughly 2.5 times the planet's radius from the centre of it.[33] That is why the giant planets have rings.

During the observations of the Cassini spacecraft scientist concluded that the rings of Saturn

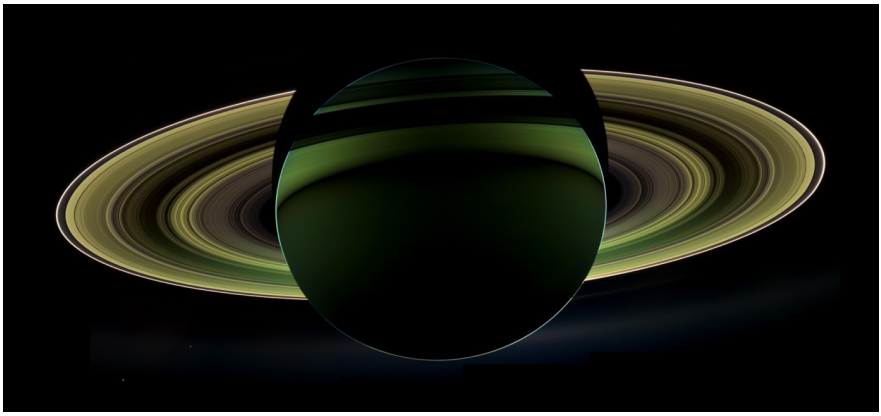

Figure 10. NASA Photojournal (https://photojournal.jpl.nasa.gov/targetFamily/Saturn)

are constantly changing. Particles in the rings are continually pushed around each other. All these observations represent that the rings are short-lived. Every second almost 40 tons of ice from the rings of Saturn rain down on the planet's atmosphere.

Discussion and Conclusion

Saturn is the second-greatest planet in the Solar System, and it is a gas giant. It is a massive, giant planet mostly made up of hydrogen and helium. It has dozens of satellites and rings around it. Even if it is not the only planet that has rings in our Solar System, its ring system is the most complex and magnificent. Its average distance from the Sun is roughly 9.5 astronomical units, that is the sunlight reaches the surface of Saturn in 80 minutes. It is almost 10 times wider than the Earth; more than 700 Earth can fit inside it. One Saturnian day takes 10.7 hours, which is the second shortest day in our Solar System. Also, it takes 29.5 years to orbit around the Sun.

Saturn's rotational axis is tilted at 26.73 degrees which causes seasons to happen. This effect is similar to the Earth's 23.5 tilted degree for its orbit around the Sun.

Saturn has 83 moons. Titan, the most famous moon of Saturn, is the only place in our solar system to have liquids in the form of lakes on its surface.

Saturn has the most complex and magnificent ring system. They are made of billions of ice, rock, and dust. The size of these particles is mainly from dust-like small particles to house-like particles. Rings may contain mountain size giant particles, too. Each ring orbits at different speeds around Saturn.

Saturn's formation is roughly 4.5 billion years ago. Also, it is in its current location almost 4 billion years ago. Observations about the planet, its satellites, and its moons are made for a long time. Dragonfly is planned spacecraft which will search for the moon of the planet, Titan. The studies are about the possible discovery of life and investigations of habitability.

I would like to thank Zeynep Çakıroğulları, one of my undergraduate students for her help in this review.

References

[1] Jerome James Brainerd, Solar System Planets Compared to Earth, The Astrophysics Spectator, 2004.

[2] Jerome James Brainerd, Characteristics of Saturn, The Astrophysics Spectator, 2004.

[3] Michael Falk, Astronomical Names for the Days of the Week, Journal of the Royal Astronomical Society of Canada, 93: 122–133, 1999.

[4] p.38-39.

[5] p.39.

[6] Saturn - The Most Beautiful Planet of our solar system, Preserve Articles, 2011

[7] David R. Williams, Saturn Fact Sheet, NASA, 2016.

[8] H. Jay Melosh, Planetary Surface Processes, Cambridge Planetary Science, Vol. 13, Cambridge University Press, 2011.

[9] Jonathan J. Fortney, Nadine Nettelman, The Interior Structure, Composition, and Evolution of Giant Planets, Space Science Reviews, 152 (1–4): 423–447, 2010.

[10] Saturn, Universe Guide, 2009.

[11] Fraser Cain, Atmosphere of Saturn, Universe Today, 2009.

[12] p.53.

[13] Glenn S. Orton, Ground-Based Observational Support for Spacecraft Exploration of the Outer Planets, Earth, Moon, and Planets, 105 (2–4): 143–152, 2009.

[14] Susan Watanabe, Saturn's Strange Hexagon, NASA, 2007.

[15] D. A. Godfrey, A hexagonal feature around Saturn's North Pole, Icarus, 76 (2): 335, 1988.

[16] C.T. Russell, Planetary Magnetospheres, Reports on Progress in Physics, 56 (6): 687–732, pp 717-718, 1993.

[17] Margaret Galland Kivelson, The current systems of the Jovian magnetosphere and ionosphere and predictions for Saturn, Space Science Reviews, 116 (1–2): 299–318, pp. 303-313, 2005.

[18] Ron Baalke, Historical Background of Saturn's Rings, Saturn Ring Plane Crossings of 1995–1996, Jet Propulsion Laboratory, 2006.

[19] James Clark Maxwell, On the stability of the motion of Saturn's rings, Cambridge England: Macmillan and Co., 1859.

[20] P.D. Nicholson et al., A close look at Saturn's rings with Cassini VIMS, Icarus, 193 (1): 182–212, 2008.

[21] Cassini, Observations nouvelles touchant le globe & l'anneau de Saturne (New observations concerning the globe and the ring of Saturn), Mémoires de l'Académie Royale des Sciences (in French), 10: 404–405, 1677.

[22] The Alphabet Soup of Saturn's Rings, The Planetary Society, 2007.

[23] Saturn now leads moon race with 62 newly discovered moons, UBC Science, University of British Columbia, 2023.

[24] Sherman Hollar, The Outer Planets: Jupiter, Saturn, Uranus, and Neptun, p. 45, 2012.

[25] Nola Taylor Redd, Titan: Facts About Saturn's Largest Moon, 2018.

[26] Robert & Bonnell Nemiroff, Jerry, Huygens Discovers Luna Saturni, Astronomy Picture of the Day, 2005.

[27] Albert Van Helden, Naming the satellites of Jupiter and Saturn, The Newsletter of the Historical Astronomy Division of the American Astronomical Society (32): 1–2, 1994.

[28] W.C Bond, Discovery of a new satellite of Saturn, Monthly Notices of the Royal Astronomical Society, 9: 1–2, 1848.

[29] V.S. Uralskaya, Discovery of new satellites of Saturn, Astronomical and Astrophysical Transactions, 15 (1–4): 249–253, 1998.

[30] Jonathan Corum, Mapping Saturn's Moons, The New York Times, 2015.

[31] Sherman Hollar, The Outer Planets: Jupiter, Saturn, Uranus, and Neptun, p. 48, 2012.

[32] Fraser Cain, Orbit of Saturn, Universe Today, 2009.

[33] What is the Roche limit?, NASA – JPL, 2009.

[34] Gary Hunt, Patrick Moore, Saturn, Early Theories, p12, 1981.

[35] R. Courtin; et al., The Composition of Saturn's Atmosphere at Temperate Northern Latitudes from Voyager IRIS spectra, Bulletin of the American Astronomical Society. 15: 831, 1967.

CHAPTER 5

ELECTRONIC AND STRUCTURAL PROPERTIES OF $APBI_3$ (A=MA,FA,NH_4,CS,RB) COMPOUNDS IN THE LIGHT OF DENSITY FUNCTIONAL THEORY

Veysel ÇELİK[1]

1 Siirt University, Faculty of Education, Department of Mathematics and Science Education, veysel3@gmail.com, ORCID No: 0000-0001-5020-8422

INTRODUCTION

Perovskite solar cells (PSCs) have emerged as a revolutionary development in photovoltaic (PV) energy over the past decade. Using materials with a perovskite structure in the active layer offers potential cost and efficiency benefits over traditional silicon-based solar cells (Kojima et al., 2009). Defined by a common chemical formula ABX_3, where A and B are metal or metalloid ions and X is typically an oxygen or halogen ion, perovskites are favored in solar cells for their optoelectronic properties (Kojima et al., 2009). Under lab conditions, PSCs have achieved conversion efficiencies nearing 26.1% (NREL, 2023). One significant benefit associated with perovskites is their capacity to undergo processing at low temperatures, hence leading to a reduction in production expenses. Additionally, PSCs can be printed on flexible substrates, paving the way for flexible PV panels. However, PSCs face challenges, including sensitivity to moisture, heat, and UV light. Some perovskites also contain lead, raising environmental concerns. In essence, while PSCs offer transformative potential for PV energy, their commercial success hinges on overcoming these challenges.

The scientific community has shown keen interest in the optoelectronic properties of methylammonium lead iodide ($MAPbI_3$) perovskites (Sharif et al., 2023; Çelik, 2023). These hybrid organic-inorganic compounds are ideal for photovoltaic devices and other optoelectronic applications. Factors like substrate composition can influence the development of perovskite crystals (Olthof and Meerholz, 2017). MAPbI3-based perovskites have shown promise in photodetection and have been integrated into electrical circuits (Soriano et al., 2023). However, concerns about their stability in ambient conditions persist. Various attempts have been undertaken to enhance stability and efficiency, including the development of 2D/3D heterostructured films (Hu et al., 2018). Despite their advantages, challenges remain in ensuring their long-term stability and optimizing device performance.

Efforts to enhance the efficiency of $MAPbI_3$-based PSCs have been numerous (Moyez and Roy, 2018; Jamal et al., 2019). Yet, stability concerns, especially regarding moisture sensitivity and degradation, persist (Jena et al., 2019). Formamidinium lead tri-iodide ($FAPbI_3$) offers better thermal stability and an energy band gap conducive to efficient solar absorption. A significant challenge with $MAPbI_3$ is its phase transition around 56°C, problematic since solar cells often operate at temperatures up to 85°C. This transition can alter its photovoltaic efficiency. Consequently, researchers are exploring alternatives like $FAPbI_3$, which offers better stability and doesn't exhibit this phase transition. Other potential replacements include ammonium ions (NH_4^+), Cs^+ ions, and Rb^+ ions, making $CsPbI_3$ and $RbPbI_3$ relevant to this discussion.

Perovskite materials hold promise across optoelectronics, photonics, and energy sectors. The $APbI_3$ perovskites, where A can be MA^+, FA^+, NH_4^+, Cs^+, or Rb^+, are particularly intriguing due to their efficiency, affordability, and superior electrical properties. To fully understand these materials, a robust theoretical framework is essential. The problem at hand can be addressed through the utilization of the Density Functional Theory (DFT) framework. This chapter aims to delve into the electrical and structural attributes of $APbI_3$ perovskites using DFT, focusing on how different A cations influence these properties and comparing the resulting changes. Through this, I hope to deepen understanding and spur further development of perovskite materials.

METHODS

The computational calculations in this study were conducted using the CASTEP software (Clark et al., 2005). CASTEP is a computational software tool that utilizes ab initio quantum mechanical methods, specifically density functional theory (DFT), to investigate the electronic structure and predict physical properties of materials in materials science research. The Perdew-Burke-Ernzerhof (PBE) exchange-correlation functional, a variant of the generalized gradient approximation (GGA), was employed across all calculations. The BFGS minimization strategy was utilized to optimize the crystal structures of $APbI_3$, where 'A' symbolizes MA^+, FA^+, NH_4^+, Cs^+, or Rb^+ (Pfrommer et al., 1997). The kinetic energy cutoff value used in the calculations is 490 eV for compounds containing MA^+, FA^+, $NH4^+$ and 250 eV for compounds containing Cs^+ and Rb^+. The Monkhorst-Pack k-point grid used to sample the Brillouin zone is 6x6x6 (Monkhorst and Pack, 1976). Convergence thresholds were set at $1.0x10^{-6}$ eV for energy and 0.05 eV/Å for forces. The electronic band structures of the optimized structures were determined by evaluating along high-symmetry k-points within the Brillouin zone. To facilitate a more comprehensive exploration of the electrical characteristics of the materials, a more precise the density of states (DOS) calculation was performed by employing a 13x13x13 k-point grid, thereby ensuring a higher level of accuracy. Norm-conserving pseudopotentials were employed for all chemical elements. The Tkatchenko-Scheffler approach was integrated into the calculations to accurately account for the van der Waals interactions within the system, providing a semi-empirical dispersion correction (McNellis et al., 2009; Tkatchenko and Scheffler, 2009).

RESULT AND DISCUSSION

$MAPbI_3$ Compound

The optimized structure of the $MAPbI_3$ perovskite structure is shown in Figure 1. The starting structure used in the calculations is cubic. The cubic structure was slightly distorted due to the effect of the relatively large MA^+ cation in the optimized structure. On the side of the molecule where the H ions are bonded to the N ion, the I ions moved towards the molecule, leaving the Pb-I-Pb line under the influence of the molecule. The calculated lattice parameters are 6.38 Å, 6.34 Å and 6.37 Å for lattice parameters *a*, *b* and *c*, respectively. The angles between the lattice vectors are calculated as approximately 90 degrees. The room temperature phase of $MAPbI_3$ is generally known as the tetragonal perovskite phase (Ong et al., 2015). However, an important point to note is that the phase stability of this material is quite sensitive to temperature, humidity and other environmental factors. In experimental study, the reported lattice parameter for the cubic phase of $MAPbI_3$ is approximately 6.30 Å. (Bonomi et al., 2020). However, it's important to note that this value can vary slightly in different studies. In comparison to the estimated values, the experimental and theoretical values exhibit a notable degree of proximity.

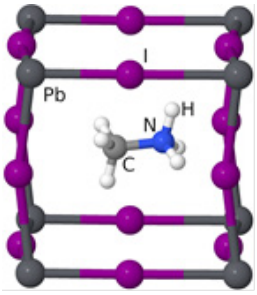

Figure 1*: Optimized $MAPbI_3$ compound.*

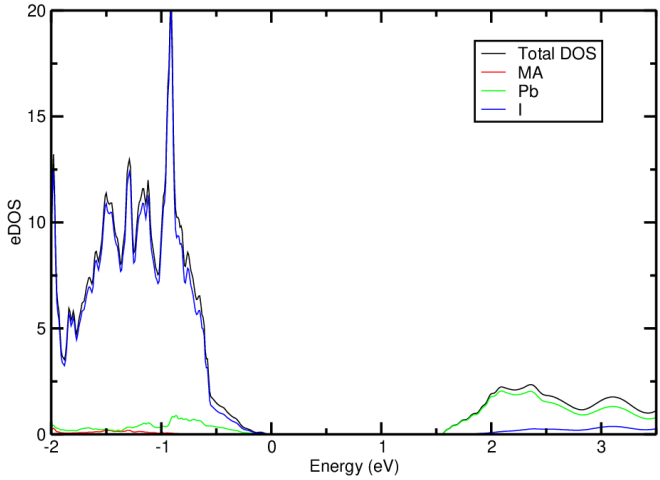

Figure 2: *The partial and total DOS patterns were acquired for the $MAPbI_3$ compound.*

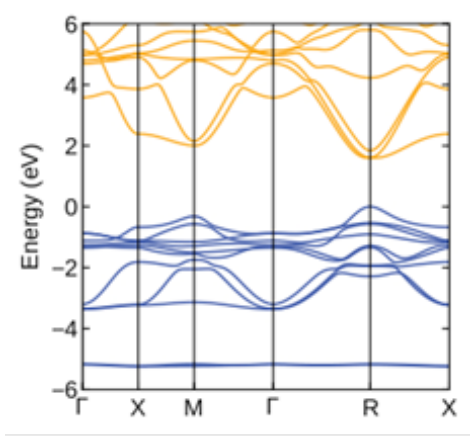

Figure 3: *Electronic band structure obtained for $MAPbI_3$.*

Density of states (DOS) patterns and band structure were obtained to examine the electronic structure. The DOS pattern depicted in Figure 2 is presented. In the valence bands, the energy levels of the I ion are dominant. Although there is a contribution from Pb ions at the valence band edge, it is weak compared to I ions. The energy levels of the MA^+ organic cation are below the valence band maximum (VBM). In the conduction band minimum (CBM), the energy levels of Pb ions are more dominant than the I ion. Like VBM, CBM consists of Pb-I hybrid energy levels. The energy levels of the MA^+ organic cation are situated higher than the CBM. Figure 3 shows the resulting band structure. $MAPbI_3$ has a semiconductor character. The lowest band gap occurs at the R symmetry point. The band gap

value here is approximately 1.59 eV. The value obtained from this study closely approximates the experimental value of around 1.61 eV (Yamada et al., 2014). The lowest band gap is around the symmetry point R and the nature of the transition is direct. However, the manner in which the transition occurs might be either direct or indirect, contingent upon the molecule's location (Çelik, 2023).

$FAPbI_3$ Compound

The $FAPbI_3$ undergoes a phase transition between the α-phase and σ-phase. The α-phase is the photoactive form, while the σ-phase is a non-perovskite form that forms at low temperatures. Considerable efforts have been undertaken to achieve the stabilization of the α-phase of $FAPbI_3$ at ambient conditions (Han et al., 2016). The alpha phase is the cubic phase and the lattice parameters value is about 6.36 Å (Weller et al., 2015). Nevertheless, the findings derived from the computations conducted in this investigation indicate that there exist modest variations in the lattice parameters. Figure 4 depicts the optimized structure derived for $FAPbI_3$. The values for the lattice parameters *a*, *b*, and *c* that were determined by the calculations were, respectively, 6.52, 6.34, and 6.37 Å. Due to the size of the FA^+ cation molecule, an elongation occurred in the lattice parameter *a*. Apart from this, the calculated values of *b* and *c* lattice parameters are highly close to the experimental value.

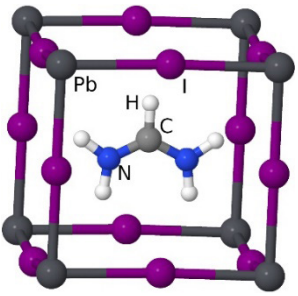

Figure 4: *Optimized $FAPbI_3$ compound.*

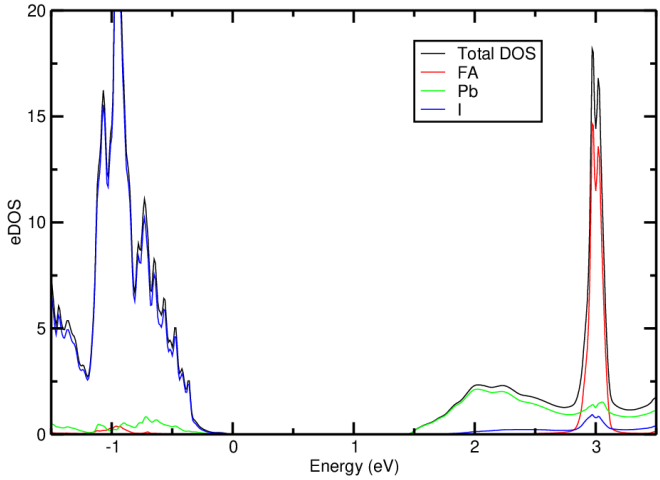

Figure 5: *The partial and total DOS patterns were acquired for the $FAPbI_3$ compound.*

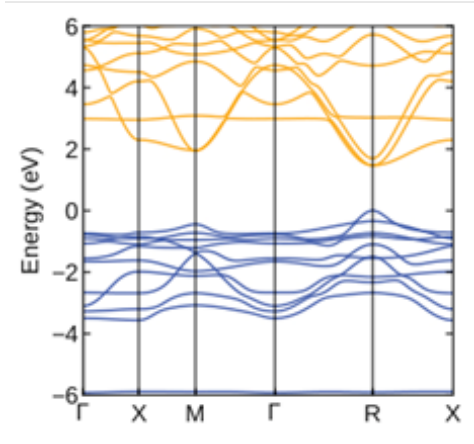

Figure 6: *Electronic band structure obtained for $FAPbI_3$.*

The Figure 5 shows the DOS pattern obtained from the calculations. In the valence band, I ion energy levels dominate. The VBM is comprised of hybrid energy levels involving the interaction between Pb and I ions. The energy levels of the FA^+ cation remain below VBM. Pb energy levels dominate at the the conduction band edge. A peak dominated by the FA^+ cation occurs approximately 1 eV above the CBM. Figure 6 illustrates the electronic band structure of $FAPbI_3$. The lowest band gap occurs around the R symmetry point. The calculated band gap is 1.47 eV. The optical analysis of $FAPbI_3$ thin films revealed that experimental band gap is in the range from 1.55 to 1.57 eV (Marí-Guaita et al., 2021). The calculated value is close to experimental values.

NH_4PbI_3 Compound

The initial structure of NH_4PbI_3 used in the calculations is cubic. The optimized structure is depicted in Figure 7. The value of the calculated lattice constant is approximately 6.29 Å. During the optimization process, the angles of the lattice vectors differed from their initial values of 90 degrees. The values of β, α and γ angles were calculated as approximately 84, 94 and 86 degrees, respectively. The NH_4^+ cation molecule was initially positioned near the middle of the inorganic lattice, attracted the I ions on the side found by the three closest hydrogens bound to the N ion during the optimization process, causing the I ions to move towards the molecule from the Pb-I-Pb direction. The likely explanation for this situation is the presence of a greater number of H-I hydrogen bonds on one side compared to the other. The aforementioned circumstance significantly influences the degradation of the cubic configuration.

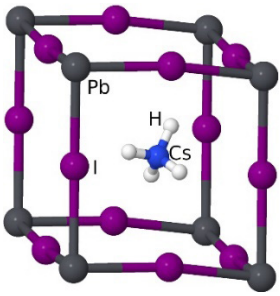

Figure 7: *Optimized NH_4PbI_3 compound.*

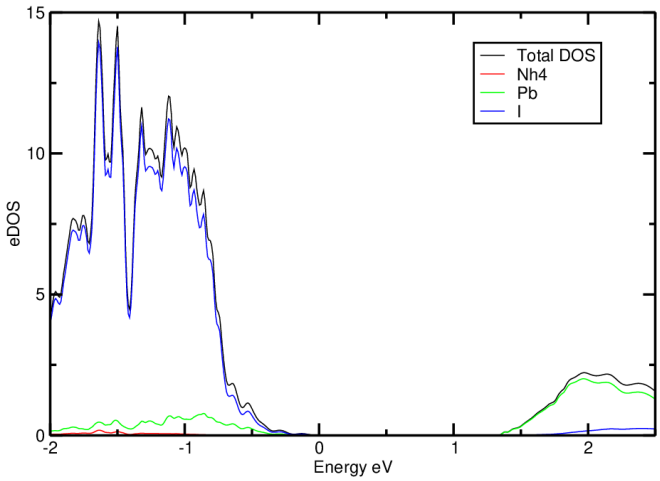

Figure 8: *The partial and total DOS patterns were acquired for the NH_4PbI_3 compound.*

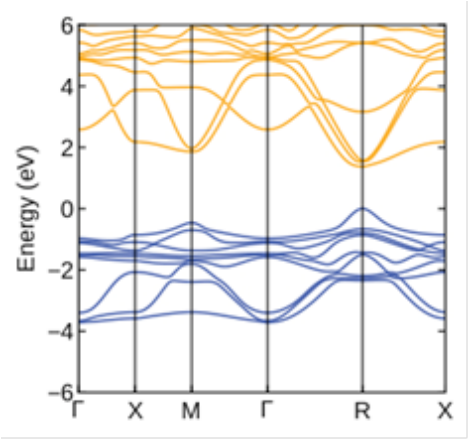

Figure 9: *Electronic band structure obtained for NH_4PbI_3*

The electronic properties of materials primarily stem from their electronic structures. An in-depth analysis for NH_4PbI_3 provides significant insights into its electronic behavior, as presented in the DOS model in Figure 8. The valence band is predominantly shaped by the electron energy levels of I ions. As commonly observed in other similar structures, the VBM prominently includes hybrid energy levels arising from the Pb-I bond where Pb energy levels dominate. This hybridization may play a crucial role in enhancing the charge transfer capabilities of the material. The role of the NH_4^+ molecule is noteworthy. Its energy levels are positioned below the VBM, suggesting that NH_4^+ may not directly participate in the material's primary charge transport processes but might be necessary for other structural or stability reasons. Shifting our focus to the CBM, we can see it is primarily composed of Pb-I energy levels. Energy states associated with Pb dominate this region. This dominance might have implications on the material's conductivity properties and its response to external stimuli, like light. The energy level of the NH_4^+ cation is found above the CBM, hinting at its potential active participation in some high-energy processes. The electronic band structure of NH_4PbI_3 is displayed in Figure 9. One of the key observations is the location of the Fermi energy level; it is located above the VBM. This positioning underscores the semiconducting character of the material, which is fundamental for potential applications in devices like solar cells or photodetectors. A significant attribute of any semiconductor material is its band gap, which determines most of its optoelectronic properties. The smallest band gap for NH_4PbI_3 has been identified near the R symmetry point. With a calculated value of 1.38 eV, this band gap can make NH_4PbI_3 suitable for specific applications, especially in cases where this energy range is critical for device performance.

$CsPbI_3$ Compound

Cesium lead iodide, commonly represented as $CsPbI_3$, belongs to the category of halide perovskites, a family of materials that has attracted considerable interest among researchers due to its promising applications in the field of photovoltaics. The compound $CsPbI_3$ exhibits distinct phase transitions in response to variations in temperature and humidity levels. The α-phase, characterized by a cubic structure, is highly favored for solar cell applications at standard room temperature. This preference stems from the possession of a direct bandgap and a notably high absorption coefficient. However, this phase is metastable at room temperature and can transition to the yellow δ-phase, which has an orthorhombic structure and is not suitable for photovoltaic applications. Efforts are ongoing in the research community to stabilize the black α-phase at ambient conditions. For this reason, the initial structures of $CsPbI_3$ used in this section are cubic.

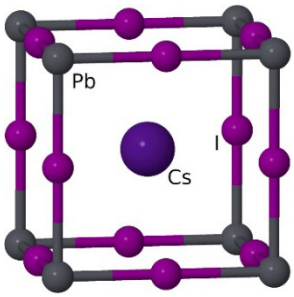

Figure 10: *Optimized $CsPbI_3$ compound.*

The optimized structure, as depicted in Figure 10, retains its cubic form with lattice parameters measuring approximately 6.30 Å. Experimental measurements have reported lattice parameter values close to this, around 6.29 Å (Trots and Myagkota, 2008). This close alignment between computational and experimental findings underscores the correctness of the modeling techniques used. Compared to organic-inorganic hybrid perovskites like $MAPbI_3$, $CsPbI_3$ offers better thermal and air stability. However, like other perovskites, $CsPbI_3$ is sensitive to moisture. For this reason, the use of shielding measures, such as encapsulation, is crucial in the manufacturing of devices to ensure their longevity and maximum performance.

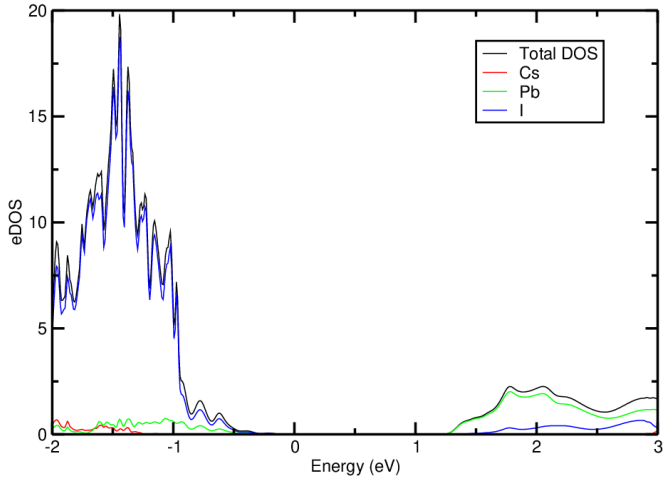

Figure 11: *The partial and total DOS patterns were acquired for the $CsPbI_3$ compound.*

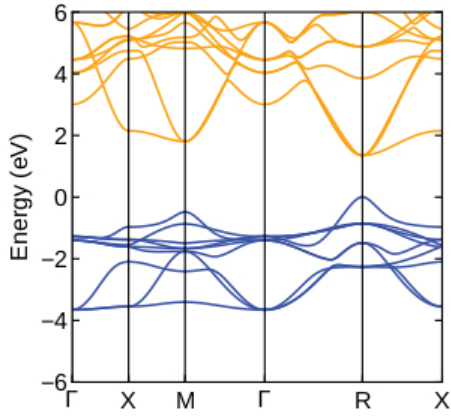

Figure 12*: Electronic band structure obtained for $CsPbI_3$.*

The DOS for $CsPbI_3$ is presented in Figure 11. The valence band predominantly features Pb-I hybrid energy levels, with I ions playing a significant role. On the other hand, the conduction band is mostly distinguished by energy levels that originate from Pb ions. The Cs ion energy levels are found below the VBM and above the CBM. The electronic band structure, shown in Figure 12, reveals a direct bandgap. While the calculations made in this study suggest a bandgap of 1.35 eV, experimental measurements typically report values closer to 1.73 eV for $CsPbI_3$ (Beal et al., 2016). The

determined band gap value exhibits a discrepancy with the observed experimental value. This larger bandgap in the experimental findings means that $CsPbI_3$ may absorb light up to approximately 700 nm, rendering it a very viable candidate for utilization in solar cell technologies. The disparity between computed and experimental bandgap values is a recognized obstacle in the area of computational materials science, which can be ascribed to several variables, including the inherent constraints of density functional theory (DFT) in accurately forecasting band gaps.

$RbPbI_3$ Compound

$RbPbI_3$, or rubidium lead iodide, is a member of the halide perovskite family. Like its counterpart $CsPbI_3$, $RbPbI_3$ has shown potential for photovoltaic applications due to its favorable electronic properties. The initial structure of $RbPbI_3$ considered in this study is cubic, similar to that of $CsPbI_3$. The optimized structure, depicted in Figure 13, retains its cubic form. The calculated lattice parameters for $RbPbI_3$ measure approximately 6.32 Å. Given the ionic radii of Cs^+ and Rb^+ ions, it's noteworthy that Rb^+ has a slightly smaller ionic radius than Cs^+. In contrast to initial expectations based on the smaller size of Rb^+ ions, it is seen that the lattice parameter of $RbPbI_3$ is slightly bigger than that of $CsPbI_3$, with a difference of around 0.02 Å. This suggests a slight elongation in the lattice structure of $RbPbI_3$ compared to $CsPbI_3$.

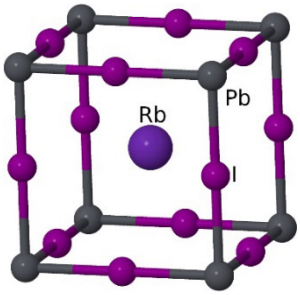

Figure 13: *Optimized $RbPbI_3$ compound.*

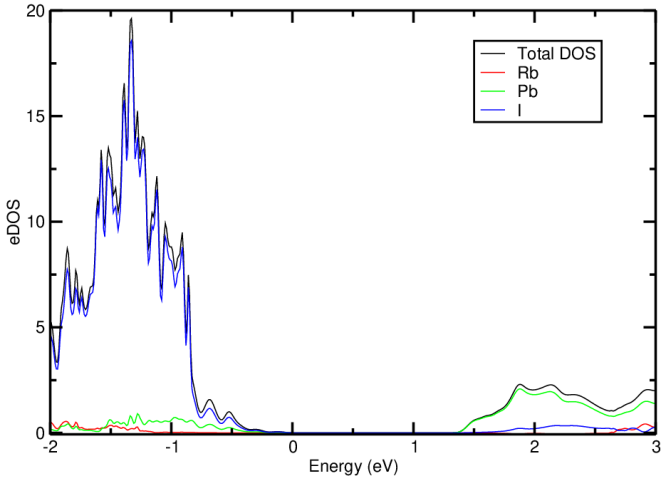

Figure 14: *The partial and total DOS patterns were acquired for the $RbPbI_3$ compound.*

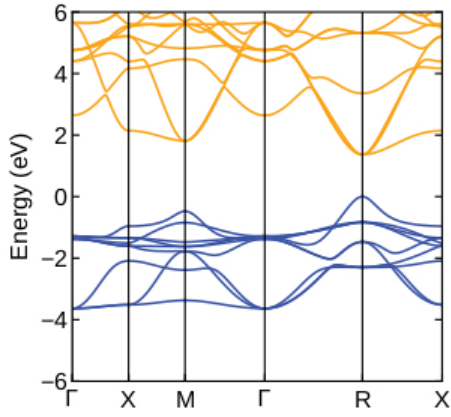

Figure 15: *Electronic band structure obtained for $RbPbI_3$.*

The Density of States (DOS) for $RbPbI_3$ is presented in Figure 14. The energy levels of the I ion predominantly occupy the valence band, similar to other perovskite structures. The VBM is characterized by Pb-I hybrid energy levels, with a pronounced contribution from I ions. Energy levels associated with the Rb^+ ion are positioned below the VBM. The conduction band, on the other hand, is primarily formed by Pb-I hybrid energy levels, with Pb ions playing a dominant role. The energy levels of the Rb^+ ion are found above the CBM. The electronic band structure of $RbPbI_3$ is illustrated in Figure 15. The band gap is direct and is identified around the R symmetry point, with a calculated value of 1.37 eV. This band gap is slightly larger than that of $CsPbI_3$, but the difference is minimal, suggesting

that both materials have similar optical properties and potential for photovoltaic applications.

Comparison of Compound

The Goldschmidt Tolerance Factor plays a crucial role in the study of crystalline materials, particularly in perovskite structures. It provides a geometric metric to predict the stability of perovskite configurations based on the ionic radii of its constituents. Given by the formula:

$$t = \frac{r_A + r_X}{\sqrt{2}(r_B + r_X)}$$

Where:

- r_A represents the ionic radius of the A-site cation.
- r_B is the ionic radius of the B-site cation.
- r_X is the ionic radius of the anion.

The key ionic radii and their respective values in *pm* are:

- $r_{MA^+} = 217\ pm$
- $r_{FA^+} = 253\ pm$
- $r_{Cs^+} = 167\ pm$
- $r_{Rb^+} = 152\ pm$
- $r_{NH_4^+} = 148\ pm$

The derived values indicate:

- A value around 1 is indicative of a likely stable cubic perovskite structure.
- Between 0.8 and 1.0, distorted perovskite structures may form.
- Values significantly outside this range suggest instability.

Table 1 shows calculated tolerance factors. Based on the tolerance factors, $MAPbI_3$ and $FAPbI_3$ seem inclined towards a stable perovskite structure. Notably, $FAPbI_3$ closely approaches the upper limit, emphasizing its potential for optimal perovskite formation-ideal for applications such as

solar cells. Conversely, the tolerance factor of $CsPbI_3$ is close to the lower bound. The values of $RbPbI_3$ and NH_4PbI_3 fall outside the optimal range, indicating potential instability. In particular, the tolerance factor of NH_4PbI_3 raises concerns regarding its compatibility with the perovskite structure.

Upon examination of Table 2, it becomes apparent that the tolerance factor exhibits a correlation with the structural characteristics derived from the computations. The tolerance factors of $FAPbI_3$, $MAPbI_3$ and $CsPbI_3$ structures are in the range of 0.8-1, showing that these structures can form the perovskite structure. As I mentioned before, a tolerance factor close to 1 indicates the formation of a cubic perovskite structure. However, since the FA^+ molecule does not have equal dimensions in all directions and is longer in one direction, the a lattice parameter is longer than the other lattice parameters. This situation disrupts the cubic structure slightly. A similar situation applies to the MA^+ molecule, although it is not as large as FA^+. $CsPbI_3$ is cubic with a Cs^+ ion at its center. However, interestingly, although the tolerance factor of $RbPbI_3$ is outside the range of 0.8-1, the structure is cubic. This may be due to the fact that it has an ion-centered structure like the $CsPbI_3$ structure.

Table 1: *Tolerance factors for various perovskite compounds*

Compound	Goldschmidt Tolerance Factor (*t*)
$FAPbI_3$	0.9866
$MAPbI_3$	0.9115
$CsPbI_3$	0.8072
$RbPbI_3$	0.7760
NH_4PbI_3	0.7676

Table 2: Lattice parameters (a,b,c), angles between lattice vectors (α, β, γ) and energy band gaps (E_g) of compounds containing different cations. The units of length, angle and band gap are Å, degree and eV respectively.

Compound	*a*	*b*	*c*	α	β	γ	E_g
$FAPbI_3$	6.52	6.34	6.37	90	90	90	1.47
$MAPbI_3$	6.38	6.34	6.37	90	90	90	1.59
$CsPbI_3$	6.30	6.30	6.30	90	90	90	1.35
$RbPbI_3$	6.32	6.32	6.32	90	90	90	1.47
NH_4PbI_3	6.29	6.29	6.29	94	84	86	1.38

The tolerance factor of the NH_4PbI_3 structure is below 0.8, like $RbPbI_3$. However, due to the fact that NH_4^+ is structurally different from the Rb^+ ion, its ionic diameter is small, and the effect of hydrogen bonds, the angles between the lattice vectors could not maintain 90 degrees during the optimization process of the structure. This result is compatible with

the tolerance factor value. This indicates that NH_4PbI_3 is unlikely to form a perovskite structure.

As mentioned at the beginning of the chapter, the starting structures used in this study are cubic. In these optimized structures, the roles of Pb and I ions in the valence band and conduction band are similar. Although the A^+ cations change in the structures, the energy levels of the A^+ cations occur below the VBM and above the CBM. Accordingly, it can be said that the effects of A^+ cations on the electronic structure are indirect. As can be seen when Table 2 is examined, the calculated band gap values are not proportional to the radius of the A^+ cation. It is mostly related to how the A^+ cations shapes the Pb-I cage.

CONCLUSIONS

The study explored various halide perovskite structures, focusing on $MAPbI_3$, $FAPbI_3$, $CsPbI_3$, $RbPbI_3$, and NH_4PbI_3. The optimized structures, electronic properties, and structural stability of these materials were critically examined. The role of the A-site cation in the structure, especially its size and geometry, was evident in determining the final optimized lattice parameters. Larger cations like MA^+ and FA^+ led to slight distortions from the ideal cubic structure. In contrast, Cs^+ and Rb^+ formed nearly perfect cubic structures, with the surprising observation that $RbPbI_3$ retained a cubic structure despite having a tolerance factor outside the typically accepted range. The NH_4PbI_3 structure, with its unique molecular geometry and hydrogen bonding capabilities, diverged significantly from the cubic form.

In the electronic properties domain, it was observed that while the A-site cation introduced different energy levels, the principal electronic characteristics (like the primary contributors to the valence and conduction bands) remained largely consistent across the different materials. The A^+ cations' energy levels were consistently found below the VBM and above the CBM, suggesting an indirect influence on the electronic structure.

The Goldschmidt Tolerance Factor provided a valuable metric to gauge the structural stability of the perovskites. As anticipated, values close to 1 favored a stable cubic structure, while values significantly deviating from this range indicated potential instability. This was especially evident in NH_4PbI_3, which demonstrated a clear departure from the cubic form, in line with its tolerance factor.

In conclusion, the inherent properties of the A-site cation in halide perovskites play a pivotal role in dictating both the electronic and structural properties of the material. While the study illuminated several interesting relationships and behaviors across the different perovskite materials, it also underscored the complexity and multifaceted nature of these com-

pounds. The insights gained can be invaluable in designing and optimizing perovskite materials for specific applications, especially in the burgeoning field of solar cell technology.

REFERENCES

Beal, R. E., Slotcavage, D. J., Leijtens, T., Bowring, A. R., Belisle, R. A., Nguyen, W. H., Burkhard, G. F., Hoke, E. T., and McGehee, M. D. (2016). Cesium lead halide perovskites with improved stability for tandem solar cells. The Journal of Physical Chemistry Letters, 7(5):746–751.

Bonomi, S., Armenise, V., Accorsi, G., Colella, S., Rizzo, A., Fracassi, F., Malavasi, L., and Listorti, A. (2020). The effect of extended ball-milling upon three-dimensional and two-dimensional perovskite crystals properties. Applied Sciences, 10(14).

Çelik, V. (2023). Theoretical investigation of the role of the organic cation in methylammonium lead iodide perovskite. The European Physical Journal B, 96(7):101.

Clark, S. J., Segall, M. D., Pickard, C. J., Hasnip, P. J., Probert, M. J., Refson, K., and Payne, M. (2005). First principles methods using CASTEP. Z. Kristall., 220:567–570.

Han, Q., Bae, S.-H., Sun, P., Hsieh, Y.-T., Yang, Y. M., Rim, Y. S., Zhao, H., Chen, Q., Shi, W., Li, G., and Yang, Y. (2016). Single crystal formamidinium lead iodide ($FaPbI_3$): Insight into the structural, optical, and electrical properties. Advanced Materials, 28(11):2253–2258.

Hohenberg, P. and Kohn, W. (1964). Inhomogeneous electron gas. Phys. Rev., 136:B864–B871.

Hu, Y., Qiu, T., Bai, F., Ruan, W., and Zhang, S. (2018). Highly efficient and stable solar cells with 2d ma3bi2i9/3d mapbi3 heterostructured perovskites. Advanced Energy Materials, 8(19):1703620.

Jamal, M., Shahahmadi, S., Abdul Wadi, M. A., Chelvanathan, P., Asim, N., Misran, H., Hossain, M., Amin, N., Sopian, K., and Akhtaruzzaman, M. (2019). Effect of defect density and energy level mismatch on the performance of perovskite solar cells by numerical simulation. Optik, 182:1204–1210.

Jena, A. K., Kulkarni, A., and Miyasaka, T. (2019). Halide perovskite photovoltaics: Background, status, and future prospects. Chemical Reviews, 119(5):3036–3103.

Kohn, W. and Sham, L. J. (1965). Self-consistent equations including exchange and correlation effects. Phys. Rev., 140:A1133–A1138.

Kojima, A., Teshima, K., Shirai, Y., and Miyasaka, T. (2009). Organometal halide perovskites as visible-light sensitizers for photovoltaic cells. Journal of the American Chemical Society, 131(17):6050–6051.

Marí-Guaita, J., Bouich, A., and Marí, B. (2021). Shedding light on phase stability and surface engineering of formamidinium lead iodide (fapbi3) thin films for solar cells. Engineering Proceedings, 12(1).

McNellis, E., Meyer, J., and Reuter, K. (2009). Azobenzene at coinage metal surfaces: Role of dispersive van der Waals interactions. Phys. Rev. B,

80:205414.

Monkhorst, H. J. and Pack, J. D. (1976). Special points for Brillouin-zone integrations. Phys. Rev. B, 13:5188–5192.

Moyez, S. A. and Roy, S. (2018). Dual-step thermal engineering technique: A new approach for fabrication of efficient ch3nh3pbi3-based perovskite solar cell in open air condition. Solar Energy Materials and Solar Cells, 185:145–152.

NREL (2023). Photovoltaic cell efficiency. Accessed: 18.09.2023.

Olthof, S. and Meerholz, K. (2017). Substrate-dependent electronic structure and film formation of mapbi3 perovskites. Scientific Reports, 7(1):40267.

Ong, K. P., Goh, T. W., Xu, Q., & Huan, A. (2015). Mechanical Origin of the Structural Phase Transition in Methylammonium Lead Iodide $CH_3NH_3PbI_3$. *The Journal of Physical Chemistry Letters*, *6*(4), 681–685.

Pfrommer, B. G., Cote, M., Louie, S. G., and Cohen, M. L. (1997). Relaxation of crystals with the quasi-Newton method. J. Comput. Phys., 131:233–240.

Sharif, R., Khalid, A., Ahmad, S. W., Rehman, A., Qutab, H. G., Akhtar, H. H., Mahmood, K., Afzal, S., and Saleem, F. (2023). A comprehensive review of the current progresses and material advances in perovskite solar cells. Nanoscale Adv., 5:3803–3833.

Soriano, S., Solis, O. E., Ramírez, D., Boix, P. P., Martínez-Pastor, J. P., and Suárez, I. (2023). Photodetection performances of mapbi3 perovskites. In 2023 23rd International Conference on Transparent Optical Networks (ICTON), pages 1–4.

Tkatchenko, A. and Scheffler, M. (2009). Accurate molecular van der waals interactions from ground-state electron density and free-atom reference data. Phys. Rev. Lett., 102:073005.

Trots, D. and Myagkota, S. (2008). High-temperature structural evolution of caesium and rubidium triiodoplumbates. Journal of Physics and Chemistry of Solids, 69(10):2520–2526.

Weller, M. T., Weber, O. J., Frost, J. M., and Walsh, A. (2015). Cubic perovskite structure of black formamidinium lead iodide, α-[hc(nh2)2]pbi3, at 298 k. The Journal of Physical Chemistry Letters, 6(16):3209–3212.

Yamada, Y., Nakamura, T., Endo, M., Wakamiya, A., and Kanemitsu, Y. (2014). Near-band-edge optical responses of solution-processed organic–inorganic hybrid perovskite ch3nh3pbi3 on mesoporous tio2 electrodes. Applied Physics Express, 7(3):032302.

CHAPTER 6

STRUCTURE AND MORPHOLOGY OF FRUITING BODIES IN MYXOMYCETES (MYXOGASTREA) I: STALK

Hayri BABA[1], Hasan AKGÜL[2],
Emre Cem ERASLAN[3], Celal BAL[4]

1 Department of Biology, Faculty of Science and Art, Hatay Mustafa Kemal University, Hatay 31060, Turkey. e-mail: hayribaba_68@hotmail.com
2 Department of Biology, Faculty of Science, Akdeniz University, Antalya 07058, Turkey.
3 Department of Biology, Faculty of Science, Akdeniz University, Antalya 07058, Turkey.
4 Oguzeli Vocational School, Gaziantep University, Gaziantep 27500, Turkey.

Introduction

Myxomycetes are known as true slime molds, plasmodial slime molds or Myxogastrea. Myxomycetes are multinuclear single-celled organisms that can produce one or more spores (Stephenson & Stempen, 1994). Myxogastrea fruitbodies could develop spontaneously in the nature. Furthermore, especially after identification with the moist chamber technique, they could be detected especially on plant surfaces (Härkönen & Ukkola, 2000). Myxomycetes can be found on different substrata such as living and dead plants and animals on the forest floor and in the canopy on bark of living trees and vines. Myxogastrea species are abundant in cool, moist and shaded areas such as rotten tree trunks, branches, alive or dead bark, decayed fruit or fruit scraps, decayed leaves and leaf debris. Myxomycetes are thus often considered "microbial predators" (Keller et al., 2008). Myxomycetes live in the environment by feeding on other microorganisms (bacteria, yeasts, fungus hyphae, blue-green bacteria and green algae) (Farr, 1981; Zümre et al., 2019).

The number of known Myxomycetes species is 1098 taxa globally (Lado, 2023). 309 taxa were identified in Turkey (Ergül et al., 2005a; Ergül et al., 2005b; Ergül et al., 2011; Ocak and Konuk, 2018; Baba et al., 2018; Baba and Sevindik, 2018; Baba and Sevindik, 2019; Baba and Atay, 2019; Baba et al., 2019; Baba and Sevindik, 2020a; Baba et al., 2020a; Baba et al., 2020b; Baba, 2021; Baba and Sevindik, 2021; Baba et al., 2021a; Baba et al., 2021b; Baba et al., 2021c; Baba and Sevindik, 2022a, Baba and Sevindik, 2022b, Baysal and Eroğlu, 2022; Eroğlu, 2021; Baba and Sevindik, 2023).

Myxomycetes are fungi-like organisms that are very common in terrestrial ecosystems. The fascinating protists; myxomycetes life cycle is illustrated in detail, including trophic stages (myxamoebae, swarm cells and plasmodia), and dormant stages (spores, microcysts, sclerotia, and fruiting bodies) (Keller et al., 2008). The fruiting body contains the spores and serves as the reproductive unit of the myxomycete life cycle. Spores are a dormant stage, usually visible as a powdery mass, disseminated by wind, and less often by insects, raindrops, or through hygroscopic and drying action of capillitial threads. Individual spores range in size from 5 to 20 μm in diameter. Spores germinate and produce one of two types of sexual gametes, myxamoebae or swarm cells. The myxamoeba is amorphous, divides by mitosis and gives rise to a population of cells capable of changing shape as they move across the substratum feeding on bacteria and other microorganisms. Swarm cells do not divide by mitosis and have two unequal, whiplash flagella attached at the anterior end that result in a distinctive corkscrew, rotating, or gyrating swimming movement (Keller et al., 2008). Unfavorable environmental conditions, such as desiccation or lack of nu-

trients, often result in the conversion of myxamoebae, and possibly swarm cells, into a dormant stage called a microcyst. Fusion of haploid gametes results in a diploid zygote, creating a large, multinucleate slime stage called a plasmodium. This amorphous, protoplasmic mass is surrounded by a cell membrane and gives the myxomycetes their common name, the "true or plasmodial slime molds". When favorable conditions plasmodium crawls out, continues feeding, matures, and then produces fruiting bodies. The plasmodial stage gradually forms mature fruiting bodies over a 24- to 48-hour period or sometimes longer in the case of larger sporophores.

Plasmodium formation and subsequent haploid chromosome number spores include one or more fructification. Plasmodium is formed by germination of spores. In the sporulation phase, these organisms form a distinctly formed spore mass within the membranous spore sac secreted by the protoplasm. The spore sacs also contain a system of non-cellular, mostly free or reticulated yarns capillitium or pseudocapillitium. Some groups have systematically important characteristic lime deposits inside, outside, or both places in the spore sac. Some species are very common, while others live in certain habitats. Myxomycetes are sensitive to light, moisture and temperature as well as the property of the substrate on which they develop. Mycetozoa members are abundant in cool, damp and shady environments such as decaying stumps, branches, live or dead tree bark, rotten fruit or fruit residues, dead leaves and leaf debris. In addition, some organic materials were collected as exceptional from herbivorous animal feces and rocks. By collecting materials that may contain spores and plasmodium from the natural environment, sporophore development is provided by the Moist chamber technique in the laboratory. The fruiting bodies of myxomycetes can occur anywhere under optimum conditions (proper humidity, heat and sufficient rotting organic matter). Many myxomycetes species have small fruit stems and it is only a few millimeters in diameter. Myxomycetes have four fruiting body forms or types, sporangium, plasmodiocarp, aethalium and pseudoaethalium. The most common fruiting body forms are a stalked sporangium (Sevindik and Akgül, 2019).

The mature fruiting body is the life cycle stage used to identify a myxomycete to species. It is primarily the combination of morphological characters inside the fruiting body such as the columella, capillitium, and spores (ornamentation, size, and color in mass), which are important in myxomycete classification and used in keys to different taxa (Martin and Alexopoulos, 1969). Fruiting bodies are based on the presence or absence of a peridium, calyculus, capillitium, pseudocapillitium, columella, pseudocolumella, stalk and hypothallus (Figure 1). Fruiting bodies are usually composed of 6 parts: hypothallus, stalk, columella, peridium, capillitium and spores. In some fruiting bodies a pseudocolumella or a pseudo-

capillitium may be present. Not all of these components are present in all fruiting body types.

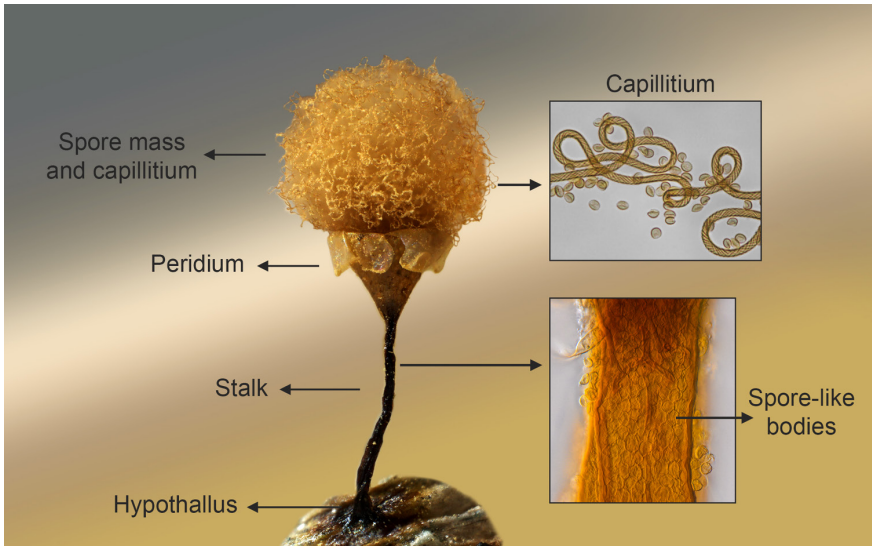

Figure 1. Fruiting bodies of a Myxomycetes (from García-Cunchillos et al., 2022)

A stalk may or may not be present as part of all sporangium. The primary function of the stalk is to support and elevate the spores above the substratum, protecting the sporangium from excessive moisture, and also aiding in the dissemination of the dry, powdery spore mass. The stalk may be useful in identifying myxomycetes such as in the Physarales where the stalk contains CaCO3 and in the Stemonitales where the stalk is either hollow or filled with fibrous strands. The hypothallus is found at the base of the stalk and may be transparent or opaque (Gray and Alexopoulos, 1968; Martin and Alexopoulos, 1969; Stephenson and Stempen 1994; Keller and Braun, 1999; Keller et al., 2008).

Material and methods

Myxomycetes are obtains by collected from the natural environment or obtained in the laboratory using by moist chamber technique. Natural myxomycete samples were collected from natural area, similar to macrofungi. For moist chamber technique different substrates; woods, barks, leaf, debris, organic plants and animal material samples were transported to the laboratory in small carton boxes. Furthermore, after the field studies, myxomycete fructifications were obtained from the moist chamber culture in laboratory. For moist chamber culture; live or dead plant materials (forest floor litter, aerial litter, wood and bark from living or dead trees) were obtained at a

number of localities. Moist chambers cultures consisted of disposable plastic petri dishes lined with filter paper. The sample material in each dish was moistened with distilled water. After a period of approximately 24 -48 hours (in summer 48 hours, in winter 24 hours), excess water in each dish was removed. Cultures were kept at room temperature (24ºC) in diffuse daylight. Examined with a stereomicroscope on a regular basis for a period of up to two months in order to detect plasmodia or fruiting bodies. When necessary, a small amount of water was added to each culture to maintain moist conditions. The moist chamber with the developing myxomycete samples was allowed to dry and the myxomycetes were dried for one week (Baba et al., 2021b). Myxomycete plasmodia or fruiting bodies were noted and recorded. Each time the cultures were checked. All fruiting bodies were removed. Air-dried and glued in small pasteboard boxes for permanent storage. The samples were photographed and identified.

The samples were identified under stereomicroscope and light microscopy. General structure, plasmodium type, fructification type, shape, colour, macroscopic measurements, the presence or absence of stalk, lime or the color and shape of the samples were examined with the stereomicroscope. In light microscopy, the capillitium, spore, shape, color, size, ornamentation, branching shape, features was observed. Samples were arranged as fungarium material and kept in the Biology Department's laboratory of Hatay Mustafa Kemal University Hatay-Turkey.

Results and discussion

The Myxomycetes are typically divided into six orders Ceratiomyxales, Echinosteliales, Liceales, Trichiales, Physarales and Stemonitales (Schnittler & Spiegel 2012). Stalk structure shows different characteristics in different taxonomic groups. As there are sessile groups and stalked groups, in some groups both sessile and stalked species, sometimes with short and long stalk structures, can be found in the same group.

The Ceratiomyxales (consist of 1 Family Ceratiomyxaceae) produce their spores on the exterior of the sporophore (exosporous) and differs considerably from the other types which are endosporous. In this type *Ceratiomyxa* J. Schröt. the sporophore consists of a matrix of highly vacuolated amorphous material that forms simple pillar-like to coralloid structures upon which the individually stalked spores are borne (Figure 2). In some *Ceratiomyxa* large colonies of stalked, 2.5–4 mm high fructifications cover often several square metres of large, decaying logs. In *Ceratiomyxa fruticulosa* (O.F. Müll.) T. Macbr. the plasmodium moves to the surface of its substrate to forms a matrix, consisting of highly vacuolated amorphous material that dries to form the basic structure of the sporophore, which is considered, by some, to be homologous to the hypothallus of other species (Clark and Haskins, 2014).

Figure 2. Exosporous sporophores of Ceratiomyxa fruticulosa

Stipes are apparently ancestral traits in the myxomycetes they would be especially useful in spore dispersal in these minute sporocarps (Clark and Haskins, 2014). The stipe in the Echinosteliales (consist of 2 Family Clastodermataceae and Echinosteliaceae*)* is a smooth hollow tube stuffed with granular debris in the lower region, and it is composed of fibrillar elements that start in the small hypothallic region and extend into the sporotheca as a generally solid columella (Clark and Haskins, 2014). Stalk in *Echinostelium* de Bary (*Echinostelium minutum* de Bary), 120-150 µm long, in transmitted light white, yellow to pale ochraceous in the lower section, colourless and translucent under the microscope, filled with a few dirt granules in the lower third, about two thirds of length filled with darker granules, diameter 10-15 µm on base, tapering to 2.5-3.5 µm on top (Figure 3).

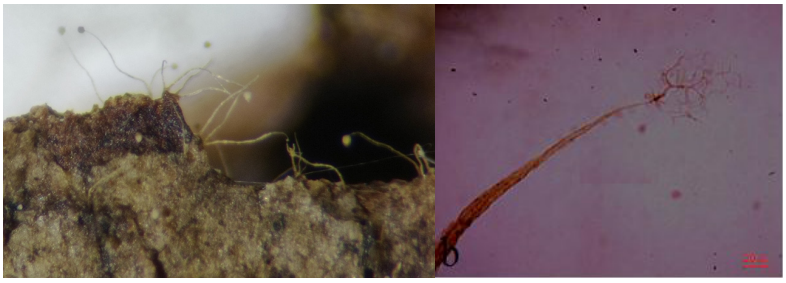

Figure 3. Stalk and capillitium of Echinostelium minutum

Clastoderma debaryanum A. Blytt stalk is erect or sometimes bent, oval swelling about ⅔ up, black and granular below the swelling, thin above swelling (Figure 4). Stalk brownish, filled with granular material bellow, translucent and tapering abruptly upwards after a droplet-like swelling. In *Barbeyella* Meyl. stalk 66% of total height, reddish brown and transparent at the base, black and opaque at the apex, tubular, stuffed near the base with refuse matter, tapered upwards.

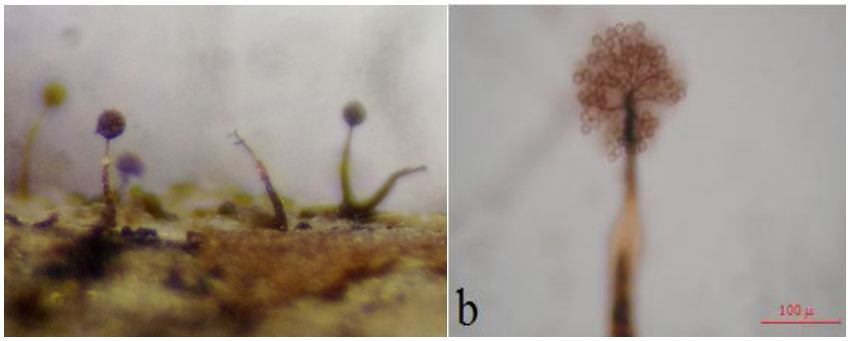

Figure 4. Stalk of Clastoderma debaryanum

In the Liceales (consist of 4 Family Cribrariaceae, Dictydiaethaliaceae, Liceaceae, Reticulariaceae), the three families apparently vary considerable in terms of the presence and morphology of the stalk. All species of Cribrariaceae are stipitate (Figure 5), although *Lindbladia tubulina* Fr. is generally a sessile, aethalium with occasional vestigial stipes (Figure 6a). The *Cribraria* Pers. species have different stipes, although some specimens may appear sessile. The stipe which has a small hypothallus and generally lacks a columella, is usually slender, dark, somewhat furrowed and continuous with the peridium and its surface net (Fiore-Donno et al. 2005), having more coppery brown sporothecae with a deeper, more urn-shaped calyculus comprising half of the height of the sporothecae and relatively longer stalks. Stalk dark brown or nearly black, slender, furrowed, 0.6-1.8 mm. long, shiny purple-brown, under transmitted light translucent-opaque red-brown, fibrous.

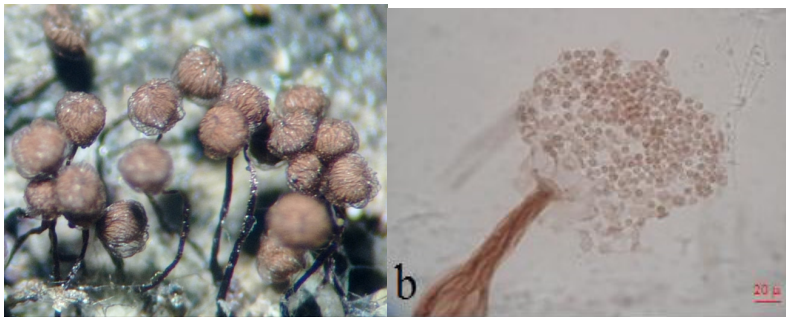

Figure 5. Stalk of Cribraria.

Dictydiaethaliaceae family has 1 genus *Dictydiaethalium* Rostaf. *Dictydiaethalium plumbeum* (Schumach.) Rostaf. fruiting bodies pseudoaethalium and sporocarps sessile concrescent to coalescent, closely compacted in a palisade layer, cylindrical (Figure 6b).

Figure 6a. Stalk of Lindbladia tubulina

Figure 6b. Stalk of Dictydiaethalium plumbeum

Liceaceae generally have small sessile sporangia with occasional constricted bases or distinct stipes. The stipe, when present, appears to be continuous with the peridium and contains amorphous materials, and thus may have a developmental system similar to that found in the Trichiales (Wrigley de Basanta & Lado 2005; Clark and Haskins, 2014). Reaching just over two-thirds of the diameter of the entire sporotheca, the hypothallus forms a stalk-like structure. *Licea* Schrad. sporotheca (40) 60–80 µm in diameter, almost spheroid. It is on a thick extension of the hypothallus, sometimes sessile, 40–45 µm at the base and 35–40 µm wide above, on a stalk-like structure (Figure 7). Stalk dull, dark, nearly black, grooved, containing refuse matter, up to 33% of the total height, 20-30 µm diam., with a membranous, ochraceous wall, closed above, filled with particles.

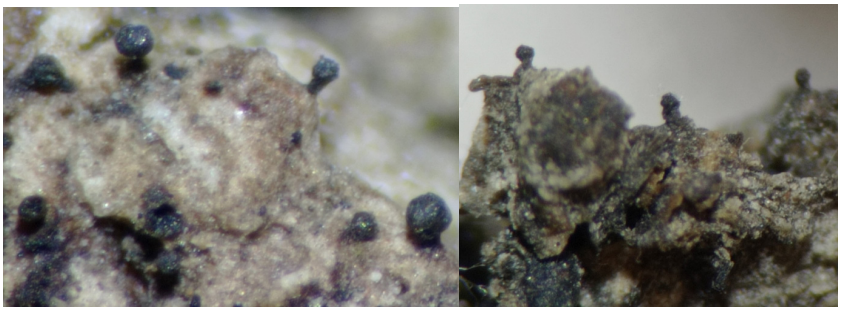

Figure 7. Stalk of Licea

Reticulariaceae family has a stipe in genera *Alwisia* Berk. & Broome and *Tubifera* J.F. Gmel. *Tubifera ferruginosa* (Batsch) J.F. Gmel. stipe is united into small groups or pseudoaethalial clusters. These stalks are also continuous with the peridium and may also be similar to the Trichiales.

Tubifera ferruginosa pseudoaethalium, sessile or borne upon a spongy, sulcate, often stalk-like hypothallus, 2-6 mm tall (Figure 8). *Alwisia* Berk. & Broome stalks cylindrical, rugose, furrowed, 2.5 mm high, 0.15 mm wide, adhering in clusters of 4-12, brownish-purple, orange-red and translucent. Stalks erect, ochraceous brown, dark rust-brown in the upper portion, thin, sinuous, irregularly gyrose, free, interlaced or partially fused with one another, forming an irregular tuft with free sporothecae at the top. Individual stalks may fuse and then separate again several times throughout its length.

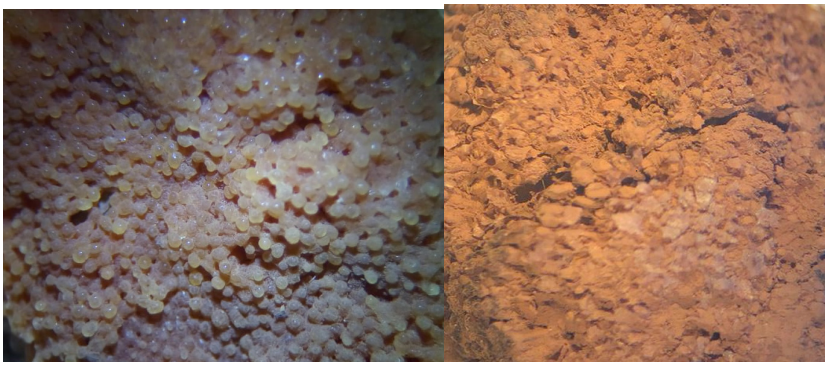

Figure 8. Stalks of Tubifera ferruginosa; united into small groups

Order Trichiales; (composed of 4 families Arcyriaceae, Dianemataceae, Minakatellaceae and Trichiaceae) when the stipe is present it never has a columella and the stalk tube often expands into a cup-shaped peridial calyculus. This order apparently has a general system of lower hypothalic development, in which the outer stalk wall continues with the peridium.

Family Arcyriaceae stalk is filled with spore-like cells, has much smaller sporocarps on longer stalks that reach 1-1.5 times the length of the almost spherical sporotheca. *Arcyria* F.H. Wigg. stalks very different in length and slender: 0.4-1.5 mm long, (18-) 23-55 (100) µm wide at the base and on top 50-70 µm wide, roughly the same diameter on top (Figure 9). Stalk often twisted, arising from a very small, disk-like hypothallus, the whole lumen densely filled with spore-like cells, these often deformed by mutual pressure, globose to ellipsoid and (9-)15-20 (23) µm diam. Stalks gradually merging into the calyculus, the latter concolorous with the sporotheca colour, slender, black. The genus *Arcyria*, which can be defined by mostly stalked sporocarps with “cellulate” stalks and a netforming capillitium without spiral bands. *Arcyriatella* Hochg. & Gottsb. stalk 3-6 mm long, 1-1.5 mm in diameter, robust, orange gray, formed by several strands, which emerge from the hypothallus and continued as veins on the base of the aethalium. *Perichaena* Fr. stalk when present, erect, cylindrical, stout,

blackened, dark brown to black, more rarely white, with calcium deposits, roughened, stuffed with granular matter, 0.1-0.7 mm long.

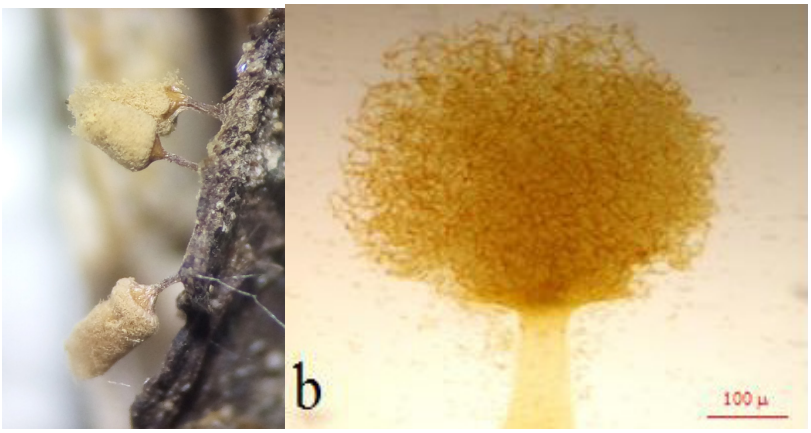

Figüre 9. Stalk of Arcyria

Family Trichiaceae sometimes sessile. Stalk more or less elongated, usually resting on a hypothallus, showing the typical opaque stalk. *Hemitrichia* Rostaf. stalk when present, ochraceous, up to 0.3 mm tall, filled with spore-like cells (Figure 10a). *Metatrichia* Ing stalk cylindrical hollow, compressed laterally, longitudinally grooved, 1.6–2.1 mm long, 0.08–0.2 mm wide, dark brown toward the apex dark red to black, red (Figure 10b).

Figure 10a. Stalk of Hemitrichia Figure 10b. Stalk of Metatrichia

Oligonema Rostaf. stalk weak, flattened, longitudinally grooved, 0.8–1.2 mm long, 0.1–0.15 mm wide, yellow. *Prototrichia* Rostaf. sporocarps sessile on a constricted base or less commonly short-stalked, rarely subplasmodiocarpous. *Trichioides* Novozh., Hooff & Jagers stalk 2/3 of

the total height of the sporocarp, straight, brownish black, nearly black by reflected light, slightly flared at the base merging at the top into the disc-shaped sporangial base, filled with amorphous material. *Trichia* Haller stalk when present sometimes cylindric, dull yellow or dark reddish or purplish-brown, dark brown or black, opaque, filled with amorphous material, sometimes long, slightly curved or straight, gradually merging into the sporotheca, plicate (Figure 11). Thin, erect, furrowed, usually short, occasionally up to 50 % of the total height gradually merging into the sporotheca, plicate, 0.4–0.7 mm long, 0.1–0.2 mm wide, brown, filled with spore-like bodies of 15–17 μm in diameter.

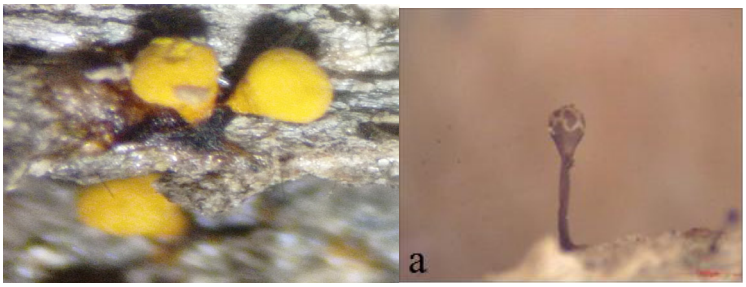

Figure 11. Stalk of Trichia

Order Physarales consist of 3 families, Didymiaceae, Elaeomyxaceae and Physaraceae. The species in the order Physarales have a typical subhypothallic developmental stipe (Guttes & Rusch 1961), and the stipe is not generally used as higher level taxonomic character other than its presence or absence. However, there appears to be useful stalk variations that can be used at the species level (Clark and Haskins, 2014).

In Didymiaceae family has sessile or different stalk structure. *Diderma* Pers. stalk when present cylindrical, sometimes common to several sporocarps and then laminar and giving the appearance of being an extension of the hypothallus, erect or slightly curved, short, 0.1-0.7 mm long x 0.09-0.4 mm wide, longitudinally striate, calcareous, whitish to brownish pink. *Lepidoderma* de Bary ex Rostaf. stipe when present, stout, dark, pale to medium brown at the base, blackish above, subcylindrical, rugulose, 0.6 mm long, 0.3-0.6 mm diam. Matsumoto (1999) has shown, in *Didymium* Schrad., that such stipe characteristics as fiber tube shape (heavily pleated or not), fiber tube thickness (thick to absent); core size and materials (present, absent, lime present or absent); and exterior lime (present or absent), can be used to help define and group the species. *Didymium* stalk distinguishing features are the rather long, ochraceous but internally limy stalks combined with an aerolate peridium (Figure 12a). Sometimes sessile stalk

when present short, buff coloured, longitudinal groove with lime crystals, and widely attached to the substrate (Clark and Haskins, 2014). Genera having lime on the stipe: *Diachea* Fr. sometimes sessile when present, usually short and stout, but sometimes over half the total height, furrowed, calcareous, with calcareous crystals throughout, wrinkled, erect, slender, attenuate upwards, reddish orange to pinkish red, white, black in the lower half, orange-red above (Figure 12b). *Physarina* Höhn. stalk conical or somewhat swollen above the middle, dull, rough, flesh-coloured or whitish, filled with lime granules, continuing into the sporotheca as a stalked, subglobose or hemispherical columella.

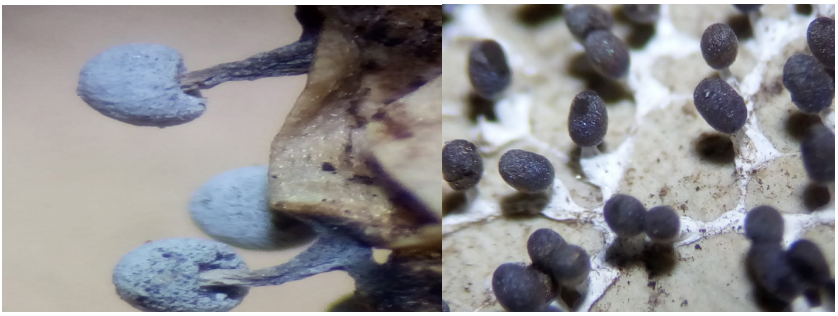

Figure 12a. Stalk of Didymium *Figure 12b. Stalk of Diachea*

In Physaraceae family has sessile or different form stalks. *Craterium* Trentep. stalk short, erect, longitudinally plicate, rising from a small hypothallus, 0.08-0.4 mm tall, up to 0.2 mm wide, black, furrowed, yellow to orange, brownish toward the base (Figure 13).

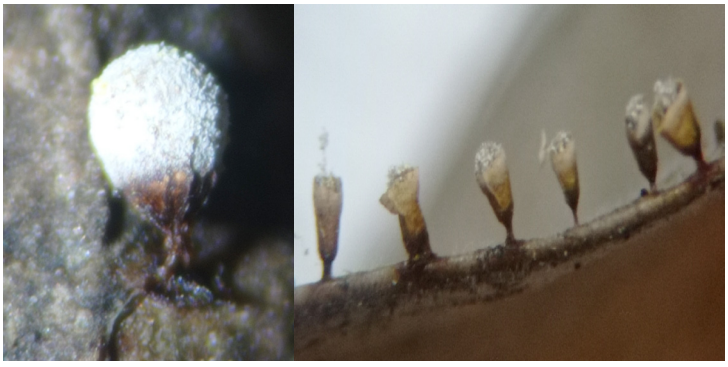

Figure 13. Stalk of Craterium

In *Leocarpus* Link genera *Leocarpus fragilis* (Dicks.) Rostaf. stalk flat, weak, pale ochraceous to pale orange, variable in length, but usually much shorter than the sporangium. In *Physarella* Peck genera *Physarella oblonga* (Berk. & M.A. Curtis) Morgan stalk, when present, terete or flattened, hollow, usually long, red, translucent, arising from an inconspicuous hypothallus. *Protophysarum* M.Blackw. & Alexop. stalk slender, subulate, stuffed with granular matter, brown, darker at the apex. *Physarum* Pers. has sessile or stalked species, colonies of small mass sporocarps on slender stems with a spherical sporotheca. Stems emerging from a very small, discoid hypothallus, slender and slender, but straight, 0.4–0.6 mm long and uniformly thick (45–55 μm) over the entire length, white, grey, brown, straw-colored, paler with passing light but uniformly coloured, fibrous, chalky or non-calcareous, with little dirt granules (Figure 14a). *Badhamia* Berk. has sessile or stalked sporophores (Figure 14b). If stalk present, can be short and black, sometimes reduced to merely a blackish base to the sporangium, expanding at the base into a small hypothallus. Sometimes thick, dark brown, lime-free, filled with granular refuse matter and almost opaque or packed with yellow lime, covered by a bright yellow membrane dotted with lime and which merges into the peridium, flaccid, very short to 2.5 mm long, mostly very pale ochraceous to white, but ochraceous at the base and colourless at the apex.

Figure 14a. Stalk of Physarum

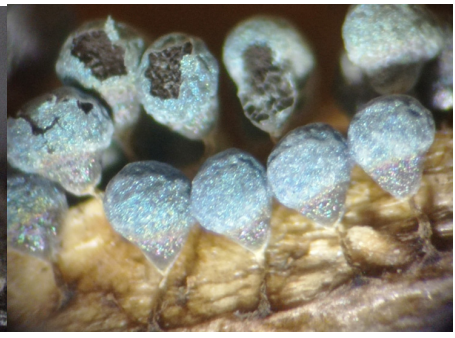

Figure 14b. Stalk of Badhamia

Order Stemonitidales consist of 1 family Stemonitidaceae characterized by their epihypothallic stipe development, all have rather similar stipes. A dark hollow or solid tube with a hypothallus and a columella consisting of extensions of the stalk fibers (Nannenga-Bremekamp et al. 1984). In a major taxonomic rearrangement of this order, Genera having hollow stipes (Clark and Haskins, 2014): *Stemonitis* Gled. stalk 1.5-6 mm long, cylindrical, dark reddish, shining black (Figure 15a), opaque (having a surface capillitial net). *Stemonaria* Nann.-Bremek., R. Sharma & Y.

Yamam. stalk long, nearly black, opaque, vaguely longitudinally striate, 20-60% of the total height (lacking a surface net). *Symphytocarpus* Ing & Nann.-Bremek. mostly sessile or short-stalked and stalk up to 0.2 mm tall, black (pseudoaethalial with no net). *Macbrideola* H.C. Gilbert stalk 0.1-0.3 mm in length, slender, hollow, tubular, widening into the hypothallus, brownish black, with a paler area, orange-yellow to yellowish brown at the base (Figure 15b). 75%-80% of the total height, attenuate upwards, black, red-brown below and opaque above, indistinctly longitudinally striate below, (scanty capillitia not forming a net). Stalk hollow, not fibrous at the base, emerging from a membranous, discoid hypothallus.

Figure 15a. Stalk of Stemonitis

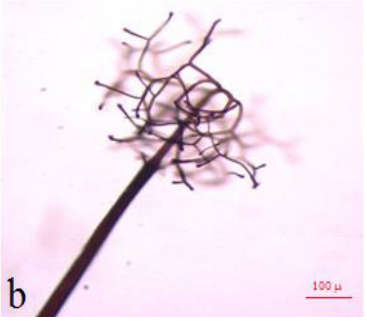

Figure 15b. Stalk of Macbrideola

Genera having solid stipes (Clark and Haskins, 2014): *Comatricha* Preuss stalk 0.5-1 mm tall, black, red or red-brown, occasionally very dark brown in the lower half, slender, usually less than half the total height, flattened and light brown at base, extending into the sporotheca as a columella (Figure 16). 50-66% of the total height fibrous at the base, with an inconspicuous hypothallus, turning to olivaceous-yellow at the base, extending into a columella equalling one to two thirds of the height of the sporotheca (stalk tube of interwoven fibers, capillitium may form a partial net), especially at the base.

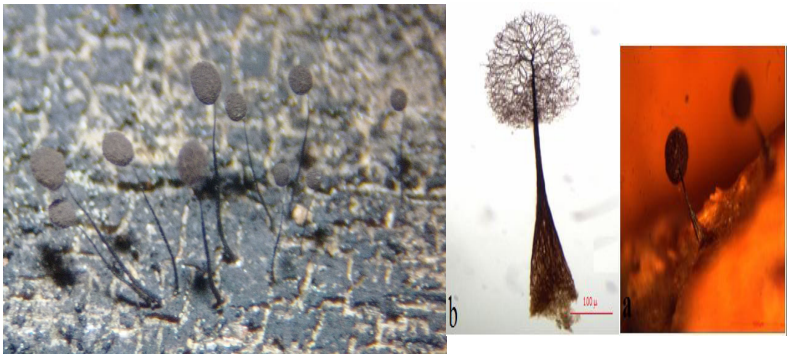

Figure 16. Stalk structure, columella and capillitium of Comatrichia

Paradiacheopsis Hertel stalk subulate with a broad, fibrous yellowish base, dark and slender above, continuing to the centre of the sporotheca as a columella, long, 0.5 mm awl-shaped, reddish brown, subulate with a broad, fibrous yellowish base, dark and slender above, tapered upwards and continuing to the centre of the sporotheca as a columella (Figure 17a), (stalk tube of interwoven fibers, capillitia dichotomously branching only). *Stemonitopsis* (Nann.-Bremek.) Nann.-Bremek. stalk black, shining, 33-50% of the total height, black, polished (Figure 17b), (stalk tube of interwoven fibers only at the base).

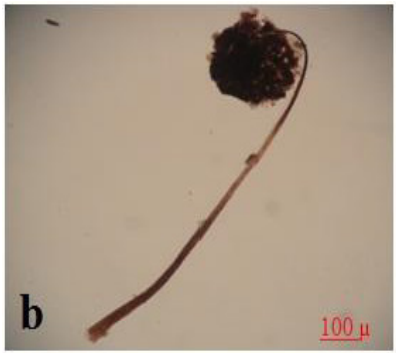

Figure 17a. Stalk of Paradiacheopsis

Figure 17b. Stalk of Stemonitopsis

Collaria Nann.-Bremek. stalk rigid, black, 66-75% of the total height, shining, very slender and long, up to 3 mm, arising from a small, membranous, brownish hypothallus (Figure 18a) (stalk tube fibers not interwoven, peridial collar on stalk). *Lamproderma* Rostaf. sessile or stipe almost 50% of the total height, black, shining, smooth, slightly swollen at the base, tapered upwards (Figure 18b), (stalk tube fibers not interwoven, peridium persistent), 0.5–0.6 mm in length, as long or only slightly longer than the sporotheca, opaque black by transmitted light, 60–100 µm wide at the base, 20–40 µm wide at the apex, continuing into a short, slightly clavate and blunt columella.

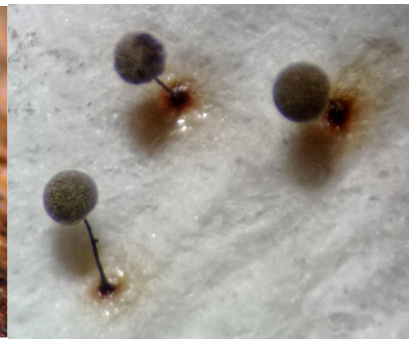

Figure 18a. Stalk of Collaria Figure 18b. Stalk of Lamproderma

The remaining genera having very short or no stipes: The stalk in *Enerthenema* Bowman black, continued into the sporotheca as a columella and tipped by a small, shining, discoid cup from which the capillitium arises, a genus with capillitium arising only from an apical cup, was not discussed. While some of these stalk characteristics are supported by DNA phylogeny others have not yet been addressed or they are contradicted (Fiore-Donno et al. 2009). The division of the genera into hollow and solid stalked groups is highly supported by these studies (a possible family level character); however, the absence of a stalk is not supported as a genus level character. *Leptoderma* G. Lister stalk short, stout, dark from enclosed refuse matter, spreading below into a dark hypothallus. *Meriderma* Mar. Mey. & Poulain sessile or stalk weak, black shining, often flattened, to 0.6 mm high up to 1 mm. *Arcyodes* O.F. Cook sessile or shortstipitate, *Calomyxa* Nieuwl. sessile or sub-sessile on a small base, *Calonema* Morgan stalk absent if present, up to 300 µm long, filled with cysts, *Echinosteliopsis* D.J. Reinh. & L.S.Olive stipitate. The stipe-less genera *Amaurochaeta* Rostaf., *Badhamiopsis* T.E. Brooks & H.W. Keller, *Brefeldia* Rostaf., *Colloderma* G. Lister, *Cornuvia* Rostaf., *Diachaeopsis* Meyl., *Dianema* Rex, *Elaeomyxa* Hagelst., *Fuligo* Haller, *Kelleromyxa* Eliasson, *Licaethalium* Rostaf., *Listerella* E. Jahn, *Minakatella* G. Lister, *Mucilago* P Micheli ex Adans., *Paradiachea* Hertel, *Semimorula* E.F. Haskins, McGuinn. & C.S. Berry, *Siphoptychium* Rostaf. *Thecotubifera* Leontyev, Schnittler, S.L. Stephenson & Novozh, *Trabrooksia* H. W. Keller and *Willkommlangea* Kuntze.

Conclusion

The stalk or stipe is an important identification character. The combination of molecular and morphological data indicate that the stalk of the myxomycete fruiting body is far less reliable as a taxonomic marker than has long been thought to be the case. The stalk may vary in length and

color and texture. In some species the stalk is opaque, while in others it is translucent. The stalk may also be coated with lime or filled with granular or sporelike structures.

References

Baba H (2021). Five new Myxomycetes (Myxogastria) records from Turkey. Phytotaxa, 507 (2): 131–143.

Baba H and Atay M (2019). Myxomycetes of Kumlu and Reyhanlı districts of Hatay/Turkey province. Biological Diversity and Conservation, 12/2 41-50.

Baba H and Sevindik M (2019). Mycetozoa of Turkey (Checklist), Mycopath 17(1):1-14.

Baba H and Sevindik M (2020a). Myxomycetes of Eşmişek Plateau (Kırıkhan-Hatay). KSU J. Agric Nat 23(4): 917-923.

Baba H and Sevindik M (2021). A New Myxomycetes record (Myxogastria) from Turkey: *Didymium listeri* Massee. KSU J. Agric Nat 24 (4): 820-823.

Baba H and Sevindik M (2022a). Myxomycetes diversity in Adana Province (Turkey) with two new records. Phytotaxa 547 (1): 031–042.

Baba H and Sevindik M (2022b). New Records of Myxogastria (Mycetozoa) from the Eastern Mediterranean Region of Turkey. Biology Bulletin, Vol. 49, No. 2, pp. 85–94.

Baba H, Altaş B and Sevindik M (2021b). Myxomycetes Diversity of Batman Province and Hasankeyf District. KSU J. Agric Nat, 24 (2): 435-441.

Baba H, Cennet E, Sevindik M (2019). Investıgatıon of Myxomycetes (Myxomycota) in Kırıkhan (Hatay Provınce). Commun. Fac. Sci. Univ. Ank. Series C Volume 29, Number 2, Pages 160-169.

Baba H, Er A, Sevindik M (2020b). Myxomycetes Diversity of Belen region of Hatay province (Turkey). Kastamonu Univ., Journal of Forestry Faculty, 20 (2): 86-96.

Baba H, Gündoğdu F and Sevindik M (2021a). Myxomycetes biodiversity in Gaziantep Province (Turkey) with four new records. Phytotaxa, 478 (1): 105–118.

Baba H, Sevindik M, Dogan M, Akgül H (2020a). Antioxidant, antimicrobial activities and heavy metal contents of some Myxomycetes. Fresenius Environmental Bulletin, Volume 29 – No. 09 pages 7840-7846.

Baba H, Sevindik M, Er A, Atay M, Doğan Y, Altaş B and Akgül A (2021c). New four Mycetozoa records from South East Anatolia-Turkey. Fresenius Environmental Bulletin, Volume 30 – No. 04 pages 3565-3574.

Baba, H., & Sevindik, M. (2018). The roles of myxomycetes in ecosystems. J Bacteriol Mycol Open Access, 6(3), 165-166.

Baba, H., & Sevindik, M. (2023). Myxomycetes (Myxogastria) of Türkiye: A checklist 2023. Mycopath, 21(1):53-67

Baba, H., Gelen, M., Sevindik, M. (2018). Taxonomic investigation of myxomycetes in Altınözü, Turkey. Mycopath, 16(1): 23-31

Baysal R and Eroğlu G (2022). Diversity of myxomycete on Konya-Beyşehir highway route. Anatolian Journal of Botany, 6(1): 55-61.

Clark J and Haskins EF (2014). Sporophore morphology and development in the myxomycetes: a review. Mycosphere, 5 (1): 153–170.

de Basanta WD and Lado C (2005). A taxonomic evaluation of the stipitate Licea. Fungal Diversity, 20; 261–314.

Ergul, C. C., Dulger, B., & Akgul, H. A. S. A. N. (2005). Myxomycetes of Mezit stream valley of Turkey. Mycotaxon, 92.

Ergul, C. C., Dulger, B., Oran, R. B., & Akgul, H. (2005). Myxomycetes of the western Black Sea region of Turkey. Mycotaxon, 93.

Ergül, C. C., & Akgül, H. (2011). Myxomycete diversity of Uludağ national park, Turkey. Mycotaxon, 116(479), 1-16.

Eroğlu G (2021). *Cribraria lepida, Physarum dictyosporum, P. diderma*, and *P. spectabile* newly recorded from Turkey. Mycotaxon, Volume 136, pp. 853–863.

Farr ML (1981). True Slime Molds. Dubuque Iowa: Wm. C. Brown Comp.

Fiore-Donno AM, Berney C, Pawlowski J, Baldauf SL. (2005). High-order phylogeny of plasmodial slime molds (Myxogastria), based on elongation factor 1-A and small subunit rRNA gene sequences. Journal of Eukaryotic Microbiology, 52; 201–210.

Fiore-Donno AM, Haskins EF, Pawlowski J, Cavalier-Smith T. (2009). *Semimorula liquescens* is a modified echinsteloid myxomycete (Mycetozoa). Mycologia, 101; 773–776.

García-Cunchillos I, Zamora JC, Ryberg M, Lado C (2022). Phylogeny and evolution of morphological structures in a highly diverse lineage of fruiting-body-forming amoebae, order Trichiales (Myxomycetes, Amoebozoa). Molecular Phylogenetics and Evolution, 177; 1-20.

Gray WD, Alexopoulos CJ (1968). Biology of the Myxomycetes. The Ronald Press, New York.

Guttes E, Rusch HP (1961). Morphological observations on growth and differentiation of *Physarum polycephalum* grown in pure culture. Developmental Biology, 3; 588–614.

Harkönen M and Ukkola T (2000). Conclusions on myxomycetes compiled over twenty-five years from 4793 moist chamber cultures. Stapfia 73, zugleich Kataloge des OO. Landesmuseums, Neue Folge Nr. 155: 105-112.

Keller HW and Braun KL (1999). Myxomycetes of Ohio: Their Systematics, Biology and Use in Teaching. Ohio Biological Survey Bulletin New Series, Volume 13, Number 2 182p.

Keller HW, Courtney MK, Sydney EE, Glenda JC, Christopher DC and Angela RS (2008). Myxomycete Plasmodia and Fruiting Bodies: Unusual Occurren-

ces and User-friendly Study Techniques. Fungi, Volume 1:1, 24-37.

Lado C (2005–2023). An on line nomenclatural information system of Eumycetozoa. Real Jardín Botánico, CSIC. Madrid, Spain. http://www.nomen.eumycetozoa.com. Last updated July 3, 2023.

Martin GW and Alexopoulos CJ (1969). The Myxomycetes. Iowa City, Univeristy of Iowa Press.

Matsumoto J. (1999). Taxonomic study on the genus Didymium (Physarales, Myxomycetes). Ph. D. Dissertation, University of Hiroshima, Japan.

Nannenga–Bremekamp NE, Yamamoto Y, Sharma R. (1984). Stemonaria, a new genus in the Stemonitaceae and two new species of Stemonitis (Myxomycetes). Konienklijke Nederlandse Akademie van Weternschappen, 87; 449–469.

Ocak İ and Konuk M (2018). Diversity and ecology of Myxomycetes from Kütahya and Konya (Turkey) with four new records. Mycobiology, 46: 215-223.

Schnittler M, Spiegel F (2012). Fruit body- forming protists: Myxomycetes and Myxomycete-like organisms. In Syllabus of Plant Families, 15th edition (ed. Frey W.).

Sevindik M and Akgül H (2019). Fruiting bodies structures of myxomycetes. J Bacteriol Mycol Open Access. 7(6):144–148.

Stephenson SL and Stempen H (1994). Myxomycetes: A Handbook of Slime Molds. Portland, USA: Tımber Press.

CHAPTER 7

BIOLOGICAL ACTIVITIES AND USES OF GENUS *Adonis*

İmran UYSAL[1], Alpaslan DAYANGAÇ[2], Nuh KORKMAZ[3], Mustafa SEVİNDİK[4], Hasan AKGÜL[5]

1 Osmaniye Korkut Ata University, Bahçe Vocational School, Department of Food Processing, Osmaniye, Turkey
2 Osmaniye Korkut Ata University, Faculty of Health Sciences Department of Nutrition and Dietics, Osmaniye, Turkey
3 Osmaniye Korkut Ata University, Science and Literature Faculty, Department of Biology, Osmaniye, Turkey.
4 Osmaniye Korkut Ata University, Science and Literature Faculty, Department of Biology, Osmaniye, Turkey.
5 Akdeniz University, Science Faculty, Department of Biology, Antalya, Turkey

Introduction

Traditional or alternative medicine, unlike modern medicine, is a method in which many natural products are used to prevent and combat diseases (Mohammed et al., 2020b). Since ancient times, people have tried natural products to combat many diseases (Mohammed et al., 2022). Among these natural products, plants have a very important position (Sevindik et al., 2017). Plants have been used by humans for different purposes such as fighting against diseases, as food, as heating, as shelter, as tools and equipment (Mohammed et al., 2020a; Korkmaz et al., 2021). They have become indispensable elements of people's diet lists. In addition to these features, they are also medically important natural products. Many studies have shown that plants have different biological activities such as antiallergic, antioxidant, antimicrobial, anticancer, anti-inflammatory, antiproliferative, antiaging, hepatoprotective, and DNA protective (Mohammed et al., 2018; Pehlivan et al., 2018; Mohammed et al., 2019; Mohammed et al., 2021; Comlekcioğlu et al., 2022; Unal et al., 2022; Kalkan et al., 2023; Sevindik et al., 2023a; Uysal et al., 2023). In this context, determining the biological activities of plants is very important in terms of their use. In this study, the intended use and biological activities of species belonging to the *Adonis* genus reported in the literature were compiled.

It is assumed that the emergence of the name of the genus *Adonis* is based on the legendary character *Adonis*, who was the lover of the goddess Aphrodite or Venus. It is a perennial herbaceous plant in the Ranunculaceae family. Its general distribution areas include the temperate regions of the northern hemisphere. It also spreads in European and Asian regions. When we look at the morphological characteristics, the lower stem leaves are generally scaly and the upper stem leaves are alternate and divided into palmate or pinnate. The flowers are radially symmetrical, bisexual and usually red, orange or yellowish. Petals vary between 5 and 30. It has numerous stamens and spirally arranged pistils, linear filaments, and single-ovulated ovaries with persistent styles and small stigma (Abduchamidov et al., 1971; Heyn and Pazy, 1989; Gostin, 2011; Shikov et al., 2014; Al-Snafi , 2016; Shang et al., 2019).

Usage Areas

It is seen that different parts of many plants in the *Adonis* genus are used in different areas. Among these areas of use, pharmacological properties are at the forefront. It has been reported that the preferred conditions in the field of health include the fight against edema formation, spasmolysis, cardiovascular conditions, insomnia, epilepsy, kidney disorders, cough and malaria treatment (Bae, 2000; Wagler, 2001; Al-Quran, 2008; Al-Snafi, 2016; Shang et al., 2019).

Biological activities

Plants are natural products responsible for many biological activities. Having different biological activities makes plants important for use (Mohammed et al., 2023a). In this study, the biological activities of species belonging to the Adonis genus reported in the literature were compiled. It has been observed that extracts such as ethyl acetate, methanol, dichloromethane, diethyl ether, water, ethanol, crude extract, butanol and alcoholic were used in in vitro and in vivo biological activity studies on species belonging to the *Adonis* genus. Biological activity studies of some species belonging to the *Adonis* genus are shown in table 1.

Table 1. Biological activity of genus Adonis

Plant species	**Biological activities**	**Extraction**	**Geographic regions**	**References**
Adonis aestivalis L.	Cytotoxic, antimicrobial, antioxidant, antiproliferative	Crude extract, methanol	Iran, Japan, Turkey	(Kubo et al., 2012; Hosseini et al., 2019; Karahan et al., 2022)
Adonis aleppica Boiss.	Antimicrobial, antioxidant, antiproliferative	Methanol	Turkey	(Karahan et al., 2022)
Adonis amurensis Regel & Radde	Cytotoxic	Crude extract	China	(Yan et al., 2022)
Adonis coerulea Maxim.	Cytotoxic, anti-inflammatory, antioxidant, acaricidal, acetylcholinesterase	Methanol	China	(Dai et al., 2020; Shang et al., 2020; Dai et al., 2022)
Adonis microcarpa DC.	Antiglycation, antiproliferation, antidiabetic, cytotoxic	Etil asetat, methanol, diklorometan, diethyl ether, water	Egypt	(Abd-Alla et al., 2021)
Adonis multiflora Nishikawa & Koji Ito	Cytotoxic	Ethanol, diklorometan, etil asetat, butanol, water, methanol	South Korea	(Jung et al., 2015)
Adonis paryadrica Boiss.	Antioxidant, antimicrobial	Methanol, ethanol	Turkey	(Mustafa, 2023; Üçüncü et al., 2020)

Adonis ramosa Franch.	Antioxidant	Aqueous, ethanol, methanol	China	(Guo et al., 2022)
Adonis vernalis L.	Allelopathic, antihyperlipidemic, anticancer, anti-inflammatory	Water, alcoholic, aqueous, methanol	Bulgaria, Pakistan, Iran, India	(Gupta et al., 2007; Lateef et al., 2012; Dragoeva et al., 2015; Sattari et al., 2020)

Antioxidant activity

Reactive oxygen species are free radicals produced as a result of metabolic activities in living organisms (Krupodorova and Sevindik, 2020). While these compounds do not cause negative effects at low levels, they can cause significant harm at high levels (Bal et al., 2019). The antioxidant defense system functions in reducing or suppressing the effects of free radicals (Akgül et al., 2020). When the antioxidant defense system is inadequate, oxidative stress occurs. As a result of oxidative stress, serious diseases such as cancer, cardiological disorders, Parkinson's, Alzheimer's, and multiple sclerosis may occur in humans (Selamoglu et al., 2020; Eraslan et al., 2021; Saridogan et al., 2021). Supplementary antioxidants may be important in preventing these diseases and reducing the effects of oxidative stress (Akgül et al., 2022). In our study, antioxidant activity studies of the *Adonis* species reported in the literature were compiled. In a study conducted in Turkey, the antioxidant status of methanol extract obtained from *Adonis aestivalis* and *Adonis aleppica* samples was analyzed using the DPPH test. As a result of the study, it was reported that the LC50 value of both plant samples used was 3.6 µg/mL (Karahan et al., 2022). In a study conducted in China, the antioxidant status of methanol extract obtained from *Adonis coerulea* sample was investigated. As a result of the study, at 100 µg/mL concentrations, SOD activities were 47.12 U/mg Prot ($p < 0.001$), respectively, 50.68 U/mg Prot at 10 µg/mL, similar to the positive agent Vc ($p < 0.001$), 50 and CAT activity at concentrations of 100 µg/mL was also reported to be significantly increased compared to the model group (Dai et al., 2022). In a study conducted in Turkey, the antioxidant properties of the methanol extract obtained from the *Adonis paryadrica* plant were examined using the CUPRAC test. As a result of the research, it was reported that it showed the highest copper reducing antioxidant power (CUPRAC) effect with 80.28 µmol TE (trolox equivalent)/g dw (Mustafa, 2023). In a study conducted in Turkey, the antioxidant status of ethanol extract obtained from the *Adonis paryadrica* plant was examined using

DPPH, FRAP, CUPRAC, ABTS and TPC tests. As a result of the study, it was reported that the DPPH SC50 value was 0.144-0.312 mg/mL, the FRAP value was 945.24-4078.57 µM, the CUPRAC value was 2.052-5.781µM, the ABTS SC50 value was 0.350-0.630 mg/mL and the TPC value was 333.26-465.56 µg/mL (Üçüncü et al., 2020). In a study conducted in China, the antioxidant status of different extracts of *Adonis ramosa* was examined through hydroxyl and superoxide radical scavenging abilities copper chelating abilities, copper-reducing antioxidant capacity, iron chelating activity, HCIO- and nitrite scavenging abilities, reactive oxygen species-scavenging abilities, iron-reducing antioxidant and β-carotene bleaching tests. As a result of the study, it was reported that the aqueous extract exhibited the highest hydroxyl and superoxide radical scavenging abilities, copper chelating abilities and copper reducing antioxidant capacity, while the ethanol extract showed the highest iron chelating activity and HClO- and nitrite scavenging abilities. It has also been reported that methanol extract shows high radical and reactive oxygen species scavenging abilities and is the best iron reducer (Guo et al., 2022).

Antimicrobial activity

In recent years, the increase in mortality from diseases caused by microorganisms has become visible (Baba et al., 2020). In particular, the emergence of resistant microorganisms has rendered the effects of the antimicrobial drugs used insufficient (Mohammed et al., 2023b). In this context, researchers' interest in new antimicrobial drugs has gradually increased. Plants have high antimicrobial activities due to the many microorganisms they encounter in the ecosystem (Bal et al., 2017; Islek et al., 2021; Sevindik et al., 2023b). In our study, antimicrobial studies reported in the literature on some species belonging to the *Adonis* genus were compiled. In a study conducted in Turkey, the antimicrobial status of methanol extract obtained from *Adonis aestivalis* and *Adonis aleppica* samples was examined. At the end of the study, it was reported to be effective against *Candida krusei, Candida parapsilosis*, *Staphylococcus aureus, Bacillus cereus, Enterococcus faecalis, Escherichia coli*, *Pseudomonas aeruginosa* and *Klebsiella pneumoniae* (Karahan et al., 2022). In a study conducted in Turkey, the antimicrobial properties of methanol extract obtained from the *Adonis paryadrica* plant were examined. As a result of the research, it was reported that among the strains used, it showed the strongest antibacterial activity against *Bacillus subtilis* with a zone diameter of 16.1 mm (Mustafa, 2023).

Other activity

Adonis species have been shown to have many biological activities other than antioxidant and antimicrobial activity studies reported in the

literature. In a study conducted in Iran, the cytotoxic activity of digitoxin, a cardiac glycoside contained in *Adonis aestivalis* extract, was examined against cervical cancer cell (HeLa) lines and human lymphocytes. As a result of the study, it was reported that the half-maximal inhibitory concentration values for cervical cancer and lymphocyte cells were 5.62 and 412.94 µg/mL, respectively (Hosseini et al., 2019). In another study conducted in Japan, it was reported that the cardenolide compound obtained from *Adonis aestivalis* extract showed cytotoxicity against malignant tumor cell lines (Kubo et al., 2012). In a study conducted in China, the cytotoxicity of pregnane glycoside A to G obtained from the extract of the *Adonis amurensis* plant was investigated on HepG2, Caco-2 and A549 cell lines. As a result of the study, it was reported that A–C and E showed inhibitory effects on the growth of HepG2 cells with LC50 values of 15.6 and 48.7 µM, and A, D and F showed inhibitory effects on the growth of A549 cells with IC50 values of 18.8, 12.4 and 30.4 µM, respectively (Yan et al., 2022). In a study conducted in China, the cytotoxicity of ACAP's methanol extract of *Adonis coerulea* against RAW 264.7 cells was evaluated and it was reported that ACAP provided in vitro safety at concentrations of 0–1,000 µg/mL (Dai et al., 2022). In a study conducted in Egypt, it was reported that the cytotoxic CC50 value of many different extracts obtained from the *Adonis microcarpa* sample on the normal lung cell line was 57.44 µM (Abd-Alla et al., 2021). In a study conducted in South Korea, it was reported that many different extracts obtained from *Adonis multiflora* specimen had cytotoxic effects against six human cancer cell lines (HCT-116, HepG2, HeLa, SK-OV-3 and SK-MEL-5 and SK-BR-3) (Jung et al., 2015). In a study conducted in Turkey, the antiproliferative status of methanol extract obtained from *Adonis aestivalis, Adonis aleppica* samples on HL-60, HCA-7 and HUVEC human cells was examined. As a result of the study, on HL-60, HCA-7 and HUVEC human cells, respectively; It was reported to be 2.05 µg/mL and 36.40 µg/mL, 36.01 µg/mL and 44.21 µg/mL, 158.10 µg/mL and 184.16 µg/mL (Karahan et al., 2022). In a study conducted in China, it was reported that methanol extract of Adonis coerulea significantly inhibited NO release after ACAP treatment (Dai et al., 2022). In another study conducted in China, it was reported that the methanol extract of *Adonis coerulea* had an acaricidal effect on Psoroptes cuniculi with IC50 values ranging between 2.38-0.56 µg/mL (Shang et al., 2020). In another study conducted in China, it was reported that silibinin, quercetin and corillagin obtained from the methanol extract of *Adonis coerulea* could inhibit AChE activity with IC50 values of 40.11 µg/mL, 46.15 µg/mL and 50.98 µg/mL, respectively (Dai et al., 2020)). In a study conducted in Egypt, it was reported that many different extracts obtained from *Adonis microcarpa* had antiglycation, antiproliferation and antidiabetic activities (Abd-Alla et al., 2021). In a study conducted in Bulgaria, it was reported

that the water extract of *Adonis vernalis* had an allelopathic effect (Dragoeva et al., 2015). A study conducted in Pakistan reported that alcoholic extract of *Adonis vernalis* showed a significant reduction in serum cholesterol and triglycerides compared to control triton-induced hyperlipidemic control (TIC) and triton-induced positive control (TIPC) (Lateef et al., 2012). In a study conducted in Iran, it was reported that silver nanoparticles (AgNPs) of the aqueous extract of *Adonis vernalis* showed anticancer properties on breast cancer (Sattari et al., 2020). In a study conducted in India, it was reported that methanol extract of *Adonis vernalis* significantly inhibited tumor necrosis factor-α (TNF-α) production by whole blood cultured cells (Gupta et al., 2007).

Conclusion

In this study, the biological activities and general characteristics of *Adonis* species reported in the literature were compiled. According to the findings, it has been observed that different *Adonis* species have biological activities such as antioxidant, antimicrobial and anticancer. In this context, it is thought that *Adonis* species can be an important natural material in pharmacological designs.

References

Abd-Alla, H. I., Hassan, A. Z., Soltan, M. M., Abdelwahab, A. B., Hanna, A. G. (2021). Potential protein antiglycation, antiproliferation, and in silico study on the antidiabetic enzymes of bioactive metabolites from Adonis microcarpa DC and their ADMET properties. Journal of Applied Pharmaceutical Science, 12(1), 106-119.

Abduchamidov, N., Hammermann, A., Sokolov, W. (1971). Adonıs Turkestanıcus–Eıne Neue Aussıchtsreıche Herz–Und Gefässwırksame Heılpflanze. Planta Medica, 20(05), 272-277.

Akgul, H., Korkmaz, N., Dayangaç, A., & Sevindik, M. (2020). Antioxidant potential of endemic Salvia absconditiflora. Turkish Journal of Agriculture-Food Science and Technology, 8(10), 2222-2224.

Akgül, H., Mohammed, F. S., Kına, E., Uysal, İ., Sevindik, M., & Doğan, M. (2022). Total Antioxidant and Oxidant Status and DPPH Free radical activity of Euphorbia eriophora. Turkish Journal of Agriculture-Food Science and Technology, 10(2), 272-275.

Al-Quran, S. (2008). Taxonomical and pharmacological survey of therapeutic plants in Jordan. J Nat Prod, 1(1), 10-26.

Al-Snafi, A. E. (2016). Adonis aestivalis: pharmacological and toxicological activities-A revew. Asian Journal of Pharmaceutical Science & Technology, 6(2), 96-102.

Baba, H., Sevindik, M., Dogan, M., & Akgül, H. (2020). Antioxidant, antimicrobial activities and heavy metal contents of some Myxomycetes. Fresenius Environmental Bulletin, 29(09), 7840-7846.

Bae, K. H. (2000). The medicinal plants of Korea. Kyo-Hak Publishing Co., Seoul, 260.

Bal, C., Akgul, H., Sevindik, M., Akata, I., & Yumrutas, O. (2017). Determination of the anti-oxidative activities of six mushrooms. Fresenius Envir Bull, 26(10), 6246-6252.

Bal, C., Sevindik, M., Akgul, H., & Selamoglu, Z. (2019). Oxidative stress index and antioxidant capacity of Lepista nuda collected from Gaziantep/Turkey. Sigma Journal of Engineering and Natural Sciences, 37(1), 1-5.

Comlekcioglu, N., Dağlı, F., Çömlekcioğlu, U., & Aygan, A. (2022). Cornus mas ve Rosa canina Meyvelerinin Antioksidan Kapasitesi ve Bazı Fitokimyasal Özellikleri. Turkish Journal of Agriculture-Food Science and Technology, 10(9), 1724-1731.

Dai, L., Li, B., Yang, X., Wang, Y., Pan, H., Zhang, J., Shang, X. (2022). The Nutritional Properties, Chemical Compositions, and Functional Characteristics of the Aerial Parts of Adonis coerulea. Frontiers in Nutrition, 9.

Dai, L., Miao, X., Li, B., Zhang, J., Pan, H., Shang, X. (2020). The active compounds and AChE inhibitor of the methanol extract of Adonis coerulea

maxim against Psoroptes cuniculi. Veterinary Parasitology, 286, 109247.

Dragoeva, A. P., Koleva, V. P., Nanova, Z. D., Georgiev, B. P. (2015). Allelopathic effects of Adonis vernalis L.: Root growth inhibition and cytogenetic alterations. Journal of Agricultural Chemistry and Environment, 4(02), 48.

Eraslan, E. C., Altuntas, D., Baba, H., Bal, C., Akgül, H., Akata, I., & Sevindik, M. (2021). Some biological activities and element contents of ethanol extract of wild edible mushroom Morchella esculenta. Sigma Journal of Engineering and Natural Sciences, 39(1), 24-28.

Gostin, I. N. (2011). Anatomical and micromorphological peculiarities of Adonis vernalis L.(Ranunculaceae). Pakistan Journal of Botany, 43(2), 811-820.

Gupta, B., Das, R. H., Das, H., Raghav, S. (2007, March). Anti-inflammatory compounds from medicinal plant Ruta graveolens. In International Symposium on Medicinal and Nutraceutical Plants 756 (pp. 389-398).

Heyn, C. C., Pazy, B. (1989). The annual species of Adonis (Ranunculaceae)—a polyploid complex. Plant systematics and evolution, 168, 181-193.

Hosseini, M., Taherkhani, M., Ghorbani Nohooji, M. (2019). Introduction of Adonis aestivalis as a new source of effective cytotoxic cardiac glycoside. Natural product research, 33(6), 915-920.

Islek, C., Saridogan, B. G. O., Sevindik, M., & Akata, I. (2021). Biological activities and heavy metal contents of some Pholiota species. Fresenius Environmental Bulletin, 30(6), 6109-6114.

Jung, J. W., Baek, N. I., Hwang-Bo, J., Lee, S. S., Park, J. H., Seo, K. H., Bang, M. H. (2015). Two New Cyototoxic Cardenolides from the Whole Plants of Adonis multiflora Nishikawa & Koki Ito. Molecules, 20(11), 20823-20831.

Kalkan, M., Aygan, A., Çömlekçioglu, N., & Çömlekçioğlu, U. (2023). Olea europaea Yapraklarının Bazı Biyoaktif Özelliklerinin Araştırılması, Antimikrobiyal ve Enzim İnhibisyon Etkinliğinin İncelenmesi. Turkish Journal of Agriculture-Food Science and Technology, 11(3), 496-504.

Karahan, F., Avşar, C., Turkmen, M., Gezici, S., Ilcim, A. (2022). Comparative Study on Phytochemical Profiles, Antiproliferative, Antimicrobial and Antioxidant Activities of Adonis Species from Turkey. Pharmaceutical Chemistry Journal, 56(5), 667-678.

Korkmaz, N., Dayangaç, A., Sevindik, M. (2021). Antioxidant, antimicrobial and antiproliferative activities of Galium aparine. J Fac Pharm Ankara, 45(3), 554-564.

Krupodorova, T., & Sevindik, M. (2020). Antioxidant potential and some mineral contents of wild edible mushroom Ramaria stricta. AgroLife Scientific Journal, 9(1), 186-191.

Kubo, S., Kuroda, M., Matsuo, Y., Masatani, D., Sakagami, H., Mimaki, Y. (2012). New cardenolides from the seeds of Adonis aestivalis. Chemical and Pharmaceutical Bulletin, 60(10), 1275-1282.

Lateef, T., Riaz, A., Zehra, A., Qureshi, S. A. (2012). Antihyperlipidemic effect of Adonis vernalis. Journal of the Dow University of Health Sciences (JDUHS), 6(2), 47-51.

Mohammed, F. S., Akgul, H., Sevindik, M., & Khaled, B. M. T. (2018). Phenolic content and biological activities of Rhus coriaria var. zebaria. Fresenius Environmental Bulletin, 27(8), 5694-5702.

Mohammed, F. S., Günal, S., Pehlivan, M., Doğan, M., Sevindik, M., & Akgül, H. (2020b). Phenolic content, antioxidant and antimicrobial potential of endemic Ferulago platycarpa. Gazi University Journal of Science, 33(4), 670-677.

Mohammed, F. S., Günal, S., Şabik, A. E., Akgül, H., & Sevindik, M. (2020a). Antioxidant and Antimicrobial activity of Scorzonera papposa collected from Iraq and Turkey. Kahramanmaraş Sütçü İmam Üniversitesi Tarım ve Doğa Dergisi, 23(5), 1114-1118.

Mohammed, F. S., Karakaş, M., Akgül, H., & Sevindik, M. (2019). Medicinal properties of Allium calocephalum collected from Gara Mountain (Iraq). Fresen Environ Bull, 28(10), 7419-7426.

Mohammed, F. S., Pehlivan, M., Sevindik, E., Akgul, H., Sevindik, M., Bozgeyik, I., & Yumrutas, O. (2021). Pharmacological properties of edible Asparagus acutifolius and Asparagus officinalis collected from North Iraq and Turkey (Hatay). Acta Alimentaria, 50(1), 136-143.

Mohammed, F. S., Sevindik, M., & Uysal, I. (2023a). Total phenolic, flavonoid, protein contents and biological activities of wild mustard. Acta Alimentaria, 52(3), 449-457.

Mohammed, F. S., Sevindik, M., Uysal, I., Sevindik, E., & Akgül, H. (2022). A Natural Material for Suppressing the Effects of Oxidative Stress: Biological Activities of Alcea kurdica. Biology Bulletin, 49(Suppl 2), S59-S66.

Mohammed, F. S., Uysal, I., & Sevindik, M. (2023b). A review on antiviral plants effective against different virus types. Prospects in Pharmaceutical Sciences, 21(2), 1-21.

Mustafa, C. Ü. C. E. (2023). Antioxidant and antimicrobial activities of methanol extracts from Adonis paryadrica (Ranunculaceae)–a critically endangered endemic species growing in the Turkish flora. International Journal of Secondary Metabolite, 10(1), 147-157.

Pehlivan, M., Mohammed, F. S., Sevindik, M., & Akgul, H. (2018). Antioxidant and oxidant potential of Rosa canina. Eurasian Journal of Forest Science, 6(4), 22-25.

Saridogan, B. G. O., Islek, C., Baba, H., Akata, I., & Sevindik, M. (2021). Antioxidant antimicrobial oxidant and elements contents of Xylaria polymorpha and X. hypoxylon (Xylariaceae). Fresenius Envir Bull. 30(5), 5400-5404.

Sattari, R., Khayati, G. R., Hoshyar, R. (2020). Preparation and physical charac-

terization of Adonis vernalis aqueous leaf extract-mediated green synthesized silver nanoparticles and its toxicity effect on breast cancer cells. Journal of Ultrafine Grained and Nanostructured Materials, 53(2), 183-189.

Selamoglu, Z., Sevindik, M., Bal, C., Ozaltun, B., Sen, İ., & Pasdaran, A. (2020). Antioxidant, antimicrobial and DNA protection activities of phenolic content of Tricholoma virgatum (Fr.) P. Kumm. Biointerface Research in Applied Chemistry, 10 (3), 5500-5506

Sevindik, M., Akgul, H., Pehlivan, M., & Selamoglu, Z. (2017). Determination of therapeutic potential of Mentha longifolia ssp. longifolia. Fresen Environ Bull, 26(7), 4757-4763.

Sevindik, M., Bal, C., Eraslan, E. C., Uysal, I., & Mohammed, F. S. (2023b). Medicinal mushrooms: a comprehensive study on their antiviral potential. Prospects in Pharmaceutical Sciences, 21(2), 42-56.

Sevindik, M., Mohammed, F. S., & Uysal, I. (2023a). Autism: plants with neuro-psychopharmacotherapeutic potential. Prospects in Pharmaceutical Sciences, 21(3), 38-48.

Shang, X. F., Miao, X. L., Dai, L. X., Guo, X., Li, B., Pan, H., Zhang, J. Y. (2020). The acaricidal mechanism and active compounds against Psoroptes cuniculi of the methanol extract of Adonis coerulea Maxim II: integrated proteomics and SPR analysis. Veterinary Parasitology, 287, 109267.

Shang, X., Miao, X., Yang, F., Wang, C., Li, B., Wang, W., Zhang, J. (2019). The genus Adonis as an important cardiac folk medicine: a review of the ethnobotany, phytochemistry and pharmacology. Frontiers in Pharmacology, 10, 25.

Shikov, A. N., Pozharitskaya, O. N., Makarov, V. G., Wagner, H., Verpoorte, R., Heinrich, M. (2014). Medicinal plants of the Russian Pharmacopoeia; their history and applications. Journal of ethnopharmacology, 154(3), 481-536.

Unal, O., Eraslan, E. C., Uysal, I., Mohammed, F. S., Sevindik, M., & Akgul, H. (2022). Biological activities and phenolic contents of Rumex scutatus collected from Turkey. Fresenius Environmental Bulletin, 31(7), 7341-7346.

Uysal, I., Koçer, O., Mohammed, F.S., Lekesiz, Ö., Doğan, M., Şabik, A.E., Sevindik, E., Gerçeker, F.O., Sevindik, M. (2023). Pharmacological and Nutritional Properties: Genus Salvia. Adv Pharmacol, 11(2), 140-155

Üçüncü, O., Baltaci, C., Akar, Z., Duzgun, A., Cuce, M., Kandemir, A. (2020). Biological activities and phytochemical screening of ethanol extracts from Adonis paryadrica (Ranunculaceae). Farmacia, 68(6), 1062-1068

Wagler, M. (2001). The homeopathic pharmacopoeia 2001: new regulations for homeopathic drugs. Deutsche Apothr. Zeit, 141, 86-89.

Yan, Y., Zhou, D., Li, X., Feng, Y., Wen, X., Wang, Y., Li, N. (2022). Pregnane glycosides from Adonis amurensis and their bioactivity. Phytochemistry, 194, 113046.

CHAPTER 8

BIOLEACHING OF METALS FROM SECONDARY SOURCES

Bengü ERTAN[1]

1 Asst. Prof.; Department of Occupational Health and Safety, Espiye Vocational School, Giresun University, Giresun, Turkey; email: bengu.ertan@giresun.edu.tr; ORCID: https://orcid.org/0000-0002-9879-9396

1. INTRODUCTION

Critical metals are characterized by supply risks and are expected to become steadily more dearth in the near future, especially given their high economic importance in key sectors such as environmental technologies, automotive, aerospace, defense, healthcare, electronics, and others. Demand for critical metals used in the manufacture of advanced technological devices is steadily increasing, while high-strength minerals are rapidly running out. Technological advances, industrial processes, rapid consumption, and the accumulation of significant quantities of valuable materials, including critical metals, in landfills have led to the emergence of a growing global industry known as "urban mining"(European Commission, 2023; Arya and Kumar, 2020; Venkata Mohan et al., 2020).

The heterogeneous and complex nature of solid waste is the major obstacle to metal recovery from waste. In addition, the varying degree of contamination of different types of waste makes it difficult to separate metals from each other and from non-metallic components. While organic matter in wastewater can be removed from the environment by various methods, the tendency of metals to dissolve and form complexes makes them difficult to separate from the environment. Traditional methods of metal recovery from waste involve pyrometallurgical and hydrometallurgical processes. While data suggest that hydrometallurgical methods are more effective compared to pyrometallurgical methods, these approaches require substantial energy and chemical consumption and necessitate the use of gas collection and dust removal systems (Krishnan et al., 2021). Due to the economic and environmental disadvantages of traditional methods, effective, environmentally friendly, cost-efficient, and sustainable biotechnological methods are preferred for metal recovery from waste (Wang and Gaustad, 2012).

2. BIOLEACHING

Microbial organisms, especially their role in the biological transformation of elements, biogeochemical cycles of metals and minerals, metal and mineral transformations, decomposition, biological degradation, and the formation of soil and sediments in the biosphere, play a significant role (Bertrand et al., 2015; Jing and Kjellerup, 2018). All microorganisms, including prokaryotes and eukaryotes, as well as complex organisms known as "higher organisms," can actively contribute to geomicrobial processes centered on the transformation of metals and minerals. While the activities of microorganisms in the transformation of organic and inorganic materials are known to microbiologists, there has been an increased awareness among researchers in geology, mineralogy, geochemistry, and related fields about the geochemical importance of microorganisms (Banfield and

Nealson, 1997; Macalady and Banfield, 2003; Warren and Haack, 2001; Gleeson et al., 2007; Konhauser, 2007; Bottjer, 2005; Gadd, 2008a; Uroz et al., 2009).

"Bioleaching" is the process of making metals in ores soluble in water through certain microorganisms naturally present in the environment (Atlas and Bartha, 1997). In these processes, metals present in ores as sulfides and oxides are dissolved in the leaching environment as metal cations (Rohwerder et al., 2003).

2.1. History

The origins of biomining date back to ancient times. In ancient civilizations, microorganisms were used for copper extraction. In the 18th century, silver was extracted from the Rio Tinto mine in Seville, Spain, and copper was mined during the Roman period. Rio Tinto (red river) is red in color due to the high concentration of ferric iron in its water, a result of natural microbial activity. It does not support fish and is not drinkable (Rawlings, 2002). The formation of acidic mine waters, a common occurrence in nature due to the breakdown of sulfide minerals during mining activities, was first attributed to the influence of microorganisms, giving rise to the field of "biohydrometallurgy" with the application of biotechnological methods in hydrometallurgy (Colmer and Hinkle, 1947). The industrial-scale application of biohydrometallurgy began in the 1950s with the bioleaching of low-grade chalcopyrite copper ore by Kennecott Copper Corporation (Utah, USA) and served as a model for many other operations. In 1986, bioleaching was applied as a pretreatment step for refractory gold-containing concentrates at the Fairview Gold Mine (South Africa) before cyanide leaching (Brierley and Brierley, 2001). Bioleaching processes are currently used in copper and cobalt recovery, pre-treatment of gold before cyanidation, and coal desulfurization (oxidizing pyrite in coal to soluble ferric sulfate) (Dresher, 2004). Bioleaching has been pilot-tested for uranium recovery (McCready and Gould, 1990), and it is estimated that approximately 20% of copper, 5% of gold, and smaller amounts of nickel, cobalt, uranium, and zinc are extracted through biomining processes (Brierley and Brierley, 2013).

2.2. Advantages

The reasons for the increasing use of biomining methods in metal recovery can be summarized as follows:

1. The limited of high-grade ore reserves on Earth and the interest in obtaining metals from ores with low metal content have led to increased attention in biomining. Compared to traditional methods that require high

temperature and pressure, bioleaching is economically favorable, requires low capital investment, low energy consumption, and is suitable for small-scale operations. It has made it economical to obtain metals from ores with a metal content of less than 0.5%, as well as from industrial wastes such as sludges (Watling, 2006; Bosecker, 1997; Brierley and Brierley, 2001).

2. Biomining allows the transformation of wastes into metals in a process closely resembling the natural biogeochemical cycle, reducing the demand for resources such as energy or storage space (Kreps et al., 1997).

3. It allows operation under conditions close to ambient pressure and temperature. The leaching solution is produced naturally by micro-organisms, creating a microclimate around the particles due to the high concentration of leaching materials during this process (Kreps, 1997). It is low cost because it does not require a sub-process cost for the use of concentrated acid/base, and there is no additional cost for the management of resulting acidic wastes. Similarly, high-temperature and high-pressure equipment is not required, making it cost-effective (Asghari et al., 2013; Bradwaj and Ting, 2013; Srichandan et al., 2014a).

4. The smelting processes used in classical pyrometallurgy result in emissions of harmful gases (e.g., SO_2), which lead to environmental pollution and contribute to global warming, as well as causing the loss of a significant portion of the metals in mineral residues. Bioleaching, on the other hand, does not cause such pollution, as it converts sulfur and reduced sulfur compounds in minerals into sulfate (Vera et al., 2013).

5. The waste generated at the end of physical-chemical processes results in the creation of acid in the atmospheric environment, causing the dissolved metals in the waste to threaten the environment (acid mine drainage). On the other hand, the waste generated at the end of bioleaching causes significantly less acid mine drainage compared to waste generated by physical-chemical processes (Bouffard and Dixon, 2004).

6. Useful oxidants, such as ferrous (Fe III), naturally present in the process, are continuously regenerated by microorganisms (Srichandan and Mishra, 2019).

2.3. Disadvantages

1. Bioleaching is a slower process compared to physical-chemical methods (Watling, 2006).

2. Toxic metals in the minerals can negatively affect microbial activity (Bryan et al., 2015).

3. Bioleaching is less effective in the recovery of metals from high-grade ores (Jalali et al., 2019).

4. In some cases, bioleaching yields can be low due to the refractory properties of ores/wastes (Pradhan et al., 2010).

5. Slow diffusion of oxidants to the ore surface due to the formation of jarosite and iron hydroxides on the ore surface can result in low metal yields (Zhao et al., 2017; Nazari et al., 2014).

6. Without a well-defined scientific strategy in material grinding, process setup, and operation, bioleaching may not be economical (Srichandan and Mishra, 2019).

2.4. Bioleaching Mechanisms

The interaction of microorganisms with minerals occurs through various mechanisms (Rawlings et al., 1999):

Indirect Interaction: During the growth of microorganisms, metabolites such as organic acids are produced, which can affect the mineral or metal compounds in the environment.

Contact Interaction: Microbial cells can attach themselves to the ore mineral within an extracellular polymeric substance (EPS). They can then mobilize metals from the mineral into the solution as metal cations.

Collaborative Bioleaching: Microbial cells attached to the ore and free microbial cells in the suspension work together to leach metals into the solution.

When a mineral or metal compound comes into contact with microorganisms, it undergoes metabolic reactions based on three fundamental principles:

Acidolysis

In a process also known to as proton-induced metal solubilization, organic acids secreted by microorganisms bind protons (H^+ ions) to the mineral surface. This weakens critical bonds and results in the detachment of metal ions from the solid surface (Brandl et al., 2001).

$$MeO + 2H^+ \rightarrow Me^{+2} + H_2O \quad (1)$$

Complexolysis

Ligand-induced metal dissolution involves the complexation of metals that have already passed into the solution through acidolysis. This stabilization occurs through complexation reactions between metal ions and organic acids. Organic ligands with two or more binding sites are more effective. This process also reduces metal toxicity towards microorganisms (Brandl et al., 2001; Burgstaller and Schinner, 1993). Amino acids secreted by microorganisms can also provide protons and participate in complexation reactions.

$$Me^{+2} + C_6H_8O_7 \rightarrow Me(C_6H_8O_7)^{-} + 3H^{+} \quad (2)$$

Redoxolysis

In this process, metals are microbially oxidized or reduced. The mobility of metals depends on their type and oxidation state. For instance, as seen in fungal leaching of manganese, the solubility of metal may result from the enzymatic reduction of highly oxidized metal compounds.

$$MnO_2 + 2e^{-} + 4H^{+} \rightarrow Mn^{+2} + 2H_2O \quad (3)$$

Soluble metals are actively transported through the cell membrane and accumulate within cells in solid particle form. This disrupts the balance between solid and dissolved metal, leading to continuous metal dissolution. Fungal cell walls, in particular, contain various functional groups such as hydroxyl, carboxyl, phosphate, amine, and sulfate groups that bind metal ions. Filamentous fungi, such as those belonging to the Aspergillus and Penicillium genera, have been reported to have a high capacity for binding heavy metals (Simate et al., 2010; Burgstaller and Schinner, 1993).

3. SECONDARY SOURCES

Secondary sources of metals can be found in electronic waste, mine waste, magnets, fluorescent lamps, optical glass, glass polishing powders, catalysts, sludge, slag, bottom ash, and fly ash. These secondary sources emerge as byproducts of processes like mining, steel processing, metallurgical operations, energy generation, and the manufacturing of electrical and electronic devices, as well as waste management. Solid waste materials containing metals are significant secondary sources of critical metals, and sometimes, it has been demonstrated that recovery of metals from secondary sources is more economically and environmentally sustainable compared to extraction from ores (Das et al., 2011; Karim and Ting, 2021; Krishnan et al., 2021).

Table 1 listed the performance achieved over different metals containing secondary sources, types of microorganisms used, and extracted metal during the bioleaching operation.

Table 1. *Selected literatüre studies on bioleaching metals from secondary sources.*

Secondary Sources	Microorganisms	Extracted metal	References
Spent automobile catalyst	Aspergillus niger (strain ZRS14)	Ce, Al, La	Hosseinzadeh et al., 2021
Waste Electrical and Electronic equipment (WEEE)	Acidithiobacillus thiooxidans	Ce, Eu, Nd, La, Y.	Marra et al., 2018
Waste Phosphors and Cracking Catalysts	Gluconobacter oxydans.	REE	Reed et al., 2016a
Cellphones Batteries	Aspergillus niger Aspergillus tubingensis	Li, Al	Alavi et al., 2021
Waste LCD (liquid crystal display) panels	Aspergillus niger	In	Cui et al., 2021
Brake pad waste	Acidithiobacillus thiooxidans, Acidithiobacillus ferrooxidans Leptospirillumferriphilum (mixed)	Cu, Zn	Zhang et al., 2019
Boron waste	Aspergillus niger	Li, Rb, Cs	Ertan, 2023
Mine tailings	Mesophilic microbial culture	As	Borja et al., 2019
Sulfidic mine tailings	Acidithiobacillus (At.) ferrooxidans and At. thiooxidans	Co, Cu	Zhang et al., 2020
Egyptian monazite	Aspergillus ficuum, Pseudomonas aeruginosa	REE	Hassanien et al., 2014

Mobile phone printed circuit board	Aspergillus fumigatus A2DS	Cu, Ni	Patel ve Lakshmi, 2021
Spent lithium-ion mobile phone batteries	Aspergillus niger	Cu, Li, Ni, Mn	Horeh et al., 2016
Spent automobile catalyst	Pseudomonas fluorescens and Bacillus megaterium.	Pt, Pd, Rh	Karim and Ting, 2022.
Steel industrial slag	Acidithiobacillus thiooxidans, Acidithiobacillus ferrooxidans, and Aspergillus niger	Mg, Zn, Cu	Hocheng et al., 2014

REE (Rare Earth Element), cerium (Ce), aluminum (Al), lanthanum (La), europium (Eu) and neodymium (Nd), yttrium (Y), lithium (Li), aluminium (Al), indium (In), copper (Cu), zinc (Zn), rubidium (Rb), cesium (Cs), arsenic (As), cobalt (Co), manganese (Mn), palladium (Pd), nickel (Ni), platinum (Pt), rhodium (Rh), magnesium (Mg)

4. CONCLUSION

Biohydrometallurgical methods have the potential to provide high selectivity and affinity in the recovery of metals from various waste categories. Furthermore, this approach is considered a reliable strategy with significant advantages over traditional leaching methods due to its simplicity, environmentally sensitive approach, and minimal energy input. In the near future, metal deposits will continue to deplete, and supply chains for industrial sectors will face challenges due to metal scarcity. The bioleaching method should be considered for the extraction of not only critical metals but also metals that do not have their own minerals, such as rubidium (Rb), from sources with low metal content, owing to its selective and economic nature. The recovery of metals from secondary sources, including waste, is not only crucial for conserving primary resources but can also serve as a resource for countries lacking primary sources of metal. Studies in biotechnology-based metal recovery from secondary sources are promising. More findings related to metal-microbe interactions, further research on the determination and optimization of parameters for the bioleaching process, can help in developing efficient, environmentally friendly, and cost-effective methods for industrial-scale metal recovery from secondary sources.

REFERENCES

Alavi, N., Partovi, K., Majlessi, M., Rashidi, M., & Alimohammadi, M. (2021). Bioleaching of metals from cellphones batteries by a co-fungus medium in presence of carbon materials. Bioresource Technology Reports, 15, 100768. https://doi.org/10.1016/j. biteb.2021.100768.

Asghari, I., Mousavi, S.M., Amiri, F., & Tavassoli, S. (2013). Bioleaching of spent refinery catalysts: a review. Industrial & Engineering Chemistry Research, 19, 1069–1081.

Arya, S., & Kumar, S. (2020). Bioleaching: urban mining option to curb the menace of Ewaste challenge. Bioengineered 11 (1), 640–660. https://doi.org/10 .1080/21655979.2020.1775988.

Atlas, R. M., & Bartha, R. (1997). Microbial Ecology: Fundamentals and Applications, Fourth Editon, Addison Wesley Longman, The Benjamin/Cumming Publishing Company, Inc., 694.

Banfield, J. F., & Nealson, K. H. (editors) (1997). Geomicrobiology: Interactions between Microbes and Minerals, Reviews in Mineralogy and Geochemistry, vol. 35. Washington, DC: Mineralogical Society of America.

Bertrand, J., Caumette, P., Lebaron, P., Matheron, R., Normand, P., & Sime-Ngando, T. (2015). Environmental Microbiology: Fundamentals and Applications. Springer Netherlands.

Bharadwaj, A., & Ting, Y.P. (2013). Bioleaching of spent hydrotreating catalyst by acidophilic thermophile Acidianus brierleyi: leaching mechanism and effect of decoking. Bioresource Technology, 130, 673–680.

Bosecker, K. (1997). Bioleaching: metal solubilization by microorganisms. FEMS Microbiology Reviews, 20: 591–604.

Bottjer, D. J. (2005). Geobiology and the fossil record: eukaryotic, microbes, and their interactions. Palaeogeogr Palaeoclimatol Palaeoecol 219, 5–21.

Bouffard, S.C., & Dixon, D.G. (2004). Heap Biooxidation of Refractory Gold Ores: Current State of the Art, Mineral Processing & Extractive Metallurgy Review, 25:159-192.

Brandl, H., Bosshard, R., & Wegmann, M.A. (2001). Computer-munching microbes: metal leaching from electronic scrap by bacteria and fungi. Hydrometallurgy, 59, 319-326.

Brierley, C.L., & Brierley, J.A. (2013) Progress in bioleaching: Part B: Applications of microbial processes by the minerals industries. Applied Microbiology and Biotechnology, 97: 7543-7552.

Brierley, J.A., & Brierley, C.L. (2001).Present and Future Commercial Applications of Biohydrometallurgy, Hydrometallurgy, 59: 233-239.

Bryan, C.G., Watkin, E.L., McCredden, T.J., Wong, Z., Harrison, S.T. & Kaksonen, A.H. (2015). The use of pyrite as a source of lixiviant in the bioleaching of electronic waste. Hydrometallurgy, 152, 33-43.

Borja, D., Nguyen, K.A., Silva, R.A., Ngoma, E., Petersen, J., Harrison, S.T., Park, J., & Kim, H. (2019). Continuous bioleaching of arsenopyrite from mine tailings using an adapted mesophilic microbial culture. Hydrometallurgy.

Burgstaller, W., & Schinner, F. (1993). Leaching of metals with fungi. Journal of Biotechnology, 27, 91-116.

Colmer, A.R., & Hinkle, M.E. (1947). The Role of Microorganisms in Acid Mine Drainage: Preliminary Report, Science, 106 (2751): 253-256.

Cui, J., Zhu, N., Mao, F., Wu, P., & Dang, Z. (2021). Bioleaching of indium from waste LCD panels by Aspergillus niger: Method optimization and mechanism analysis. Sci. Total Environ. 790, 148151. https://doi.org/10.1016/j.scitotenv.2021.148151.

Das, A. P., Sukla, L. B., Pradhan, N., & Nayak, S. (2011). Manganese biomining: A review. Bioresource technology, 102(16), 7381–7387. https://doi.org/10.1016/j.biortech.2011.05.018

Dresher, W.H. (2004). Copper Applications in Mining and Extraction, http://www.copper.org/innovations/2004/05/

Ertan, B. (2023). Extraction of High-value Metals from Boron Waste by Bioleaching Using Aspergillus niger. Transactions of Indian Institue of Metals. https://doi.org/10.1007/s12666-023-03013-0.

Gadd, G. M. (2008a). Bacterial and fungal geomicrobiology: a problem with communities? Geobiology 6, 278–284.

Gleeson, D., McDermott, F., & Clipson, N. (2007). Understanding microbially active biogeochemical environments. Adv Appl Microbiol 62, 81–104.

Grohol, M., & Veeh, C. (2023). Study on the critical raw materials for the EU 2023 – Final report.. European Commission, Directorate-General for Internal Market, Industry, Entrepreneurship and SMEs, Publications Office of the European Union. https://data.europa.eu/doi/10.2873/725585.

Hansford, G.S. & Vargas, T. (2001). Chemical and Electrochemical Basis of Bioleaching Process. Hydrometallurgy, 59, 135-145.

Hassanıen, W. A. G., Desouky, O. A. N., & Hussıen, S. S. E. (2013). Bioleaching of some Rare Earth Elements from Egyptian Monazite using Aspergillus ficuum and Pseudomonas aeruginosa. Walailak Journal of Science and Technology (WJST), 11(9), 809–823. Retrieved from https://wjst.wu.ac.th/index.php/wjst/article/view/481

Hocheng, H., Su, C., & Jadhav, U. U. (2014). Bioleaching of metals from steel slag by Acidithiobacillus thiooxidans culture supernatant. Chemosphere, 117, 652-657.

Horeh, N. B., Mousavi, S. M., & Shojaosadati, S. A. (2016). Bioleaching of valuable metals from spent lithium-ion mobile phone batteries using Aspergillus niger. Journal of power sources, 320, 257-266.

Hosseinzadeh, F., Rastegar, S.O. & Ashengroph, M. (2021). Bioleaching of rare

earth elements from spent automobile catalyst as pretreatment method to improve Pt and Pd recovery: Process optimization and kinetic study, Process Biochemistry 105, 1–7, https://doi.org/10.1016/j.procbio.2021.03.022.

Jalali, F., Fakhari, J. & Zolfaghari, A. (2019). Response surface modeling for lab-scale column bioleaching of low-grade uranium ore using a new isolated strain of Acidithiobacillus Ferridurans. Hydrometallurgy.

Jing, R., & Kjellerup, B. V. (2018). Biogeochemical cycling of metals impacting by microbial mobilization and immobilization. Journal of environmental sciences (China), 66, 146–154. https://doi.org/10.1016/j.jes.2017.04.035

Karim, S., & Ting, Y.-P. (2021). Recycling pathways for platinum group metals from spent automotive catalyst: A review on conventional approaches and bio-processes. Resour. Conserv. Recycl. 170, 105588. https://doi.org/10.1016/j. resconrec.2021.105588.

Karim, S., & Ting, Y. P. (2022). Bioleaching of platinum, palladium, and rhodium from spent automotive catalyst using bacterial cyanogenesis. Bioresource Technology Reports, 18, 101069.

Konhauser, K. (2007). Introduction to Geomicrobiology. Oxford: Blackwell.

Krebs, W., Brombacher, C., Bosshard, P.P., Bachofen, R., & Brandl, H. (1997). Microbial recovery of metals from solids. FEMS Microbiology Reviews, 20: 605–617. https://doi.org/10.1111/j.1574-6976.1997.tb00341.x.

Krishnan, S., Zulkapli, N.S., Kamyab, H., Taib, S.M., Din, M.F., Majid, Z.A., Chaiprapat, S., Kenzo, I., Ichikawa, Y., Nasrullah, M., Chelliapan, S., & Othman, N. (2021). Current technologies for recovery of metals from industrial wastes: An overview. Environmental Technology and Innovation, 101525.

Macalady, J., & Banfield, J. F. (2003). Molecular geomicrobiology: genes and geochemical cycling. Earth Planet Sci Lett 209, 1–17.

Marra, A., Cesaro, A., Rene, E. R., Belgiorno, V., & Lens, P. N. L. (2018). Bioleaching of metals from WEEE shredding dust. Journal of environmental management, 210, 180–190. https://doi.org/10.1016/j.jenvman.2017.12.066

McCready, R.G., & Gould, W.D. (1990). Bioleaching of Uranium, Ehrlich, H.L. and Brierly, C.L. (Eds.), Microbial Mineral Recovery, McGraw-Hill, New York, p.107.

Nazari, B., Jorjani, E., Hani, H., Manafi, Z., & Riahi, A. (2014). Formation of jarosite and its effect on important ions for Acidithiobacillus ferrooxidans bacteria. Transactions of Nonferrous Metals Society of China, 24, 1152-1160.

Pradhan, D., Mishra, D., Kim, D.J., Ahn, J.G., Chaudhury, G.R. & Lee, S.W. (2010). Bioleaching kinetics and multivariate analysis of spent petroleum catalyst dissolution using two acidophiles. Journal of Hazardous Materials, 175, 267–273.

Patel, F., & Lakshmi, B. (2021). Bioleaching of copper and nickel from mobile phone printed circuit board using Aspergillus fumigatus A2DS. Brazilian Journal of Microbiology, 52(3), 1475-1487.

Rawlings, D. E., Tributsch, H., & Hansford, G. S. (1999). Reasons why'Leptospirillum'-like species rather than Thiobacillus ferrooxidans are the dominant iron-oxidizing bacteria in many commercial processes for the biooxidation of pyrite and related ores. Microbiology-Reading, 145(1), 5-14.

Rawlings, D. E. (2002). Heavy Metal Mining Using Microbes, Annual Review of Microbiology, 56:65-91.

Reed, D.W., Fujita, Y., Daubaras, D.L., Jiao, Y., & Thompson, V.S. (2016a). Bioleaching of Rare Earth Elements from Waste Phosphors and Cracking Catalysts Title: Bioleaching of Rare Earth Elements from Waste Phosphors and Cracking Catalysts.

Rohwerder, T., Gehrke, T., Kinzler, K., & Sand, W. (2003). Bioleaching review part A: progress in bioleaching: fundamentals and mechanisms of bacterial metal sulfide oxidation. Applied microbiology and biotechnology, 63(3), 239–248. https://doi.org/10.1007/s00253-003-1448-7

Simate, G.S., Ndlovu, S., & Walubita, L.F. (2010). The fungal and chemolithotrophic leaching of nickel laterites — Challenges and opportunities. Hydrometallurgy, 103, 150-157.

Srichandan, H., Pathak, A., Singh, S., Blight, K., Kim, D.J., & Lee, S.W. (2014a). Sequential leaching of metals from spent refinery catalyst in bioleaching-bioleaching and bioleaching-chemical leaching reactor: comparative study. Hydrometallurgy 150, 130–143.

Srichandan, H., & Mishra, S. (2019). Bioleaching approach for extraction of metal values from secondary solid wastes: A critical review. Hydrometallurgy. 189. 105122. 10.1016/j.hydromet.2019.105122.

Uroz, S., Calvaruso, C., Turpault, M.-P., & Frey-Klett, P. (2009). Mineral weathering by bacteria: ecology, actors and mechanisms. Trends Microbiol 17, 378–387

Venkata Mohan, S., Amulya, K., & Annie Modestra, J. (2020). Urban biocycles – Closing metabolic loops for resilient and regenerative ecosystem: A perspective. Bioresources Technology, 306, 123098. https://doi.org/10.1016/j.biortech.2020.123098.

Vera, M., Schippers, A., & Sand, W. (2013). Progress in bioleaching: fundamentals and mechanisms of bacterial metal sulfide oxidation—part A. Applied Microbiology.

Wang, X., & Gaustad, G. (2012). Prioritizing material recovery for end-of-life printed circuit boards. Waste management (New York, N.Y.), 32(10), 1903–1913. https://doi.org/10.1016/j.wasman.2012.05.005

Warren, L. A., & Haack, E. A. (2001). Biogeochemical controls on metal be-

haviour in freshwater environments. Earth Sci Rev 54, 261–320.

Watling, H. R. (2006). The bioleaching of sulphide minerals with emphasis on copper sulphides – a review. Hydrometallurgy, 84: 81–108.

Zhang, M., Guo, X., Tian, B., Wang, J., Qi, S., Yang, Y., & Xin, B. (2019). Improved bioleaching of copper and zinc from brake pad waste by low-temperature thermal pretreatment and its mechanisms. Waste Management, 87, 629–635. https://doi.org/ 10.1016/j.wasman.2019.02.047.

Zhang, R., Hedrich, S., Römer, F., Goldmann, D., & Schippers, A. (2020). Bioleaching of cobalt from Cu/Co-rich sulfidic mine tailings from the polymetallic Rammelsberg mine, Germany Hydrometallurgy, 197, Article 105443.

Zhao, K., Gu, G., Qiu, G., & Wang, X. (2017). Study on the jarosite mediated by bioleaching of pyrrhotite using Acidthiobacillus ferrooxidans . Bioscience Journal, 33(3), 721–729. https://doi.org/10.14393/BJ-v33n3-33824.

CHAPTER 9

ZINC OXIDE NANOPARTICLES - FUNDAMENTALS AND APPLICATIONS

Olcay GENÇYILMAZ[1]

1 Assoc. Prof. Dr., Çankırı Karatekin University, ORCID ID: 0000-0002-7410-2937

1. Nanoparticle and Nanotechnology

The term "nano" has its roots in the Greek word "nanos", which denotes a measure of length at the scale of one billionth of a meter (Boholm, 2016). However, the term "nano" itself does not signify a specific unit of measurement. Rather, it is used for all units of measurement, but usually in units of length, mass, and time. It is worth noting that a nanometer scale is 80,000 times smaller than the diameter of a human hair, 7,000 times smaller than red blood cells, and hundreds of times smaller than the common cold virus (Raffa et al., 2010). Nanotechnology is the technology achieved with particles ranging in size from 1 to 100 nanometers. The concept of nanotechnology was initially introduced in 1959 through a conference led by the renowned scientist, Richard Feynman. In this lecture, Feynman introduced the concept of individually controlling atoms and molecules using sensitive instruments while discussing nanotechnology. This gave rise to the possibility of creating materials of new sizes, possessing distinct physical and chemical features (Demir, 2021). Nanotechnology was initially coined in 1974 by Norio Taniguchi, a Japanese professor at Tokyo's Norio Taniguchi University. The term aimed to identify objects with exceptional accuracy and minimal size. The scanning tunneling microscope was the historic launch and revolution of the nanoworld when it was invented in 1981 by two scientists, Gerd Bing, and the scientist Henrik Rohr, who won the Nobel Prize in Physics in 1986 for this great invention. Subsequently, the progression and evolution of nanotechnology persisted, culminating in the invention of the atomic force microscope, an improved instrument that enables the investigation of applications of nano-objects with dimensions ranging from 1 to 100 nanometers (Dosekova et al., 2017).

Nanotechnology has emerged as a key and highly complex technological domain requiring extensive research and study. Nanotechnology has emerged as a promising technology with applications in many critical areas such as biology, chemistry, and physics (Abdulkadeer, 2016; Öztürk et al., 2016). The superior properties of nanoparticles, over bulk materials, are attributable to their increasingly augmented surface area relative to particle size. The significant differences between nanomaterials and bulk materials lie in their melting point, electronic structure, conductivity, and temperature properties (Yokoyama et al., 2008).

Nanotechnology finds its application in diverse fields, ranging from medicine, optoelectronics, defense, environment, food, to agriculture. Biomedical applications of nanotechnology include tissue engineering, assisting in vaccine development, treating wounds, burns, and diabetes patients, along with manufacturing dental fillings, prostheses, conducting drug delivery, and bioimaging. Nanoparticles prove vital in bioscience in

their anti-cancer and anti-bacterial properties (Xu et al., 2020). They find use in disciplines, including computers, diodes, solar cells, fuel cells, and energy in optoelectronic applications. Besides, they have applications in fields such as textiles, cosmetics, paints, spacecraft, and aircraft. Moreover, they are employed in environmental applications such as desalination of drinking water and air purification. Their use can be seen in agriculture and the fertilizer industry, as well as soil and food processing and packaging (Bavasso et al. 2016).

In nanotechnology, nanoparticles are categorized into semiconductors, metals, and polymers based on their chemical composition. Chemical nano-manufacturing techniques, including the sol-gel, vapor condensation, and mechanical grinding methods are commonly employed; however, they can be costly (Shankar et al., 2004). Zinc oxide has received particular attention from researchers due to its unique properties, which have been further emphasized by recent developments in nanotechnology. Due to its unique optical and electromagnetic properties, it serves as an antibody against fungi and cancer. Additionally, it acts as a catalyst in numerous vital cellular interactions, thereby playing a significant role in medical applications (Padalia and Chanda, 2017).

In recent years, significant advances have been made in nanotechnology for generating diverse nanomaterials using advanced techniques and materials. Environmental pollution resulting from the use of hazardous chemicals is a significant issue when producing nanoparticles using chemical methods. Therefore, biological techniques for nanoparticle synthesis have been proposed as an alternative to their chemical counterparts (Jafarirad et al., 2016). The green synthesis method for nanoparticle production, however, offers an environmentally friendly alternative due to its safety and lack of collateral damage, low cost, energy efficiency, and speed. As a result, it has captured the attention of researchers in recent years (Abd-Elsalam 2021).

2. Zinc Oxide Nanoparticles

Zinc oxide is an inorganic compound with the chemical formula ZnO that is insoluble in water. It is biodegradable and has low toxicity, making it a valuable substance. Due to its unique properties, this oxide is considered one of the most important among semiconductor metals. In materials science, its distinct chemical and physical properties generate significant interest for various applications. In addition to this, zinc oxide particles are favoured for their ease of manufacture, low cost, and lightweight nature (Shaba et al. 2021). Zinc oxide exhibits many properties similar to those of titanium dioxide TiO2, including chemical stability at room temperature and transparency in the visible and infrared spectra (Janotti and Van de Walle, 2009). Zinc oxide nanoparticles are available in a powdered form,

featuring high-temperature resistance, high toughness, a very large surface area, and large photocatalytic activity. The substance is non-harmful and exhibits considerable stability across different environmental circumstances. Additionally, it possesses a sizeable band gap of 3.36 eV (Padmavathy and Vijayaraghavan, 2008).

Zinc oxide belongs to the group (II-VI) of semiconductors, which are situated between ionic and covalent semiconductors. Zinc oxide can exist in various structures including one-dimensional (1D) formations such as nanolines, nano-helices, nanobelts, and nanowires, two-dimensional (2D) structures such as nanoplates and nanospheres, as well as three-dimensional (3D) structures such as flowers. Among these, one-dimensional structures are the most common (Kołodziejczak-Radzimska and Jesionowski 2014). Zinc oxide is a material that exhibits excellent optical properties owing to its high spectral response in both the visible and ultraviolet regions. These characteristics can be altered by introducing impurities or forming the substance into granules. Zinc oxide also possesses notable electrical conductivity and n-type conductivity. The some important properties of zinc oxide in Table 1 (Dakua and Afzulpurkar 2013).

Table 1. *Main properties of ZnO (Dakua and Afzulpurkar 2013)*

Properties	Values
Piezoelectric coefficient	12 pC/N
Exciton binding energy	60 MeV
Refractive index	2.008
Energy band gap	3.36 eV
Intensity	5.606 $g.cm^{-3}$
Melting point	1975 ^{o}C
Boiling point	2360 ^{o}C
Static dielectric constant	8.75
Molecular weight	81.38
Lattice energy	964 kcal/mole
Colour	White

3. Zinc Oxide Nanoparticle Applications

Zinc oxide (ZnO) nanoparticles have gained significant attention in various fields due to their unique properties and wide range of applications. One of the key areas where ZnO nanoparticles have been extensively studied is in biomedical applications (Jiang et al., 2018). ZnO nanoparticles have shown excellent biocompatibility, low toxicity, and economic viability, making them suitable for use in various biomedical applications (Jiang et al., 2018). They have been explored for drug delivery systems, biosensors, and as antimicrobial agents (Jiang et al., 2018). In fact, ZnO nanoparticles have

demonstrated potent bactericidal activity against both Gram-positive and Gram-negative bacteria (Azam et al., 2012). Studies have shown that ZnO nanoparticles exhibit significant growth inhibition against a broad spectrum of microorganisms (Jones et al., 2008). Apart from biomedical applications, ZnO nanoparticles have also found applications in agriculture. They have been used in the development of nanofertilizers and as a means to enhance plant growth and productivity (Sabir et al., 2014).

ZnO nanoparticles have also been investigated for their potential in revolutionizing agriculture through their use in gas sensors, optical devices, and solar cells (Sabir et al., 2014). In addition, ZnO nanoparticles have been utilized in the field of nanotechnology. They have been used in the fabrication of nanorods, which have shown promise in various applications such as cosmetics, polymer films, and chemical sensors (Sotiriou et al., 2014; Khun et al., 2013). ZnO nanoparticles have also been studied for their photocatalytic activity and have been used in the synthesis of Ag-decorated ZnO nanoparticles for enhanced photocatalysis (Khan et al., 2020). Furthermore, the unique properties of ZnO nanoparticles have led to their use in environmental applications. They have been investigated for their potential in reducing DNA damage and for their UV absorption properties, which make them suitable for use in transparent UV protection films (Sotiriou et al., 2014). Overall, ZnO nanoparticles have shown great potential in various fields including biomedical applications, agriculture, nanotechnology, and environmental applications. Their excellent biocompatibility, antimicrobial activity, and unique properties make them a versatile material with a wide range of applications. Fig. 1 shows schematic diagram of ZnO nanoparticles application areas.

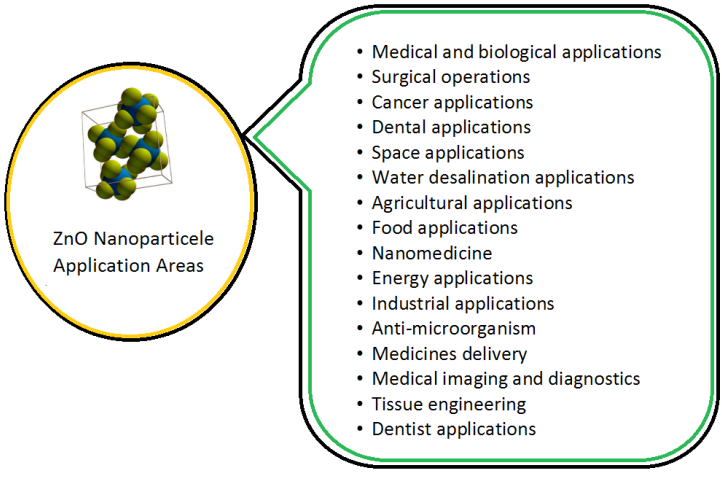

Figure 1. *Application areas of ZnO nanoparticles*

3.1. Medical and biological applications

Zinc oxide particles possess unique physical, chemical, and biological properties that render them applicable in medical and biological settings. They can eliminate the bacterial cell membrane, making them ideal for antibacterial, antifungal, and antiviral applications. Their large surface area in proportion to their size makes them useful for delivering drugs in smaller amounts and with enhanced safety and efficacy. Owing to its unique optical and magnetic characteristics, it has diverse applications in bio-imaging and disease diagnosis equipment (Jiang et al. 2018).

3.2. Dental applications

Zinc oxide nanoparticles are a suitable material for traditional dental treatments and to mitigate complications associated with such treatments. It is worth noting that the utilization of nanotechnology in dental practice has many promising applications that ensure efficient oral care. In orthodontics, nanoprobes are utilised to effectively manage the tissue encompassing the tooth, adjust and manoeuvre the tooth with ease, and increase the longevity of nano fillings (Moradpoor et al., 2021). Fig. 2 shows generally dental applications of ZnO nanoparticles.

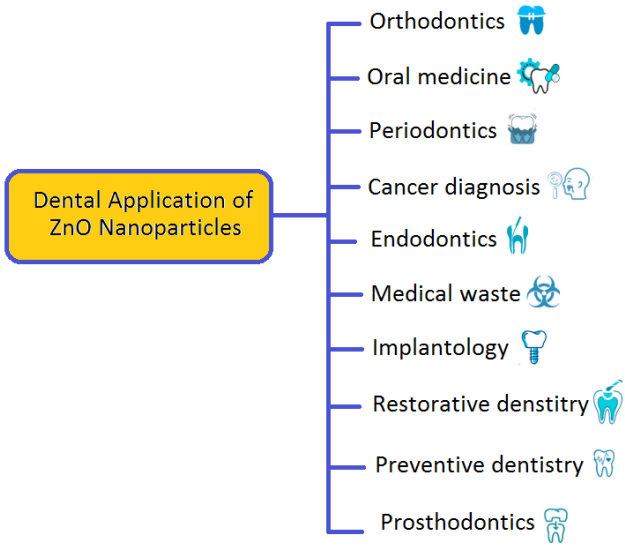

Figure 2. *The dental applications of ZnO nanoparticles*

Dental nanotechnology encompasses nanomaterials and tissue engineering techniques, which are employed to alleviate chronic dentinal hypersensitivity by using biological nanomaterials. In orthodontic proce-

dures, it offers a painless and superior alternative to conventional methods during the manipulation of gingival tissues. Nanobots constitute a further application of nanomaterials within dental practices. Nanobots possess the capability to navigate through delicate human tissues using certain kinetic methods. They are also capable of developing a technology resilient enough to operate under such conditions, penetrate cells securely, and observe nerve impulse movements of nerve cells. Nanobots may be controlled and modified by programming them with pertinent information using particular computers, or by utilising specific notifications directly transmitted by the dentist using audio signals. Additionally, a nano-toothpaste is manufactured, converting the organic matter that is stuck on the gums into a harmless and odourless vapour. Ivory robots are employed to exterminate and eradicate bacteria that cause diseases inside the teeth (Patil et al. 2008).

3.3. Industrial applications

Zinc oxide nanoparticles have a multitude of industrial applications. Furthermore, light-emitting diodes (LEDs) are implemented in the production process of electronic devices, solar cells, lasers, rubber, ceramics, paints, textiles, cosmetics, and other industrial productions, resulting in an immersive range of uses. It is worth noting that the use of materials and devices containing nanoparticles imparts increased durability, reduced weight and size, and greater utility within electronic devices, as substantiated by Hahn (2011).

3.4. Food applications

Zinc oxide particles have potential applications in enhancing food products, treatment, protection against rapid spoilage, and preservation through antioxidant coatings. Furthermore, antimicrobial agents can be added to food packaging to boost its quality and safety (Espitia et al. 2016).

3.5. Agricultural applications

Zinc oxide nanoparticles serve as a substitute for various harmful chemicals used in agricultural goods. They have multiple applications in the agricultural field, as they are suitable for enhancing the quality of products while reducing their costs. By undergoing processes such as filtration and hydrolysis, these nanomaterials facilitate the production of exceptional plant nutrients for crops in minimal quantities without causing any adverse effects (Sabir et al. 2014).

3.6. Water desalination applications

Zinc oxide nanoparticles can be employed in desalinating drinking water, purging industrial waste from it, and converting toxic chemicals

into non-hazardous substances (Rambabu et al., 2021). The past few years have witnessed an upsurge in research activity pertaining to this aspect. Exploiting the photocatalytic nature of ZnO nanoparticles results in the production of highly effective photocatalysts. Exploiting the photocatalytic nature of ZnO nanoparticles results in the production of highly effective photocatalysts.

3.7. Space applications

Zinc oxide nanoparticles find extensive usage in space technology, with their applications being varied and diverse. Specifically, they have proven to be valuable in the manufacturing It makes spacecraft lighter and thus increases fuel efficiency. Furthermore, their nanocoating on space vehicles allows for the construction of more heat-resistant crafts, thereby further enhancing their utility (Shirshneva-Vaschenko et al., 2019).

3.8. Energy applications

Zinc oxide nanomaterials have numerous applications in renewable energy, including solar and wind energy. For instance, nanomaterial-based solar cells exhibit greater energy density, durability, and efficiency in comparison to conventional solar cells (Imran et al., 2017). The usage of nanomaterials in this domain is highly innovative. Ongoing research is being conducted on devices that are capable of generating more electrical energy than mechanical energy, while also possessing faster speeds and increased durability.

3.8. Nanomedicine

Nanomedicine is a crucial and foremost application of nanotechnology due to its intimate association with human life and health. It constitutes the implementation of medical nanotechnology into biological sensors and devices that employ nanomaterials whose dimensions approach those of various biological molecules. Such nanomaterials offer utility in many research and medical domains. The incorporation of nanomaterials into biology has resulted in considerable progress in diagnostic devices, physical therapy, contrast agents and analytical tools (Nayak et al., 2018).

Recent progress in nanotechnology has facilitated the development of novel medical and therapeutic techniques, distinct from those currently employed in disease diagnosis and treatment. For instance, nanotechnology operates through innovative means of drug delivery in the human body, with remarkable precision to target cells throughout. In addition to combatting life-threatening conditions like cancer, nanomedicine and its potential uses are being investigated extensively by research establishments world-

wide. The US Food and Drug Administration approved Doxil as the first nanomedicine for cancer treatment. In 1995, it was utilized to remedy adult carcinomas comprising ovarian cancer, multiple myeloma, and Kaposi's sarcoma, which are infrequent malignancies that target immunocompromised individuals like those who have HIV (Wibroe et al. 2016).

Early detection devices are used for nano-diagnosis of various diseases that can potentially be fatal to the human body. This type of diagnosis involves preparation and recovery from molecular and cellular diseases. The implementation of medical nanotechnology can significantly enhance the accuracy of disease diagnosis within the human body by introducing sensitive nanodevices with the advanced ability to study and detect illnesses at an early stage. Furthermore, these devices offer objective data on identifying harmful particles, quantifying their concentration, detecting cancerous cells, and facilitating their treatment. Nanomaterials possess unique attributes such as distinctive structures, optical properties, magnetic behaviour, and chemical reactivity, which render them valuable in diagnostic imaging and tumour localization within the human anatomy. Nanoparticles differ from non-nanoscale materials due to their significantly larger surface area relative to their size and enhanced adaptability. These properties result from the modified quantitative effect of the nanoscale (Souri et al., 2022).

Nanotechnology has facilitated novel drug delivery approaches, demonstrating the remarkable potential of targeting human cells with nanoparticles. Such methods can significantly mitigate the consumption of drugs and related side effects by administration of minuscule amounts of active substances to precise areas of affliction, eliciting short-lived biochemical reactions. Nanotechnology facilitates drug administration to a particular region of the body over a set duration while yielding low consumption and biological savings through molecular targeting nano-device technology. A key advantage of the implementation of nanoparticles in medical devices is the production of minute nano-devices that can be implanted into the human body. These devices function faster and are more responsive than traditional methods of drug delivery. Nanomedicine endeavours to offer significant novel research equipment and gadgets with the possibility of clinical implementation in the forthcoming future. The National Nanotechnology Initiative anticipates a wide range of applications in drug development, encompassing novel modes for delivering therapies and medications, and imaging techniques like magnetic resonance and ultrasound (Roco 2003).

3.9. Cancer applications

Cancer is a top cause of death in the United Kingdom, and its incidence is on the rise. Nanotechnology is poised to play an important role in can-

cer treatment, particularly in magnetic resonance imaging, due to the unique properties and small size of nanoparticles. A high number of functional groups are linked to nanoparticles due to their large surface area, relative to their size. Nanoparticles have different collecting patterns at the tumor site. Research in the field of nanotechnology is focused on developing nanoparticles capable of both carrying drugs to the tumor site and imaging the tumor non-invasively. It has been discovered that nanoparticles between 10 and 100 nanometers in size can traverse blood vessels, break through capillary barriers and ultimately reach cancerous cells (Wang et al., 2008).

3.10. Medicines delivery

Nanotechnology is focused on enhancing the therapeutic effectiveness of drug molecules within medicine. Medical technology places significant importance on accurately delivering drugs through biological processes in the body using drug carriers. Investigations into the interaction of drug molecules with cells center around modulating the size and shape of these molecules and the chemical traits of their surfaces. Researchers in high-precision nanomaterial nanomedicine technology are currently focusing on drug delivery to body tissues. There is also an emphasis on controlling these molecules, which enables high efficacy, minimal side effects, low drug consumption, and low treatment cost. Nanoparticles, nanotubes and nanocapsules are the most promising forms of drug delivery, as they have a myriad of applications. They are particularly efficient at delivering small drug particles and a variety of biomolecules, including plasmid DNA, proteins and peptides. Fig. 3 illustrates the nanoparticle-mediated drug release mechanism as described by Goldberg et al. in 2007 (Goldberg *et al.* 2007).

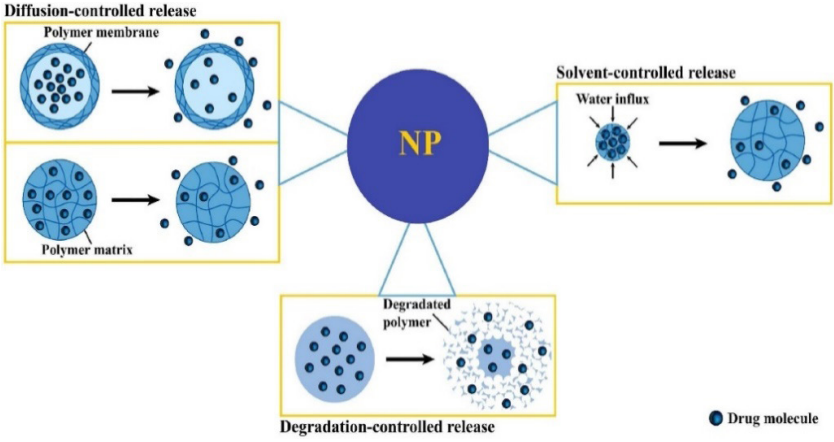

Figure 3. *Continuous mechanisms of drug release from nanoparticles (Souri et al. 2022)*

3.11. Medical imaging and diagnostics

Early disease detection is a key aim of nanotechnology, enabling prompt intervention and reducing complications and additional symptoms. The key factor for making these determinations is molecular imaging and the detection of cellular processes. Nanoparticles are particularly useful in creating contrast and combining multiple features. New designs of molecular imaging contrast media comprise materials appropriate for creating contrast, including fluorescent and paramagnetic, super magnetic, or electron-dense materials. Nano-mediated imaging permits the monitoring of all motilities that materialize in the living tissues of the human body, allowing medical professionals to accurately supervise the progression of medicines in the patient's tissues.

It can be challenging to study certain cells within the body. This has led scientists to utilise coloring techniques to identify them. Additionally, cells emit light waves at various wavelengths, meaning they do not function in a consistent or uniform manner. These factors present a range of obstacles for medical imaging and diagnosis. However, researchers employed nanoparticles to overcome this challenge. Molecules exhibit diverse responses to wave frequencies owing to their intrinsic properties. The application of nanotechnology has facilitated the production of biological tests that can measure the activity of lab equipment with utmost swiftness, precision, and adaptability. To identify particular microbes, magnetic nanoparticles were employed as markers in combination with antibodies. For instance, certain gold nanoparticles are utilized in conjunction with a DNA section to comprehend gene sequence in some samples. The integration of nanoholes in DNA analysis has facilitated the conversion of its unit array into electrical signals. The use of nanoparticles as a contrast agent has further improved the quality and dispersion of ultrasound and magnetic resonance images. Additionally, surgeons can easily locate tumors during surgical operations thanks to the shiny nanoparticles, making the eradication process more efficient (Cormode et al., 2009).

3.12. Anti-microorganism

Excessive and unintentional use of antibiotics causes the development of genetic factors that heighten resistance, leading to amplification in bacterial numbers. This, in turn, increases bacterium resistance to drugs and promotes the spread of biofilms, endangering public health. Antimicrobial agents in the form of nanoparticles or nanocomposites at sizes below 100 nanometers have recently been introduced. Owing to its size, the large surface area of the object results in enhanced interaction with microorganisms, which leads to an improvement in its antimicrobial activity. Certain studies suggest that nanoparticles attack gram-negative bacteria, penetrat-

ing the cell wall and altering the cell membrane's permeability. As a result, an increase in the permeability of the cell membrane has been observed. Controlling the entry of substances through the cytoplasmic membrane is challenging and inevitably fatal for bacterial cells. Nanotechnology biofilm applications combat microbes by destroying their cell membranes, transmitting electrical charges, mechanically killing them, and preventing the emergence of superbugs. Biofilms are formed by a cluster of elongated atomic chains capable of penetrating the cell wall. These chains carry substantial positive charges that draw negatively charged bacteria towards them (Natan and Banin, 2017).

3.13. Surgical operations

Nanorobots are an additional application of nanotechnology in the medical field. In surgical practice, these tiny robots aid doctors during critical and hazardous surgeries. By means of a specialized device, the physician can easily guide and operate the nanorobot with significant accuracy and efficiency. This technique is superior, more precise and less risky compared to conventional surgical methods. The surgical technique involves the use of a manipulative stick by the surgeon to operate the robot's arm which comprises of sensitive instruments and a miniature camera. The stick facilitates the conversion of a large movement into a smaller one, delivering a high level of surgical precision. Fig. 4 illustrates a surgical procedure where each step can be executed, and the video is regularly updated during the cell dissection process (Song et al., 2012).

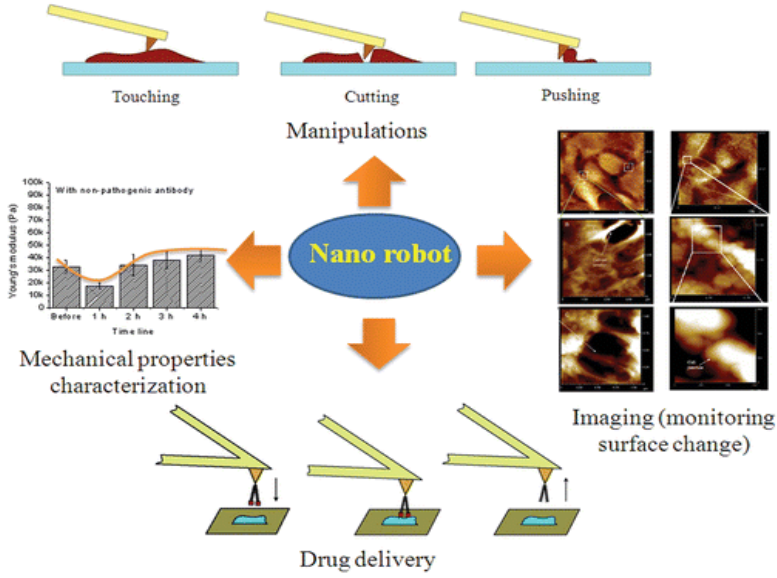

Figure 4. *Mechanism of surgery with a nanorobot (Song et al. 2012)*

3.14. Tissue engineering

Medical nanotechnology has an important application in tissue engineering. Growth factors based on suitable nanomaterials are used to produce, repair and remodel damaged tissues. Tissue engineering could replace conventional treatments like artificial implants or organ transplants. Nanoparticles such as graphene and carbon nanotubes are used as reinforcing agents to make polymeric nanocomposites with high strength and are mechanically biodegradable for bone tissue engineering applications. When added to the polymer matrix at reduced concentrations (~ 0.2 wt %), these nanoparticles notably enhance the compressive and bending mechanical properties of the polymeric nanocomposites (Lalwani et al., 2013).

References

Abd-Elsalam, K. A. (2021), Zinc-Based Nanostructures for Environmental and Agricultural Applications. Elsevier.

Abdulkadeer, M. A. (2016), Synthesis and Characterization of the Golden Nanoparticles and their medical Applications by Using (LALP) Technique, University of Anbar, 128 page, Anbar.

Azam, A., Ahmed, Oves M. M., Khan, Habib S., Memic, A. (2012), Antimicrobial activity of metal oxide nanoparticles against Gram-positive and Gram-negative bacteria: a comparative study, 7, 6003-6009.

Bavasso, I., Vilardi, G., Stoller, M., Chianese, A., Di, Palma, L. (2016), Perspectives in nanotechnology based innovative applications for the environment, Chemical Engineering, 47, 1-6.

Cormode, D. P., Skajaa, T., Fayad, Z. A ., Mulder, W. J. M. (2009), Nanotechnology in medical imaging: probe design and applications, Arteriosclerosis, thrombosis, and vascular biology, 29(7), 992–1000.

Dakua, I. and Afzulpurkar, N. (2013), Piezoelectric energy generation and harvesting at the nano-scale: materials and devices, Nanomaterials and Nanotechnology, 3, 21-31.

Demir, N. (2021), Nanotechnology in cosmetics: opportunities and challenges, NanoEra, 1(1), 19–23.

Dosekova, E., Filip, J., Bertok, T., Both, P., Kasak, P. , Tkac, J. (2017), Nanotechnology in glycomics: applications in diagnostics, therapy, imaging, and separation processes, Medicinal research reviews, 37(3), 514–626.

Espitia, P. J. P., Otoni, C. G.,Soares, N. F. F. (2016), Zinc oxide nanoparticles for food packaging applications, Antimicrobial food packaging, 5(5), 1447-1464.

Goldberg, M., Langer, R., Jia, X. (2007), Nanostructured materials for applications in drug delivery and tissue engineering, Journal of Biomaterials Science, Polymer Edition, 18(3), 241–268.

Hahn, Y. B. (2011), Zinc oxide nanostructures and their applications, Korean Journal of Chemical Engineering, 28(9), 1797–1813.

Imran, M., Haider, S., Ahmad, K., Mahmood, A., Al-Masry, W. A. (2017), Fabrication and characterization of zinc oxide nanofibers for renewable energy applications, Arabian Journal of Chemistry, 10, S1067–S1072.

Jones, N., Ray, B., Ranjit, K. T., Manna, A. C. (2008), Antibacterial activity of ZnO nanoparticle suspensions on a broad spectrum of microorganisms, FEMS Microbiology Letters, 279 (1), 71–76.

Janotti, A., Van de Walle, C. G. (2009), Fundamentals of zinc oxide as a semiconductor, Reports on progress in physics, 72(12), 126501.

Jafarirad, S., Mehrabi, M., Divband, B., Kosari-Nasab, M. (2016), Biofabrication of zinc oxide nanoparticles using fruit extract of Rosa canina and their toxic potential against bacteria: a mechanistic approach, Materials Science and Engineering: C, 59, 296–302.

Jiang, J., Pi, J., Cai, J. (2018), The advancing of zinc oxide nanoparticles for biomedical applications, Bioinorganic chemistry and applications, 1062562, 1-19.

Khan, M. S., Dhavan, P. P., Jadhav, B. L., Shimpi, N. G. (2020), Ultrasound-Assisted Green Synthesis of Ag-Decorated ZnO Nanoparticles UsingExcoecaria agallochaLeaf Extract and Evaluation of Their Photocatalytic and Biological Activity, 5 (41), 12660-12671.

Kołodziejczak-Radzimska, A., Jesionowski, T. (2014), Zinc oxide—from synthesis to application: a review, Materials, 7(4), 2833–2881.

Khun, K., Ibupoto, Z. H., AlSalhi, M. S. Atif, M., Ansari, A. A., Willander, M. (2013), Fabrication of Well-Aligned ZnO Nanorods Using a Composite Seed Layer of ZnO Nanoparticles and Chitosan Polymer, Material, 6 (10), 4361-4374.

Lalwani, G., Henslee, A. M., Farshid, B., Lin, L., Kasper, F. K., Qin, Y. X., Mikos, A. G., Sitharaman, B. (2013), Two-dimensional nanostructure-reinforced biodegradable polymeric nanocomposites for bone tissue engineering, Biomacromolecules, 14(3), 900–909.

Moradpoor, H., Safaei, M., Mozaffari, H. R., Sharifi, R., Imani, M. M., Golshah, A., Bashardoust, N. (2021), An overview of recent progress in dental applications of zinc oxide nanoparticles, RSC Advances, 11(34), 21189–21206.

Natan, M. ,Banin, E. (2017), From nano to micro: using nanotechnology to combat microorganisms and their multidrug resistance, FEMS microbiology reviews, 41(3), 302–322.

Nayak, C., Chandra, I., Singh, P., Singh, S. K. (2018), Omics-based nanomedicine. Synthetic Biology, Fronteir Genetic, 12, 227–248.

Öztürk, Ö., Asıkuzun, E., Hacıoglu, Z. B., Safran, S. (2016), Characteristics of ZnO:Er nano thin films produced different thickness using different solvent by sol-gel method, Journal of Polytechnic, 1, 37-45.

Padmavathy, N., Vijayaraghavan, R. (2008), Enhanced bioactivity of ZnO nanoparticles an antimicrobial study, Science and technology of advanced materials 9(3), 035004.

Padalia, H., Chanda, S. (2017), Characterization, antifungal and cytotoxic evaluation of green synthesized zinc oxide nanoparticles using Ziziphus nummularia leaf extract, Artificial cells, nanomedicine, and biotechnology, 45(8), 1751–1761.

Raffa, V., Vittorio, O., Riggio, C., Cuschieri, A. (2010), Progress in nanotechnology for healthcare. Minimally Invasive Therapy & Allied Technologies, 19(3), 127–135.

Rambabu, K., Bharath, G., Banat, F., Show, P. L. (2021), Green synthesis of zinc oxide nanoparticles using Phoenix dactylifera waste as bioreductant for effective dye degradation and antibacterial performance in wastewater treatment, Journal of hazardous materials, 402, 23560.

Roco, M. C. (2003), Nanotechnology: convergence with modern biology and medicine, Current opinion in biotechnology, 14(3),337–346.

Patil, M., Mehta, D. S., Guvva, S. 2008. Future impact of nanotechnology on medicine and dentistry. Journal of Indian society of periodontology, 12(2): 34-40.

Sabir, S., Arshad, M., Chaudhari, S. K. (2014), Zinc oxide nanoparticles for revolutionizing agriculture: synthesis and applications, The Scientific World Journal, 925494, 1-8.

Shaba, E. Y., Jacob, J. O., Tijani, J. O., Suleiman, M. (2021), A critical review of synthesis parameters affecting the properties of zinc oxide nanoparticle

and its application in wastewater treatment, Applied Water Science, 11(2), 1–41.

Shankar, S. S., Rai, A., Ankamwar, B., Singh, A., Ahmad, A. S. S. (2004), Biological synthesis of triangular gold nanoprisms, Nature materials, 3(7); 482–488.

Shirshneva-Vaschenko, E. V., Shirshnev, P. S., Snezhnaia, Z. G., Sokura, L. A., Bougrov, V. E., Romanov A. E. (2019), Zinc oxide aluminum doped slabs for heat-eliminating coatings of spacecrafts, Acta Astronautica, 163, 107–111.

Song, B., Yang, R., Xi, N., Patterson, K. C., Qu, C., Lai, K. W. C. (2012), Cellular-level surgery using nano robots, Journal of laboratory automation, 17(6), 425–434.

Souri M., Soltani M., Kashkooli F. M., Shahvandi M. K., Chiani M., Shariati F., Merhabi M. R., Munn L. L. (2022), Towards principled design of cancer nanomedicine to accelerate clinical translation, Materials Today Bio, 13(100208), 1-30.

Sotiriou, G. A., Watson, C., Murdaugh, K. M., Darrah, T. H., Pyrgiotakis, G., Elder, A., Brain, J. D., Demokritou, P. (2014), Engineering safer-by-design silica-coated ZnO nanorods with reduced DNA damage potential, Environmental Science: Nano,1, 144-153.

Wang, X., Yang, L., Chen, Z., Shin, D. M. (2008), Application of nanotechnology in cancer therapy and imaging, CA: a cancer journal for clinicians, 58(2), 97–110.

Wibroe, P., Ahmadvand, D., Oghabian, M. A., Yaghmur, A., Moghimi, S. M. (2016), An integrated assessment of morphology, size, and complement activation of the PEGylated liposomal doxorubicin products Doxil®, Caelyx®, DOXOrubicin, and Sina Doxosome, Journal of Controlled Release, 221, 1–8.

Xu, L., Wang, Y. Y., Huang, J., Chen, C. Y., Wang, Z. X., Xie, H. (2020), Silver nanoparticles: Synthesis, medical applications and biosafety, Theranostics, 10(20), 8996.

Yokoyama, T., Masuda, H., Suzuki, M., Ehara, K., Nogi, K., Fuji, M., Fukui, T., Suzuki, H., Tatami, J., Hayashi, K., Toda, K. (2008), Basic properties and measuring methods of nanoparticles', in Nanoparticle technology handbook. Elsevier, pp. 3–48, London.

CHAPTER 10

XYLANASES AND XYLANASE CODING GENES OF ANAEROBIC RUMEN FUNGI

Uğur ÇÖMLEKCIOĞLU[1]

1 Osmaniye Korkut Ata Üniversitesi, Fen Edebiyat Fakültesi, Biyoloji Bölümü, Osmaniye, Türkiye

ANAEROBIC FUNGI IN THE RUMEN MICROBIOTA

The main stored carbon source in nature is plant cell walls and plant cell wall material is the main food of many ruminants (Akin, 1993). Therefore, the rumen is highly adapted for the fermentation of plant cell walls. The cell walls of forage plants that make up the diet of ruminants are complex because they contain protein and many structural carbohydrates. In addition, the structure of the plant cell wall varies greatly depending on the plant species, plant part, tissue type, age of the plant, as well as environmental factors such as temperature, photoperiod, moisture and soil minerals in the plant (Weimer, 1992). Rumen contains one of the most complex microbial ecosystems in nature, and there are bacteria, archaea, protozoa, fungi and bacteriophages in rumen ecosystem (Itabashi, 2004).

Rumen fungi have a very important role in the breakdown of plant cell wall elements by rapidly colonizing and secreting hydrolytic enzymes (Dehhaghi et al., 2020). Rumen fungi are more advantageous than other microorganisms in the degradation of lignocelluloses with the effective enzymes they produce and the rhizomycelium they have. Therefore, rumen fungi play an important role in the degradation of lignocellulosic biomass in rumen (Liang et al., 2020). Most of the enzymes that degrade polysaccharides are localized in the rhizoids, rhizomycelium, but are also secreted extracellularly (Lowe et al., 1987). It has also been reported that anaerobic fungal zoospores produce polysaccharide-degrading enzymes (Williams and Orpin, 1987). Immunofluorescence techniques have shown that enzymes are localized in vesicles, rhizoids, and cell wall surface of ribosome-rich vegetative cells, starting from the germination of zoospores. Enzyme production decreases considerably at the time of sporulation (Breton et al., 1995).

The surface substances of lignin are effectively removed by rumen fungi, thereby significantly increasing the accessibility of degradable cellulose and hemicellulose, so that efficient degradation of lignocellulosic biomass by other rumen microorganisms can be achieved (Yue et al., 2013). The polysaccharide-degrading enzyme activity of anaerobic rumen fungi was approximately 3-6 times higher than that of aerobic fungi such as *Trichoderma reesei*, *T. viridae* and *Aspergillus oryzae* used in many industrial processes (Lee et al., 1999). Additionally, rumen fungi are better than rumen bacteria at breaking down structural barriers in plants because of their ability to extensively degrade some lignified tissues, partially degrade and weaken more resistant tissues, and penetrate the cuticle barrier in forages (Akin and Borneman, 1990). Scanning electron microscope (SEM) photographs in Figure 1 show intensive colonization of wheat straw by *Neocallimastix* sp.

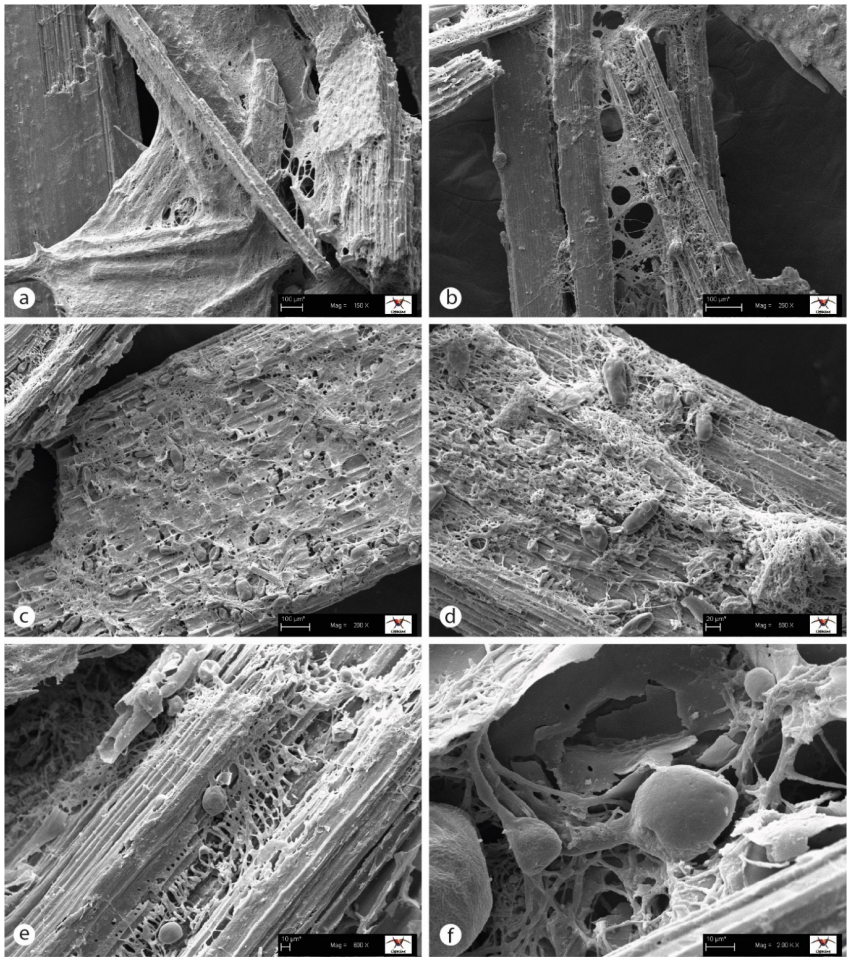

Figure 1. The SEM micrographs of wheat straw incubated for 72 h with Neocallimastix sp. Antibiotic mix added to the culture to inhibit the bacterial growth. Wheat straw was extensively colonized with rhizomycellium (a-b), and sporangia (c-d) of Neocallimastix sp. Colonization of anaerobic fungi on plant fragments showing development of sporangia of Neocallimastix sp. (e-f). The fungal culture was prepared in the Biotechnology laboratory of Biology Department in Kahramanmaras Sutcu Imam University. The SEM micrographs were taken at Research Center for University and Industry Collaboration of Kahramanmaras Sutcu Imam University.

XYLAN AND XYLANASES

The plant cell wall contains three basic polymers. These are cellulose, hemicellulose, and lignin. These structures are generally called lignocellulose (Thomson, 1993). Xylan is the main hemicellulose component of the plant cell wall and is the second most abundant polysaccharide on earth after cellulose (Kulkarni et al., 1999). The amount of xylan varies accord-

ing to the plant. Xylan protects cellulose against enzymatic degradation. When xylan is removed from the plant, cellulose is more susceptible to cellulolytic hydrolysis (Donev et al., 2018). Hemicellulose comprises 15% to 35% of lignocellulosic biomass and differs from cellulose due to its diverse forms, shorter chains, and branching. Like cellulose, it consists of 1,4-linked β-D-pyranol residues such as glucose, mannose, and xylose. The extent of branching and functional groups varies based on the feedstock source. Hemicellulose, a heteropolymer, comprises monosaccharides like pentose, hexoses, acetylated sugars, and uronic acids, with variations used in plant classification (Naidu et al., 2018).

Xylanases (EC 3.2.1.8) are key enzymes for the degradation of xylan and act on the xylan backbone, randomly cleaving the β-1,4-glycosidic bonds between xylopyranosyl residues (Katahira et al., 2004; Malgas et al., 2019). Xylanases have been classified mainly as glycosyl hydrolase family (GH) 10 and 11 based on their amino acid sequence similarity and hydrophobic cluster analysis of the catalytic domains. Compared to xylanases in other GH families, GH11 xylanases are advantageous for many biotechnological applications due to their high substrate selectivity and diverse properties such as high catalytic activity, small size and a range of optimum pH and temperature values (Walia et al., 2017).

Xylanase production has been reported from many organisms such as fungi, bacteria, yeast, marine algae, but the main sources of xylanases are fungi and bacteria. Microbial xylanases have received great attention for application in the feed, food, bioenergy and paper-pulp industries over the past few decades (Wang et al., 2015). Anaerobic fungi have a wide variety of enzymes, for example *Orpinomyces* sp. C1A has been reported to have 357 glycoside hydrolases, 24 polysaccharide lyases, 92 carbohydrate esterases in its genome (Youssef et al., 2013). It was observed that the xylanase is the most active enzyme among all the endo-polysaccharide hydrolase enzymes of anaerobic fungi studied (Borneman et al., 1989).

XYLANASES OF ANAEROBIC FUNGI

Enzymes required to degrade xylan are produced at high levels in both monocentric and polycentric rumen fungi (Comlekcioglu et al., 2011). Xylanase production have been reported for species belong to the genera of *Neocallimastix* (Mountfort and Asher, 1989), *Piromyces* (Dagar et al., 2018; Paul et al., 2010), *Orpinomyces* (Dagar et al., 2018; Ljungdahl, 2008), *Anaeromyces* (Dagar et al., 2018; Novotná et al., 2010), *Caecomyces* (Matsui and Ban-Tokuda, 2008), *Cyllamyces* (Comlekcioglu et al., 2011), *Liebetanzomycespolymorphus* (Joshi et al., 2018), and *Pecoramyces* (Hanafy et al., 2017). Rumen fungi have xylanases both from GH10 and GH11 (Gruninger et al., 2018). Rumen fungi mostly secretes the xy-

lanase enzyme into the culture medium, and only a small amount (<10%) has been reported to be associated with fungal rhizoids (Gomez de Segura et al., 1998; Mountfort and Asher, 1989), while there are also species with significant cellular activity (Lowe et al., 1987).

Although xylan is an important inducer for xylanase production of rumen fungi, xylanase has also been produced in media containing different carbon sources such as wheat straw, cellulose, cellobiose, glucose or xylose (Comlekcioglu U. et al., 2012; Mountfort and Asher, 1989). According to this result, it could be concluded that xylanase is produced at basal level by rumen fungi and increases with the presence of xylan (Lowe et al., 1987). On the other hand, some reports demonstrated the decrease in enzyme production of rumen fungi in the presence of glucose (Henske et al., 2018; Morrison et al., 1990; Williams et al., 1994).

Studies have shown that the xylanases of *Neocallimastix* sp. and *Orpinomyces* sp. are endo-hydrolytic, producing mainly xylobiose, xylotriose and slightly higher xylo-oligosaccharides as products (Comlekcioglu et al., 2014; Liu et al., 2005; Mountfort and Asher, 1989). The subsequent degradation of xylo-oligomers into xylose showed that xylan hydrolysis first started with xylanase and then continued with β-xylosidase (Pearce and Bauchop, 1985). Although most of the β-xylosidase enzyme of *Neocallimastix* sp. is inside the cell, a significant amount is also released outside the cell (Comlekcioglu et al., 2011; Gomez de Segura et al., 1998). For efficient enzyme production of rumen fungi, it is important to keep the concentration of fermentation products, especially acetic acid, at a low level to avoid inhibition of fungal growth and enzyme production using continuous or repeated batch culture systems (Srinivasan et al., 2001). Co-cultures can be a solution to remove fermentation products, for example, the co-culture of *N. frontalis* and *Methanobrevibacter ruminantium* showed high xylanase activity (Wei et al., 2016).

XYLANASE CODING GENES OF ANAEROBIC FUNGI

The detailed characterization of the enzyme systems of anaerobic fungi has been achieved by cloning the enzyme genes. As a result of sequence analysis, horizontal transfer of genes between bacteria and anaerobic fungi in rumen was proposed because of the significant homology between rumen fungal and bacterial xylanases and concluded as xylanase genes of rumen fungi have prokaryotic origin (Comlekcioglu et al., 2010; Gilbert et al., 1992; Zhou et al., 1994). Additionally, it has been observed that rumen fungi carry various catalytic domains with the same or different catalytic properties on a single polypeptide (Gilbert et al., 1992; Xue et al., 1992). The *xylA* gene of *N. patriciarum* contains 2 highly homologous catalytic domains (Gilbert et al., 1992). The catalytic domains of this enzyme were

examined separately in terms of enzyme production in *E. coli* and it was observed that the second domain produced more enzymes than the first domain or the full enzyme carrying two domains (Xue et al., 1995).

Besides catalytic domains, dockerin domains play an important role in the formation of the cellulosome complex known in rumen fungi and the presence of dockerin domain was found in the genes of *xynA* of *N. patriciarum*, *xyn11A* and *xyn11B* of *N. frontalis*, *xynA* of *O. joyonii*, and *xynA* of *Orpinomyces* sp. (Garcia-Vallvé et al., 2000). Dockerin domains allow polysaccharidases to attach to the scaffolding protein and form cellulosome complexes (Raghothama et al., 2001). Dockerin domains in rumen fungal genes can be found single or in pairs. It was found that the double dockerin domain binds to the cellulosome complex more tightly than the single dockerin domain (Nagy et al., 2007). It has been reported that optimum temperature and thermal stability increase when dockerin domains are removed from *xyn11A* and *xyn11B* genes isolated from *N. frontalis* (Huang et al., 2005), on the other hand, deletion of non-catalytic domains of *xynC* from *N. patriciarum* reduced xylanase activity (Liu et al., 1997).

Unlike other rumen fungal xylanases, the XynC enzyme also showed carboxymethylcellulase activity (Liu et al., 1999). Another bifunctional xylanase enzyme was XynS20E from *N. patriciarum* which has axetylxylan esterase and xylanase activities (Pai et al., 2010). As observed in XynC and XynS20E, multiple catalytic activities can be found in an enzyme, on the other hand, multiple enzyme production can be achieved by constructing co-expression vectors. *xynA-7* of *Neocallimastix* sp. and the bifunctional *celA-5* of *Orpinomyces* sp. were co-expressed on a single vector in *E. coli* and thus *E. coli* produced xylanase, carboxymethylcellulase and lichenase enzymes (Comlekcioglu et al., 2017).

The crystal structure of XynCDBFV of *N. patriciarum* revealed that this xylanase had a typical GH11 β-jelly-roll fold, but had an extended N-terminal region consisting of 11 amino acids which is found unique among GH11 xylanases (Cheng et al., 2014b). Mutant xylanases generated using directed evolution of the XynA of *Orpinomyces* sp. PC-2 showed higher thermostability than wild-type XynA (Trevizano et al., 2012). Additionally, a large increase in the specific activity of the XynA of *Orpinomyces* sp. PC-2 was achieved by removing the 27 amino acid residue from the N-terminal of XynA (Ventorim et al., 2018). On the other hand, thermostability of XynCDBFV of *N. patriciarum* was improved based on C-terminus replacement using site-directed mutagenesis (Han et al., 2017). The xylanase (Xyn1B) of *Neocallimastix* sp. GMLF1 was firstly expressed and characterized in *Escherichia coli* (Comlekcioglu et al., 2010), then Xyn1B found to be resistant to xylanase inhibitor protein (XIP), and authors suggested that XIP-resistant xylanase may have an advantage in saccharifica-

tion of barley malt (Zhu et al., 2020).

The *xylP*, *xynF1* and *xylAr10* (isolated from *Piromyces finnis*, uncultured ruminal fungus and *Anaeromyces robustus*, respectively) were expressed by cloning into *Pichia pastoris* (Kalinina et al., 2020; Leng et al., 2018; Wen et al., 2021). *xyn11B* of *N. frontalis* was expressed both in *P. pastoris* and *P. methanolica*, and it was suggested that the purification of xylanase would be easier with the *P. pastoris* while *P. methanolica* produced more xylanase (Tsai and Huang, 2008). *xynR8* of an uncultured rumen fungus was cloned and expressed in *Lactococcus reuteri* which was isolated from the gastrointestinal tract of broiler chickens (Liu et al., 2005). Then, two truncated XynR8 with different lengths were expressed by *L. reuteri*, and it was found that the specific activity of these truncated XynR8 enzymes were higher than the wild type XynR8 (Cheng et al., 2014a). Also, residues N41 and N58 which are important in stabilizing two loops and the structure of XynR8, were mutated to D, and as a result, while N41D mutation improved the tolerance of XynR8 to pH2.0, N58D mutation enhanced both the activity and acid tolerance of XynR8 (Chen et al., 2012).

INDUSTRIAL POTENTIAL OF ANAEROBIC FUNGAL XYLANASES

The xylanase activity of the rumen fungus *Piromyces* is more than three times higher than the enzymes produced by *Trichoderma reesei* and *Aspergillus nidulans*, which are widely used for enzyme production in industry today (Solomon et al., 2016). All anaerobic fungi carry at least a xylanase gene but can also carry genes encoding xylanases with different characteristics (Comlekcioglu, 2023), however, the research on the industrial usage of rumen fungal xylanases is remained limited.

Cellulase-free xylanase enzymes has significantly gained attention during recent years for enhancing brightness during paper-pulp processing (Dutta et al., 2020). A few research was made for pulp bleaching using rumen fungal xylanases. The bleaching of eucalyptus kraft pulp with XynA16 of *Orpinomyces* sp. was resulted with decrease in kappa number, increase in brightness and release of chromophores (Comlekcioglu et al., 2014). The total relative active chlorine savings of the pretreatment of eucalyptus kraft pulp with the xylanase of *Orpinomyces* sp. PC-2 over the acid pretreatment was found to be nearly 23% (Meng et al., 2015). The effects of *Orpinomyces* sp PC-2 xylanase treatment on the fiber surface properties of high yield pulp were investigated and an increase in the atomic oxygen-carbon ratio, a decrease in lignin content and an improvement in the physical strength-related properties of the pulp were observed (Liu et al., 2016).

A recent study demonstrated the utilization of ArXyn10 originating from the anaerobic rumen microorganism *Anaeromyces robustus* in bread making as an application prospect in food industry. In this study, ArXyn10 improved the quality by reducing the hardness and chewiness of the bread (Wen et al., 2021). A novel glycoside hydrolase family 10 (GH10) xylanase gene, ArXyn10c20 obtained from *A. robustus*, has been effectively synthesized and expressed in *Pichia pastoris* GS115. Its application in bread production led to remarkable improvements: a significant reduction in bread hardness (by 42.2%), gumminess (by 45.3%), and chewiness (by 55.4%), accompanied by an 18.7% increase in reducing sugar content. These findings underscore the immense potential of the newly discovered ArXyn10c20 xylanase in the food industry (Liu et al., 2022). In summary, anaerobic fungal xylanases represent a promising and unexplored asset that holds significant potential for a wide array of biotechnological applications.

CONCLUSION

Rumen fungi are beneficial microorganisms for ruminants, therefore, a better understanding of the enzyme systems of anaerobic rumen fungi is significantly important for the gut health of the ruminants. Furthermore, the rich enzymatic variety of rumen fungi possess a significant application potential for different industries such as feed, food, paper, textile, pharmaceuticals, and biofuels. However, studies on regulation, function, production, structures, and functional mechanisms of complex enzyme system of rumen fungi are still limited. In more than 40 years since the discovery of anaerobic fungi, culture-based studies on rumen fungi have resulted in the discovery of new species, and 20 genera have been reported for rumen fungi: *Aestipascuomyces, Agriosomyces, Aklioshbomyces, Anaeromyces, Buwchfawromyces, Caecomyces, Capellomyces, Cyllamyces, Feramyces, Ghazallomyces, Joblinomyces, Khoyollomyces, Liebetanzomyces, Neocallimastix, Oontomyces, Orpinomyces, Paucimyces, Pecoramyces, Piromyces,* and *Tahromyces* (Stabel et al., 2021). Although the rumen fungi species discovered in the last decade have increased, there is not enough information about the enzymatic properties of many of them. Moreover, metagenomic studies have revealed that there are undiscovered rumen fungal species yet (Edwards et al., 2017; Rabee et al., 2019). Recent advances in molecular techniques can isolate the enzyme genes of rumen fungi without the need for culture techniques and enable them to be expressed heterologously in different hosts. However, it is also necessary to culture the rumen fungi and carry out detailed research on their enzyme systems for sustainable livestock production by reducing the environmental footprint.

REFERENCES

Akin, D.E. 1993. Perspectives of Cell Wall Biodegradation—Session Synopsis, In: Forage Cell Wall Structure and Digestibility. 73-82.

Akin, D.E., Borneman, W.S., 1990. Role of Rumen Fungi in Fiber Degradation. Journal of Dairy Science 73, 3023-3032.

Borneman, W.S., Akin, D.E., Ljungdahl, L.G., 1989. Fermentation products and plant cell wall-degrading enzymes produced by monocentric and polycentric anaerobic ruminal fungi. Applied and Environmental Microbiology 55, 1066-1073.

Breton, A., Gaillard-Martine, B., Gerbi, C., de Ségura, B.G., Durand, R., Kherratia, B., 1995. Location by fluorescence microscopy of glycosidases and a xylanase in the anaerobic gut fungi Caecomyces communis, Neocallimastix frontalis, and Piromyces rhizinflata. Current Microbiology 31, 224-227.

Chen, Y.-C., Chiang, Y.-C., Hsu, F.-Y., Tsai, L.-C., Cheng, H.-L., 2012. Structural modeling and further improvement in pH stability and activity of a highly-active xylanase from an uncultured rumen fungus. Bioresource Technology 123, 125-134.

Cheng, H.-L., Hu, C.-Y., Lin, S.-H., Wang, J.-Y., Liu, J.-R., Chen, Y.-C., 2014a. Characterization of two truncated forms of xylanase recombinantly expressed by Lactobacillus reuteri with an introduced rumen fungal xylanase gene. Enzyme and Microbial Technology 64-65, 6-10.

Cheng, Y.-S., Chen, C.-C., Huang, C.-H., Ko, T.-P., Luo, W., Huang, J.-W., Liu, J.R., Guo, R.-T., 2014b. Structural Analysis of a Glycoside Hydrolase Family 11 Xylanase from Neocallimastix patriciarum: Insights into the molecular basis of a thermophilic enzyme. Journal of Biological Chemistry, 289(16), 11020-11028.

Comlekcioglu, U., 2023. Screening, Cloning and Characteristics of the Common Xylanase Gene in Anaerobic Fungi. Iranian Journal of Applied Animal Science 13, 113-119.

Comlekcioglu, U., Aygan, A., Yazdic, F.C., Ozkose, E., 2011. Effects of various agro-wastes on xylanase and b-xylosidase production of anaerobic ruminal fungi. J Sci Indus Res 70, 293-299.

Comlekcioglu, U., Gunes, M., Altun, H., Ekiz, D.O., Aygan, A., 2017. Coexpression of rumen fungal xylanase and bifunctional cellulase genes in Escherichia coli. Brazilian Archives of Biology and Technology 60.

Comlekcioglu, U., Ozkose, E., Tutus, A., Akyol, I., Ekinci, M., 2010. Cloning and characterization of cellulase and xylanase coding genes from anaerobic fungus Neocallimastix sp. GMLF1. Int J Agric Biol 12, 691-696.

Comlekcioglu, U., Tutus, A., Cicekler, M., Gunes, M., Aygan, A., 2014. Application of recombinant xylanase from Orpinomyces sp. in elemental chlorine-free bleaching of kraft pulps. Rom Biotechnol Lett 19, 8941-8950.

Comlekcioglu U., Yazdic F.C., Keser S., Kelleci B.M., Battaloglu G., E., O., 2012. Effects of Carbon Sources on Enzyme Production of Neocallimastix sp. ve Orpinomyces sp. Kafkas Üniversitesi Veterinerlik Fakültesi Dergisi 18, 799-806.

Dagar, S.S., Kumar, S., Mudgil, P., Puniya, A.K., 2018. Comparative evaluation of lignocellulolytic activities of filamentous cultures of monocentric and polycentric anaerobic fungi. Anaerobe 50, 76-79.

Dehhaghi, M., Kazemi Shariat Panahi, H., Salehi Jouzani, G., Nallusamy, S., Gupta, V.K., Aghbashlo, M., Tabatabaei, M. 2020. Anaerobic Rumen Fungi for Biofuel Production, In: Salehi Jouzani, G., Tabatabaei, M., Aghbashlo, M. (Eds.) Fungi in Fuel Biotechnology. Springer International Publishing, Cham, 149-175.

Donev, E., Gandla, M.L., Jönsson, L.J., Mellerowicz, E.J., 2018. Engineering Non-cellulosic Polysaccharides of Wood for the Biorefinery. Frontiers in Plant Science 9.

Dutta, P.D., Neog, B., Goswami, T., 2020. Xylanase enzyme production from Bacillus australimaris P5 for prebleaching of bamboo (Bambusa tulda) pulp. Materials Chemistry and Physics 243, 122227.

Edwards, J.E., Forster, R.J., Callaghan, T.M., Dollhofer, V., Dagar, S.S., Cheng, Y., Chang, J., Kittelmann, S., Fliegerova, K., Puniya, A.K., Henske, J.K., Gilmore, S.P., O'Malley, M.A., Griffith, G.W., Smidt, H., 2017. PCR and Omics Based Techniques to Study the Diversity, Ecology and Biology of Anaerobic Fungi: Insights, Challenges and Opportunities. Frontiers in Microbiology 8.

Garcia-Vallvé, S., Romeu, A., Palau, J., 2000. Horizontal Gene Transfer of Glycosyl Hydrolases of the Rumen Fungi. Molecular Biology and Evolution 17, 352-361.

Gilbert, H.J., Hazlewood, G.P., Laurie, J.I., Orpin, C.G., Xue, G.P., 1992. Homologous catalytic domains in a rumen fungal xylanase: evidence for gene duplication and prokaryotic origin. Molecular Microbiology 6, 2065-2072.

Gomez de Segura, B., Durand, R., Fèvre, M., 1998. Multiplicity and expression of xylanases in the rumen fungus Neocallimastix frontalis. FEMS Microbiology Letters 164, 47-53.

Gruninger, R.J., Nguyen, T.T.M., Reid, I.D., Yanke, J.L., Wang, P., Abbott, D.W., Tsang, A., McAllister, T., 2018. Application of Transcriptomics to Compare the Carbohydrate Active Enzymes That Are Expressed by Diverse Genera of Anaerobic Fungi to Degrade Plant Cell Wall Carbohydrates. Frontiers in Microbiology 9.

Han, N., Miao, H., Ding, J., Li, J., Mu, Y., Zhou, J., Huang, Z., 2017. Improving the thermostability of a fungal GH11 xylanase via site-directed mutagenesis guided by sequence and structural analysis. Biotechnology for Biofuels 10, 133.

Hanafy, R.A., Elshahed, M.S., Liggenstoffer, A.S., Griffith, G.W., Youssef, N.H., 2017. Pecoramyces ruminantium, gen. nov., sp. nov., an anaerobic gut fungus from the feces of cattle and sheep. Mycologia 109, 231-243.

Henske, J.K., Gilmore, S.P., Haitjema, C.H., Solomon, K.V., O'Malley, M.A., 2018. Biomass-degrading enzymes are catabolite repressed in anaerobic gut fungi. AIChE Journal 64, 4263-4270.

Huang, Y.-H., Huang, C.-T., Hseu, R.-S., 2005. Effects of dockerin domains on Neocallimastix frontalis xylanases. FEMS Microbiology Letters 243, 455-460.

Itabashi, H., 2004. Recent Topics in Rumen Microbiology with Particular Reference to Animal Production in Japan. Microbes and Environments 19, 270-275.

Joshi, A., Lanjekar, V.B., Dhakephalkar, P.K., Callaghan, T.M., Griffith, G.W., Dagar, S.S., 2018. Liebetanzomycespolymorphus gen. et sp. nov., a new anaerobic fungus (Neocallimastigomycota) isolated from the rumen of a goat. MycoKeys, 89-110.

Kalinina, A.N., Borshchevskaya, L.N., Gordeeva, T.L., Sineoky, S.P., 2020. Expression of the Xylanase Gene from Pyromyces finnis in Pichia pastoris and Characterization of the Recombinant Protein. Applied Biochemistry and Microbiology 56, 787-793.

Katahira, S., Fujita, Y., Mizuike, A., Fukuda, H., Kondo, A., 2004. Construction of a Xylan-Fermenting Yeast Strain through Codisplay of Xylanolytic Enzymes on the Surface of Xylose-Utilizing Saccharomyces cerevisiae Cells. Applied and Environmental Microbiology 70, 5407-5414.

Kulkarni, N., Shendye, A., Rao, M., 1999. Molecular and biotechnological aspects of xylanases. FEMS Microbiology Reviews 23, 411-456.

Lee, S.S., Shin, K.J., Kim, W.Y., Ha, J.K., Han, I.K., 1999. The Rumen Ecosystem : As a Fountain Sources of Nobel Enzymes - Review. Asian-Australas J Anim Sci 12, 988-1001.

Leng, J., Liu, X., Zhang, C., Zhu, R., Mao, H., 2018. Gene cloning and expression of fungal lignocellulolytic enzymes from the rumen of gayal (Bos frontalis). The Journal of General and Applied Microbiology 64, 9-14.

Liang, J., Nabi, M., Zhang, P., Zhang, G., Cai, Y., Wang, Q., Zhou, Z., Ding, Y., 2020. Promising biological conversion of lignocellulosic biomass to renewable energy with rumen microorganisms: A comprehensive review. Renewable and Sustainable Energy Reviews 134, 110335.

Liu, J.-H., Selinger, B.L., Tsai, C.-F., Cheng, K.-J., 1999. Characterization of a Neocallimastix patriciarum xylanase gene and its product. Canadian Journal of Microbiology 45, 970-974.

Liu, J.-H., Selinger, L.B., Cheng, K.-J., Beauchemin, K.A., Moloney, M.M., 1997. Plant seed oil-bodies as an immobilization matrix for a recombinant

xylanase from the rumen fungus Neocallimastix patriciarum. Molecular Breeding 3, 463-470.

Liu, J.-R., Yu, B., Lin, S.-H., Cheng, K.-J., Chen, Y.-C., 2005. Direct cloning of a xylanase gene from the mixed genomic DNA of rumen fungi and its expression in intestinal Lactobacillus reuteri. FEMS Microbiology Letters 251, 233-241.

Liu, Y.-y., Liu, M.-r., Li, H.-l., Li, B.-y., Zhang, C.-h., 2016. Characteristics of high yield pulp fibers by xylanase treatment. Cellulose 23, 3281-3289.

Liu, Z., Wen, S., Wu, G., Wu, H., 2022. Heterologous expression and characterization of Anaeromyces robustus xylanase and its use in bread making. European Food Research and Technology 248, 2311-2324.

Ljungdahl, L.G., 2008. The Cellulase/Hemicellulase System of the Anaerobic FungusOrpinomycesPC-2 and Aspects of Its Applied Use. Annals of the New York Academy of Sciences 1125, 308-321.

Lowe, S.E., Theodorou, M., Trinci, A., 1987. Cellulases and xylanase of an anaerobic rumen fungus grown on wheat straw, wheat straw holocellulose, cellulose, and xylan. Applied and environmental microbiology 53, 1216-1223.

Malgas, S., Mafa, M.S., Mkabayi, L., Pletschke, B.I., 2019. A mini review of xylanolytic enzymes with regards to their synergistic interactions during hetero-xylan degradation. World Journal of Microbiology and Biotechnology 35, 187.

Matsui, H., Ban-Tokuda, T., 2008. Studies on Carboxymethyl Cellulase and Xylanase Activities of Anaerobic Fungal Isolate CR4 from the Bovine Rumen. Current Microbiology 57, 615-619.

Meng, Q., Fu, S., Li, B., Lucia, L.A., 2015. The Impact of Xylanase and Hot Acid Pretreatment on HexAs in Eucalyptus Kraft Pulp Bleaching. Journal of Wood Chemistry and Technology 35, 239-250.

Morrison, M., Mackie, R.I., Kistner, A., 1990. Evidence that Cellulolysis by an Anaerobic Ruminal Fungus Is Catabolite Regulated by Glucose, Cellobiose, and Soluble Starch. Applied and Environmental Microbiology 56, 3227-3229.

Mountfort, D.O., Asher, R.A., 1989. Production of xylanase by the ruminal anaerobic fungus Neocallimastix frontalis. Applied and Environmental Microbiology 55, 1016-1022.

Nagy, T., Tunnicliffe, R.B., Higgins, L.D., Walters, C., Gilbert, H.J., Williamson, M.P., 2007. Characterization of a Double Dockerin from the Cellulosome of the Anaerobic Fungus Piromyces equi. Journal of Molecular Biology 373, 612-622.

Naidu, D.S., Hlangothi, S.P., John, M.J., 2018. Bio-based products from xylan: A review. Carbohydrate Polymers 179, 28-41.

Novotná, Z., Procházka, J., Šimůnek, J., Fliegerová, K., 2010. Xylanases of anaer-

obic fungus Anaeromyces mucronatus. Folia Microbiologica 55, 363-367.

Pai, C.-K., Wu, Z.-Y., Chen, M.-J., Zeng, Y.-F., Chen, J.-W., Duan, C.-H., Li, M.-L., Liu, J.-R., 2010. Molecular cloning and characterization of a bifunctional xylanolytic enzyme from Neocallimastix patriciarum. Applied Microbiology and Biotechnology 85, 1451-1462.

Paul, S.S., Deb, S.M., Punia, B.S., Singh, D., Kumar, R., 2010. Fibrolytic potential of anaerobic fungi (Piromyces sp.) isolated from wild cattle and blue bulls in pure culture and effect of their addition on in vitro fermentation of wheat straw and methane emission by rumen fluid of buffaloes. Journal of the Science of Food and Agriculture 90, 1218-1226.

Pearce, P.D., Bauchop, T., 1985. Glycosidases of the rumen anaerobic fungus Neocallimastix frontalis grown on cellulosic substrates. Applied and Environmental Microbiology 49, 1265-1269.

Rabee, A.E., Forster, R.J., Elekwachi, C.O., Kewan, K.Z., Sabra, E.A., Shawket, S.M., Mahrous, H.A., Khamiss, O.A., 2019. Community structure and fibrolytic activities of anaerobic rumen fungi in dromedary camels. Journal of Basic Microbiology 59, 101-110.

Raghothama, S., Eberhardt, R.Y., Simpson, P., Wigelsworth, D., White, P., Hazlewood, G.P., Nagy, T., Gilbert, H.J., Williamson, M.P., 2001. Characterization of a cellulosome dockerin domain from the anaerobic fungus Piromyces equi. Nature Structural Biology 8, 775-778.

Solomon, K.V., Haitjema, C.H., Henske, J.K., Gilmore, S.P., Borges-Rivera, D., Lipzen, A., Brewer, H.M., Purvine, S.O., Wright, A.T., Theodorou, M.K., Grigoriev, I.V., Regev, A., Thompson, D.A., O'Malley, M.A., 2016. Early-branching gut fungi possess a large, comprehensive array of biomass-degrading enzymes. Science 351, 1192-1195.

Srinivasan, K., Murakami, M., Nakashimada, Y., Nishio, N., 2001. Efficient production of cellulolytic and xylanolytic enzymes by the rumen anaerobic fungus, Neocallimastix frontalis, in a repeated batch culture. Journal of Bioscience and Bioengineering 91, 153-158.

Stabel, M., Schweitzer, T., Haack, K., Gorenflo, P., Aliyu, H., Ochsenreither, K., 2021. Isolation and Biochemical Characterization of Six Anaerobic Fungal Strains from Zoo Animal Feces. Microorganisms 9, 1655.

Thomson, J.A., 1993. Molecular biology of xylan degradation. FEMS Microbiology Letters 104, 65-82.

Trevizano, L.M., Ventorim, R.Z., de Rezende, S.T., Silva Junior, F.P., Guimarães, V.M., 2012. Thermostability improvement of Orpinomyces sp. xylanase by directed evolution. Journal of Molecular Catalysis B: Enzymatic 81, 12-18.

Tsai, C.T., Huang, C.-T., 2008. Overexpression of the Neocallimastix frontalis xylanase gene in the methylotrophic yeasts Pichia pastoris and Pichia methanolica. Enzyme and Microbial Technology 42, 459-465.

Ventorim, R.Z., de Oliveira Mendes, T.A., Trevizano, L.M., dos Santos Camargos, A.M., Guimarães, V.M., 2018. Impact of the removal of N-terminal non-structured amino acids on activity and stability of xylanases from Orpinomyces sp. PC-2. International Journal of Biological Macromolecules 106, 312-319.

Walia, A., Guleria, S., Mehta, P., Chauhan, A., Parkash, J., 2017. Microbial xylanases and their industrial application in pulp and paper biobleaching: a review. 3 Biotech 7, 11.

Wang, Q., Luo, Y., He, B., Jiang, L.-S., Liu, J.-X., Wang, J.-K., 2015. Characterization of a Novel Xylanase Gene from Rumen Content of Hu Sheep. Applied Biochemistry and Biotechnology 177, 1424-1436.

Wei, Y.-Q., Long, R.-J., Yang, H., Yang, H.-J., Shen, X.-H., Shi, R.-F., Wang, Z.-Y., Du, J.-G., Qi, X.-J., Ye, Q.-H., 2016. Fiber degradation potential of natural co-cultures of Neocallimastix frontalis and Methanobrevibacter ruminantium isolated from yaks (Bos grunniens) grazing on the Qinghai Tibetan Plateau. Anaerobe 39, 158-164.

Weimer, P.J., 1992. Cellulose Degradation by Ruminal Microorganisms. Critical Reviews in Biotechnology 12, 189-223.

Wen, S., Wu, G., Wu, H., 2021. Biochemical characterization of a GH10 xylanase from the anaerobic rumen fungus Anaeromyces robustus and application in bread making. 3 Biotech 11, 406.

Williams, A.G., Orpin, C.G., 1987. Glycoside hydrolase enzymes present in the zoospore and vegetative growth stages of the rumen fungi Neocallimastix patriciarum, Piromonas communis, and an unidentified isolate, grown on a range of carbohydrates. Canadian Journal of Microbiology 33, 427-434.

Williams, A.G., Withers, S.E., Orpin, C.G., 1994. Effect of the carbohydrate growth substrate on polysaccharolytic enzyme formation by anaerobic fungi isolated from the foregut and hindgut of nonruminant herbivores and the forestomach of ruminants. Letters in Applied Microbiology 18, 147-151.

Xue, G.-p., Denman, S.E., Glassop, D., Johnson, J.S., Dierens, l.M., Gobius, K.S., Aylward, J.H., 1995. Modification of a xylanase cDNA isolated from an anaerobic fungus Neocallimastix patriciarum for high-level expression in Escherichia coli. Journal of Biotechnology 38, 269-277.

Xue, G.-P., Gobius, K.S., Orpin, C.G., 1992. A novel polysaccharide hydrolase cDNA (celD) from Neocallimastix patriciarum encoding three multi-functional catalytic domains with high endoglucanase, cellobiohydrolase and xylanase activities. Microbiology 138, 2397-2403.

Youssef, N.H., Couger, M.B., Struchtemeyer, C.G., Liggenstoffer, A.S., Prade, R.A., Najar, F.Z., Atiyeh, H.K., Wilkins, M.R., Elshahed, M.S., 2013. The Genome of the Anaerobic Fungus Orpinomyces sp. Strain C1A Reveals the Unique Evolutionary History of a Remarkable Plant Biomass Degrader. Applied and Environmental Microbiology 79, 4620-4634.

Yue, Z.-B., Li, W.-W., Yu, H.-Q., 2013. Application of rumen microorganisms for anaerobic bioconversion of lignocellulosic biomass. Bioresource Technology 128, 738-744.

Zhou, L., Xue, G.P., Orpin, C.G., Black, G.W., Gilbert, H.J., Hazlewood, G.P., 1994. Intronless celB from the anaerobic fungus Neocallimastix patriciarum encodes a modular family A endoglucanase. Biochemical Journal 297, 359-364.

Zhu, D., Liu, X., Xie, X., Yang, S., Lin, H., Chen, H., 2020. Characteristics of a XIP-resistant xylanase from Neocallimastix sp. GMLF1 and its advantage in barley malt saccharification. International Journal of Food Science & Technology 55, 2152-2160.

CHAPTER 11

KKT-TYPE OPTIMALITY CRITERIA FOR FUZZY VALUED FRACTIONAL OPTIMIZATION

Hasan DALMAN[1]

1 Associate Professor , Batman University, Department of Mathematics, ORCID: https://orcid.org/0009-0008-6574-3215

1. Introduction

Zadeh introduced the application of fuzzy set theory to mathematical programming in 1965 (Zadeh, 1965). In 1970, Bellman and Zadeh proposed aggregation algorithms to enhance the optimization of fuzzy collections (Bellman & Zadeh, 1970). Zimmermann (1978) was the first to successfully employ fuzzy set theory in multi-objective optimization, marking a significant milestone in this field. In 1991, Zimmermann coined the term "fuzzy-valued optimization" to describe the modeling of real-world problems with fuzzy parameters (Zimmermann, 1991). These issues encompass constraints, objective functions, or a combination of both, and numerous approaches have been developed to address them (Zimmermann, 1991).

Fuzzy function-based optimization is a complex subfield of fuzzy optimization, and it involves optimization problems where the objective function and/or constraints exhibit fuzzy values. This specialized area was pioneered by Wu in 2007, who extensively explored the intricacies of fuzzy function-based optimization (Wu, 2007). Wu (2009a) made substantial advancements by introducing Karush-Kuhn-Tucker (KKT) optimality criteria specifically tailored to this category of fuzzy optimization problems. Furthermore, in 2009, Wu (2009b) extended this line of research by incorporating level-wise differentiability and Hukuhara differentiable fuzzy functions into the framework. Rufián-Lizana et al. (2012) further contributed to the advancement of knowledge in this domain by conducting comprehensive research on fuzzy function-based optimization challenges, building upon the foundational work.

Chalco-Cano et al. (2013a) delved into the complexities of differential calculus for functions with fuzzy interval values and employed the generalized Hukuhara differentiability paradigm for a thorough examination of optimization problems featuring interval-valued objective functions. They introduced KKT conditions based on generalized Hukuhara derivatives, capable of handling two distinct order relations within the interval space (Chalco-Cano et al., 2013b). Moreover, Chalco-Cano et al. (2016) proposed KKT-type optimality criteria for non-differentiable functions within fuzzy optimization contexts, with a focus on improving the understanding of fuzzy optimization with interval-valued objectives. Their work centered on the sophisticated concepts of

Generalized Hukuhara (GH) differentiability and pseudo-invex fuzzy-valued functions, as detailed in their studies (Chalco-Cano et al., 2013a, 2013b, 2016).

It's noteworthy that there has been extensive research on fractional optimization problems (Pop & Stancu-Minasian, 2008). Dinkelbach (1967) developed a parametric approach for transforming fractional optimization into non-fractional optimization, while Jagannathan (1966) explored the relationship between parametric and fractional optimization. Su and Hang (2022) investigated non-smooth multi-objective fractional optimization problems with set, generalized inequality, and equality constraints, providing conditions for local weak minimizers with primary and secondary optimality constraints. In 2023, Thuy and Su addressed an uncertain non-smooth multi-objective fractional semi-infinite optimization problem with resistant Karush-Kuhn-Tucker optimality constraints. Su and Hang (2023) established second-order optimality requirements for both rigorous and weak local Pareto minima in a local Lipschitz multi-objective fractional optimization problem with inequality constraints.

Recently, Agarwal et al. (2023) successfully tackled Fuzzy-valued Interval Fractional Optimization Problems (FVIFOPs) by leveraging level-wise differentiability and Hukuhara differentiable fuzzy functions. Additionally, Chalco-Cano et al. (2016) outlined a methodology for addressing fuzzy-valued optimization problems, delving into the properties of fuzzy-valued functions in various scenarios with a focus on their behavior at specific points. The study brings attention to the underexplored research area of Fuzzy Valued Interval Fractional Optimization (FIVFOP). Consequently, this investigation concentrates on FIVFOP to identify effective solutions based on the findings of Chalco-Cano et al. (2016). Using a scalar weighting technique, FIVFOP is initially transformed into a Fractional Optimization Problem (FOP). Subsequently, the FOP is converted into a single-objective non-fractional optimization problem utilizing the Dinkelbach (1967) method. The efficient solution is derived by presenting KKT conditions using the Lagrange multipliers method within the Maple 2023 program. Finally, a numerical example is presented to demonstrate the accuracy of the proposed solution methodology.

2. Preliminaries

The symbol $\mathcal{K}_C$ r denotes the set of closed intervals on the real number line, which is defined as:

$$\mathcal{K}_C = \{[a^L, a^U] | \ a^L, a^U \in \mathbb{R}, a^L \leq a^U\}.$$

Definition 1: A fuzzy set on $\mathbb{R}^n$ can be defined in mathematics as a mapping ρ that assigns a value between 0 and 1 to each element in $\mathbb{R}^n$. The set of all items in $\mathbb{R}^n$ whose assigned value by ρ is larger than or equal to α, and is referred to as the α - level set of a fuzzy set ρ and is denoted as $[\rho]^\alpha$. A fuzzy set's support ρ is the set of all elements in $\mathbb{R}^n$ whose given value by ρ is positive, and is denoted as $\text{supp}(\rho)$.

Definition 2: A fuzzy interval is defined as a fuzzy set ρ on the real number line $\mathbb{R}$, which must adhere to the following criteria: ρ is a continuous function that assigns membership values between 0 and 1 to elements in the real number universe $\mathbb{R}$. The membership function is required to exhibit upper semi-continuity and possess a peak value of 1 at some specific point x_0. This condition implies that the membership function must satisfy a particular type of triangle inequality. Moreover, the set of points characterized by a positive membership function must be compact, and $[\rho]^0$ also must be compact.

2.1. Operations on Fuzzy Intervals

Let $\mathcal{F}_C$ represent the set of all fuzzy intervals. For any ρ in $\mathcal{F}_C$, $[\rho]^\alpha$ is a member of $\mathcal{K}_C$ for α values ranging from 0 to 1, both inclusive.

The fuzzy intervals ρ and ϵ in $\mathcal{F}_C$, represented by $\left[\rho_\alpha^L, \rho_\alpha^L\right]$ and $\left[\epsilon_\alpha^L, \epsilon_\alpha^L\right]$ respectively, may be combined together to form $\rho + \epsilon$, and scalar multiplication $\lambda\rho$ can be defined for any real number λ:

$$(\rho+\epsilon)(x)=\sup_{y+z=x}\min\{\rho(y),\epsilon(z)\}$$

$$(\lambda\rho)(x)=\begin{cases}\rho\left(\dfrac{x}{\lambda}\right), & \text{if } \lambda\neq 0,\\ 0, & \text{if } \lambda=0.\end{cases}$$

Moreover $\forall\alpha\in[0,1]$:

$$\left[\rho+\epsilon^{\alpha}\right]=\left[\rho^{L}+\epsilon^{L}{}_{\alpha},\rho^{R}+\epsilon^{R}{}_{\alpha}\right]=\left[\rho_{\alpha}^{L}+\epsilon_{\alpha}^{L},\rho_{\alpha}^{R}+\epsilon_{\alpha}^{R}\right] \quad (1)$$

$$\left[\lambda\rho^{\alpha}\right]=\left[\min\left\{\lambda\rho_{\alpha}^{L},\lambda\rho_{\alpha}^{R}\right\},\max\left\{\lambda\rho_{\alpha}^{L},\lambda\rho_{\alpha}^{R}\right\}\right] \quad (2)$$

Definition 3: Stefanini (2010) developed the concept of generalized Hukuhara (GH) difference between two fuzzy intervals. If the GH-difference between ρ and ϵ exists (denoted by $\rho\ominus_{GH}\epsilon=w$), it exists only if w is a real number. This notion is an expansion of Hukuhara's (1967) Hukuhara difference. According to Stefanini and Bede (2009) and Stefanini (2010), the GH-difference between two intervals can be written using α-levels as $[\rho\ominus_{GH}\epsilon]^{\alpha}=[\rho]^{\alpha}\ominus_{GH}[\epsilon]^{\alpha}$. The phrase $[\rho\ominus_{GH}\epsilon]^{\alpha}$ is defined as $\left[\min\{\rho_{\alpha}^{L}+\epsilon_{\alpha}^{L},\rho_{\alpha}^{R}+\epsilon_{\alpha}^{R}\},\max\{\rho_{\alpha}^{L}+\epsilon_{\alpha}^{L},\rho_{\alpha}^{R}+\epsilon_{\alpha}^{R}\}\right]$ for all $\alpha\in[0,1]$.

Wu (2007) developed the notion of level-wise differentiable fuzzy functions by depending on endpoint function differentiability at all levels. However, Chalco-Cano et al. (2016) revealed that Wu's 2007 definition is not universally applicable. In other words, they demonstrated that, contrary to popular belief, certain fuzzy-valued functions are not convex and lack derivatives at their endpoint positions. As a result, they presented a broader method, arguing that even though endpoint functions cannot be identified at particular points, their overall behavior may still be studied.

Two fuzzy functions GH-differentiable, $\mathcal{F}$ and $\mathcal{G}$, they can be represented by interval-valued functions $\mathcal{F}_{\alpha}$ and $\mathcal{G}_{\alpha}$ that are also GH-

differentiable for any α in the closed interval [0, 1]. In this case, the following relationship holds:

$$\left[\mathcal{F}'(x)\right]^{\alpha} = \mathcal{F}_{\alpha}(x) \quad \text{and} \quad \left[\mathcal{G}'(x)\right]^{\alpha} = \mathcal{G}_{\alpha}(x) \tag{3}$$

where the GH-differentiability is defined.

The fuzzy interval-valued function $\mathcal{F} - v \cdot \mathcal{G}$ is also GH-differentiable if $\mathcal{F}$ and $\mathcal{G}$ are GH-differentiable fuzzy functions and v is any real number.

Lemma 1: A real-valued function for these fuzzy interval functions:

$$(\mathcal{F}_{\alpha}^{L}(x_0) + \mathcal{F}_{\alpha}^{R}(x_0) - v \cdot (\mathcal{G}_{\alpha}^{L}(x_0) + \mathcal{G}_{\alpha}^{R}(x_0))) : K \to \square \tag{4}$$

is differentiable at x_0 for each α ∈ [0, 1], if $\mathcal{F}$ and $\mathcal{G}$ are both GH-differentiable at x_0 and v is any real number. Furthermore, the following equality holds:

$$\frac{\partial(\mathcal{F}_{\alpha}^{L}(x_0) - v \cdot \mathcal{G}_{\alpha}^{L}(x_0) + \mathcal{F}_{\alpha}^{R}(x_0) - v \cdot \mathcal{G}_{\alpha}^{R}(x_0))}{\partial x_i} = \frac{\partial(\mathcal{F}_{\alpha}^{L}(x_0) + \mathcal{F}_{\alpha}^{R}(x_0) - v \cdot (\mathcal{G}_{\alpha}^{L}(x_0) + \mathcal{G}_{\alpha}^{R}(x_0))}{\partial x_i} \tag{5}$$

Proof: The given statement is defined for $\alpha \in [0,1]$, so we will prove it for a specific α. According to the GH-differentiability definition (see Bede and Stefanini (2013)), both $\mathcal{F}$ and $\mathcal{G}$ are GH-differentiable at x_0 for the chosen α (see Chalco-Cano et al. (2016)). This implies the following:

$$\left[\mathcal{F}'(x_0)\right]^{\alpha} = \mathcal{F}'_{\alpha}(x_0) \quad \text{and} \quad \left[\mathcal{G}'(x_0)\right]^{\alpha} = \mathcal{G}'_{\alpha}(x_0)$$

Now, let's take the derivative of both sides of the equation with respect to x_i:

$$\frac{\partial}{\partial x_i}\left(\mathcal{F}_{\alpha}^{L}(x_0) - v \cdot \mathcal{G}_{\alpha}^{L}(x_0) + \mathcal{F}_{\alpha}^{R}(x_0) - v \cdot \mathcal{G}_{\alpha}^{R}(x_0)\right) =$$

$$\frac{\partial}{\partial x_i}\left(\mathcal{F}_{\alpha}^{L}(x_0) + \mathcal{F}_{\alpha}^{R}(x_0) - v \cdot (\mathcal{G}_{\alpha}^{L}(x_0) + \mathcal{G}_{\alpha}^{R}(x_0))\right)$$

It is worth noting that if $\mathcal{F}$ and $\mathcal{G}$ are GH-differentiable at x_0, then $\frac{\partial \mathcal{F}}{\partial x_i}(x_0)$ and $\frac{\partial \mathcal{G}}{\partial x_i}(x_0)$ is a fuzzily defined interval (see Chalco-Cano et al. (2013)). Therefore, the equation can be written as follows:

$$\frac{\partial\left(\mathcal{F}_\alpha(x_0)-v\cdot\mathcal{G}_\alpha(x_0)\right)}{\partial x_i}=\frac{\partial}{\partial x_i}\left(\mathcal{F}_\alpha^L(x_0)+\mathcal{F}_\alpha^R(x_0)-v\cdot(\mathcal{G}_\alpha^L(x_0)+\mathcal{G}_\alpha^R(x_0))\right)$$

The proof is completed by demonstrating that the left-hand side and right-hand side of this equation for any real valued v are equal to each other.

3. Problem Formulations and Methods

In this section, information is provided regarding the transformation of fuzzy fractional optimization problems into single-objective classical optimization problems.

3.1. Fuzzy Fractional Optimization (FFOP)

The fuzzy fractional optimization problem (FFOP) is a type of optimization problem where the objective function is a ratio of two fuzzy functions. The FFOP is defined as follows:

$$\text{FFOP}: \begin{cases} \min\left(\dfrac{\mathcal{F}(x)}{\mathcal{G}(x)}\right) \\ \text{subjectto} \begin{cases} \dot{\psi}_i(x)\le 0, & i=1,\ldots,m, \\ \dot{\xi}_j(x)=0, & j=1,\ldots,r, \\ x\in X \end{cases} \end{cases} \tag{6}$$

where $\dot{\psi}_i$ and $\dot{\xi}_j$ are real-valued functions defined on the set K.

The feasible set of FFOP (6) is denoted as:

$$X=\left\{x\in K|\ \dot{\psi}_i(x)\le 0,\dot{\xi}_j(x)=0,(j=1,\ldots,n,i=1,\ldots,r)\right\}.$$

Definition 4 (Efficient Solution): In the context of FFOP (6), a practical solution denoted by x^* is classified as an efficient solution if there exists

no alternative solution, based on the function $\frac{\mathcal{F}(x)}{\mathcal{G}(x)}$, in the set X that is superior to x^*. In other words, if there is no $x^o \in X \setminus \{x^*\}$ such that $\frac{\mathcal{F}(x^o)}{\mathcal{G}(x^o)} \prec \frac{\mathcal{F}(x^*)}{\mathcal{G}(x^*)}$.

Proof: Assume that x^* is an efficient solution, and there exists an alternative solution x^o in the set $X \setminus \{x^*\}$ such that $\frac{\mathcal{F}(x^o)}{\mathcal{G}(x^o)} \prec \frac{\mathcal{F}(x^*)}{\mathcal{G}(x^*)}$. This implies that $\frac{\mathcal{F}(x^o)}{\mathcal{G}(x^o)} < \frac{\mathcal{F}(x^*)}{\mathcal{G}(x^*)}$, which means that x^o is strictly better than x^* according to the objective function. However, this contradicts the definition of x^* as an efficient solution, which states that there should be no alternative solution superior to x^*. Therefore, our assumption that there exists an alternative solution x^o that is better than x^* is incorrect, and as a result, x^* is indeed an efficient solution.

Definition 5 (Strongly Efficient Solution):

A feasible solution to FFOP (6) is called a strongly efficient solution if there is no solution x^o in the set X that is strictly better than x^* according to the same function $\frac{\mathcal{F}(x)}{\mathcal{G}(x)}$. That is, if no $x^o \in X \setminus \{x^*\}$ exists such that $\frac{\mathcal{F}(x^o)}{\mathcal{G}(x^o)} \prec \frac{\mathcal{F}(x^*)}{\mathcal{G}(x^*)}$.

Proof: Assume that x^* is a strongly efficient solution, and there exists an alternative solution x^o in the set $X \setminus \{x^*\}$ such that $\frac{\mathcal{F}(x^o)}{\mathcal{G}(x^o)} \prec \frac{\mathcal{F}(x^*)}{\mathcal{G}(x^*)}$. This implies that $\frac{\mathcal{F}(x^o)}{\mathcal{G}(x^o)} \prec \frac{\mathcal{F}(x^*)}{\mathcal{G}(x^*)}$, which means that x^o is strictly better than x^* according to the objective function. However, this

contradicts the definition of x^* as a strongly efficient solution, which states that there should be no alternative solution strictly better than x^*.

In conclusion, the definitions of efficient and strongly efficient solutions in the FFOP are established, and the proof demonstrates that these solutions are characterized by the absence of alternative solutions that are better or strictly better according to the objective function $\frac{\mathcal{F}(x)}{\mathcal{G}(x)}$.

3.2. Fuzzy Valued Interval Fractional Optimization Problem (FVIFOP)

The problem given above is a fuzzy problem, and this problem can be easily transformed into the following FVIOP using the provided equations:

$$\left[\mathcal{F}(x_0)\right]^{\alpha} = \mathcal{F}_{\alpha}(x_0) = \left[f_{\alpha}^{L}(x_0), f_{\alpha}^{R}(x_0) \right] \tag{7}$$

and

$$\left[\mathcal{G}(x_0)\right]^{\alpha} = \mathcal{G}_{\alpha}(x_0) = \left[g_{\alpha}^{L}(x_0), g_{\alpha}^{R}(x_0) \right] \tag{8}$$

This transformation allows us to work with a FVIOP in the context of fuzzy optimization.

$$\text{FIVFOP:} \quad \begin{cases} \min\left(\dfrac{\left[\mathcal{F}(x)\right]^{\alpha}}{\left[\mathcal{G}(x)\right]^{\alpha}}\right) = \min\left(\dfrac{\mathcal{F}_{\alpha}(x)}{\mathcal{G}_{\alpha}(x)}\right) = \min\left(\dfrac{[f_{\alpha}^{L}(x), f_{\alpha}^{R}(x)]}{[g_{\alpha}^{L}(x), g_{\alpha}^{R}(x)]}\right) \\ \text{subject to} \quad \{\text{constraints of FFOP (6)} \end{cases} \tag{9}$$

where $\dot{\psi}_i$ and $\dot{\xi}_j$ are real-valued functions defined on the set K.

3.3. Fractional Optimization Problem(FOP)

The problem given in (9) is a multiobjective fuzzy-valued, interval-based, and fractional optimization problem. Furthermore, even after a partial ordering, endpoint functions may not have level-wise derivatives at some places, or if they do, the function may not be convex. In this instance, the derivative of the sum of endpoint functions rather than the individual derivatives of endpoint functions may be required (Chalco-Cano et al., 2016). This allows us to convert the problem with interval functions into

a Fractional Optimization Problem (FOP) with a single real-valued objective function.

$$\text{FOP:} \quad \begin{cases} \min\left(\dfrac{f_\alpha^L(x)+f_\alpha^R(x)}{g_\alpha^L(x)+g_\alpha^R(x)}\right) \\ \text{subject to} \quad \{\text{constraints of FFOP (6)} \end{cases} \tag{10}$$

3.4. Single Objective Optimization Problem (SOOP)

Dinkelbach's 1967 technique allows for the translation of FOP (11) into a SOOP, as follws:

$$\text{SOOP:} \quad \begin{cases} \min\left(\left(f_\alpha^L(x)+f_\alpha^R(x)\right)-v\left(g_\alpha^L(x)+g_\alpha^R(x)\right)\right) \\ \text{ssubject to} \quad \{\text{constraints of FFOP (6)} \end{cases} \tag{11}$$

We may use KKT conditions to get the optimal solution to SOOP (11) because it is a real valued single-objective optimization problem. To begin, consider the following Lagrange function that corresponds to SOOP (11):

$$L_\alpha(x,\mu,\pi)=\left(\left(f_\alpha^L(x)+f_\alpha^R(x)\right)-v\left(g_\alpha^L(x)+g_\alpha^R(x)\right)\right)+\mu_i(\alpha)\dot{\psi}_i(x)+\pi_j(\alpha)\dot{\xi}_j(x) \tag{12}$$

where α represents a parameter between 0 to 1, x is the decision variable, $\mu(\alpha)$ and $\eta(\alpha)$ are Lagrange multipliers, f_α^L, f_α^R, g_α^L, and g_α^R are functions associated with the left and right endpoints, and $\dot{\psi}_i(x)$ and $\dot{\xi}_j(x)$ represent constraint functions.

KKT conditions are key equations and restrictions that aid in determining the optimality and feasibility of solutions to mathematical optimization problems. The following statements describe these conditions, which are based on the Lagrange function:

1. To ensure that a solution is optimal, the gradient of the Lagrange function with respect to the decision variable x must be equal to zero:

$$\nabla_x L_\alpha\left(x^*,\mu^*(\alpha),\pi^*(\alpha)\right)=0$$

2. The Lagrange multipliers must be greater than or equal to zero:

$$\mu_i^*(\alpha) \geq 0, \quad i = 1, \ldots, m$$

$$\pi_j^*(\alpha) \geq 0, \; j = 1, \ldots, r$$

3. The constraint functions of an optimization problem must satisfy the constraints equations:

$$\dot{\psi}_i(x^*) \leq 0, i = 1, \ldots, m,$$

$$\dot{\xi}_j(x^*) = 0, j = 1, \ldots, r$$

4. The relationship between the Lagrange multipliers and inequality constraint functions is demonstrated through the KKT complementarity conditions:

$$\mu_i^*(\alpha) \cdot \dot{\psi}_i(x) = 0, \quad i = 1, \ldots, m$$

By utilizing the KKT conditions, we can readily assess the optimality and feasibility of solutions in mathematical optimization problems. The generalized KKT conditions are stated in the subsequent theorem.

Theorem 3: Suppose the real-valued constraint functions $\dot{\psi}_i(x)$ and $\dot{\xi}_j(x)$ for SOOP (11) are both convex and differentiable on K. Assume that the fuzzy functions $F : K \to \mathcal{F}_C$ and $G : K \to \mathcal{F}_C$ are GH-differentiable, and the real-valued functions $\left(f_\alpha^L + f_\alpha^R\right)$ and $v.\left(g_\alpha^L + g_\alpha^R\right)$ are convex on K for all $\alpha \in [0,1]$. If there exist non-negative real-valued values $\mu_i(\alpha)$ and $\pi_j(\alpha)$ for $i = 1, \ldots, m,$ and $j = 1, \ldots, r$, then the following KKT conditions hold:

1. $\nabla\left(\left(f_\alpha^L + f_\alpha^R\right) - v\left(g_\alpha^L + g_\alpha^R\right)\right)(x^*) + \sum_{i=1}^{m} \mu_i^*(\alpha) \nabla \dot{\psi}_i(x^*) + \sum_{j=1}^{r} \pi_j^*(\alpha) \nabla \dot{\xi}_j(x^*) = 0, \quad \forall \alpha \in [0,1],$

2. $\sum_{i=1}^{m} \mu_i^*(\alpha) \nabla \dot{\psi}_i(x^*) = 0.$

Then, x^* is an optimal solution to SOOP (11).

Proof: If both $\mathcal{F}$ and $\mathcal{G}$ are functions that possess GH-differentiability, and if v is a real scalar, it follows that the objective function of problem (11) exhibits differentiability across the entire domain X for all $\alpha \in [0,1]$. The satisfaction of Conditions (1) and (2) consequently establishes that x^* represents a KKT point within the context of SOOP (11) for all $\alpha \in [0,1]$.

Given the convex and real-valued nature of both the objective and constraint functions defined on the set K within SOOP (11), x^* emerges as an optimal solution for this problem across the entire range of $\alpha \in [0,1]$. Moreover, since SOOP (11) serves as a weighted scalar formulation of the more general FVIOP (9), featuring strictly positive weighting coefficients, it logically follows that x^* embodies a Pareto-efficient solution for FVIOP (9) over the entire span of $\alpha \in [0,1]$. In accordance with Definitions 4 and 5, x^* attains the status of an efficient solution within the domain of FFOP (6).

4. A Numerical Example

Consider the following optimization problem, which corresponds to FFOP (6):

$$\begin{cases} Z(x_1, x_2) = \min\left(\dfrac{\tilde{3}x_1 + \tilde{2}x_2^2}{\tilde{2}x_1}\right) \\ \text{subject to}: \begin{cases} (x_1 - 2)^2 + x_2^2 - 4 \le 0, \\ x_1, x_2 \in X \end{cases} \end{cases} \tag{13}$$

where $\tilde{3} = (2,3,5)$ and $\tilde{2} = (1,2,4)$ denote triangular fuzzy numbers.

Here, $F(x_1, x_2) = \tilde{3}x_1 + \tilde{2}x_2^2$, $G(x_1) = \tilde{2}x_1$, $[\tilde{2}]^\alpha = [1+\alpha, 4-2\alpha]$ and $[\tilde{3}]^\alpha = [2+\alpha, 5-2\alpha]$ for all $\alpha \in [0,1]$.

We derive from equations (1) and (2)

$$[F(x_1,x_2)]_\alpha = \begin{cases} \left((2+\alpha)x_1+(1+\alpha)x_2^2,(5-2\alpha)x_1+(4-2\alpha)x_2^2\right), & \text{if } x_1 \geq 0, x_2 \in \square; \\ \left((5-2\alpha)x_1+(1+\alpha)x_2^2,(2+\alpha)x_1+(4-2\alpha)x_2^2\right), & \text{if } x_1 < 0, x_2 \in \square. \end{cases}$$

and

$$[G(x_1)]^\alpha = \begin{cases} \left((1+\alpha)x_1,(4-2\alpha)x_1\right), & \text{if } x_1 \geq 0; \\ \left((4-2\alpha)x_1,(1+\alpha)x_1\right), & \text{if } x_1 < 0. \end{cases}$$ for any α between 0 to 1.

Then comes the depiction of the first function's end point:

$$f_\alpha^L(x) = \begin{cases} (2+\alpha)x_1+(1+\alpha)x_2^2 & x_1 \geq 0, x_2 \in \square, \\ (5-2\alpha)x_1+(1+\alpha)x_2^2 & x_1 < 0, x_2 \in \square. \end{cases} \tag{14}$$

and

$$f_\alpha^R(x) = \begin{cases} (5-2\alpha)x_1+(4-2\alpha)x_2^2 & x_1 \geq 0, x_2 \in \square, \\ (2+\alpha)x_1+(4-2\alpha)x_2^2 & x_1 < 0, x_2 \in \square, \end{cases} \tag{15}$$

as well as the end point representation of the second function:

$$g_\alpha^L(x) = \begin{cases} (1+\alpha)x_1 & \text{if } x_1 \geq 0; \\ (4-2\alpha)x_1 & \text{if } x_1 < 0. \end{cases} \tag{16}$$

and

$$g_\alpha^R(x) = \begin{cases} (4-2\alpha)x_1 & \text{if } x_1 \geq 0; \\ (1+\alpha)x_1 & \text{if } x_1 < 0. \end{cases} \tag{17}$$

It is obvious that $f_\alpha^L(x)$ $f_\alpha^R(x)$ $g_\alpha^L(x)$ and $g_\alpha^R(x)$ are not differentiable at $x=(0,0)$ and convex. As a result, $F \text{and} G$ cannot be differentiated level-wise, and $F \text{and} G$ is also not convex at $x=(0,0)$. Nonetheless, the sum of end point functions

$$f_\alpha^L(x)+f_\alpha^R(x) = (7-\alpha)x_1+(5-\alpha)x_2^2 \tag{18}$$

and

$$g_\alpha^L(x)+g_\alpha^R(x)=(5-\alpha)x_1 \tag{19}$$

are differentiable and convex (see Chalco-Cano et al. (2016)).

Since $f_\alpha^L(x)+f_\alpha^R(x)$ and $g_\alpha^L(x)+g_\alpha^R(x)$ are differentiable at $x=(0,0)$, then for FFOP (13), the real valued multiobjective optimization problem corresponding to FVIFOP (9) is as follows:

$$\begin{cases} Z_\alpha(x_1,x_2)=\min\left(\dfrac{f_\alpha^L(x),\ f_\alpha^R(x)}{g_\alpha^L(x),\ g_\alpha^R(x)}\right),\alpha\in[0,1] \\ \text{subject to}:\begin{cases}(x_1-2)^2+x_2^2-4\le 0,\\ x_1,x_2\in X\end{cases}\end{cases} \tag{19}$$

As a result, we write the real valued objective function of the preceding multiobjective optimization problem in equal weighted method as follows:

$$Z_\alpha(x_1,x_2)=\min\left(\frac{f_\alpha^L(x)+f_\alpha^R(x)}{g_\alpha^L(x)+g_\alpha^R(x)}\right)=\min\left(\frac{(7-\alpha)x_1+(5-\alpha)x_2^2}{(5-\alpha)x_1}\right). \tag{20}$$

FFOP (10) is transformed into the following nonlinear fractional optimization problem depending on the α parameter, and FOP (10) matches to this.

$$\begin{cases} Z_\alpha(x_1,x_2)=\min\left(\dfrac{(7-\alpha)x_1+(5-\alpha)x_2^2}{(5-\alpha)x_1}\right),\alpha\in[0,1] \\ \text{subject to}:\{\text{constraints of problem (19)}\}\end{cases} \tag{21}$$

The problem in (19) was solved using Maple 2023 software with the α parameter set to 0.2. The objective function value of the fractional nonlinear optimization problem was determined to be 1.417, with $x_1=0.896$ and $x_2=-2.34299373514663\times10^{-10}$. The surface and point plots for $\alpha=0.2$ are also shown in Figures 1 and 2, respectively.

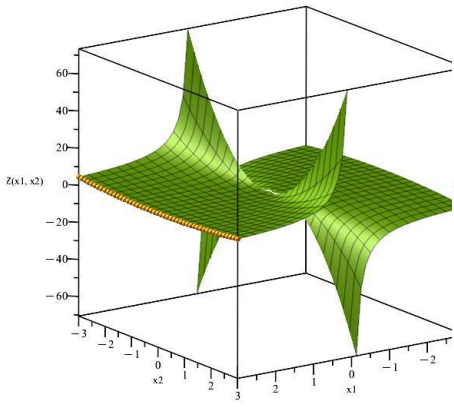

Figure 1: Surface of the fractional nonlinear optimization problem (21) for $\alpha = 0.2.$

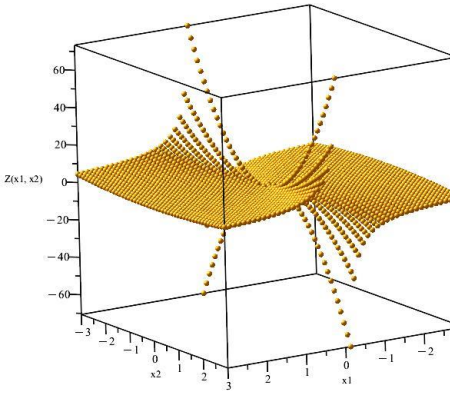

Figure 2 Points of the fractional nonlinear optimization problem (21) for $\alpha = 0.2.$

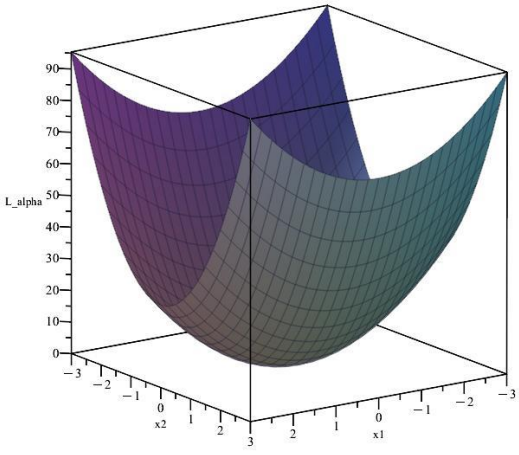

Figure 3: Surface of non- fractional problem (24) for $\alpha = 0.2$ and $\mu = -\frac{\alpha}{2} + 3.$

Moreover, using Dinkelbach's (1967) technique, we may convert it to a non-fractional nonlinear function corresponding to SOOP (11) as:

$$\left(\left(f_\alpha^L + f_\alpha^R\right) - v\left(g_\alpha^L + g_\alpha^R\right)\right)(x) = \left((7-\alpha)x_1 + (5-\alpha)x_2^2\right) - v\left((5-\alpha)x_1\right) \tag{22}$$

FFOP (10) can thus be reduced to a single objective nonlinear optimization problem as follows:

$$\begin{cases} Z_\alpha(x_1, x_2) = \min\left((7-\alpha)x_1 + (5-\alpha)x_2^2\right) - v\left((5-\alpha)x_1\right) \\ \text{subject to} \quad \{\text{constraints of problem (19)} \end{cases} \tag{23}$$

where v is any real number.

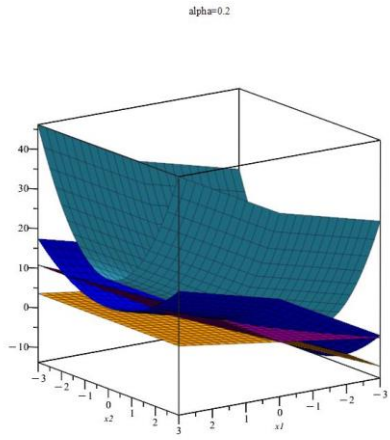

Figure 4: Surface of FVIOP(19) at $\alpha = 0.2$.

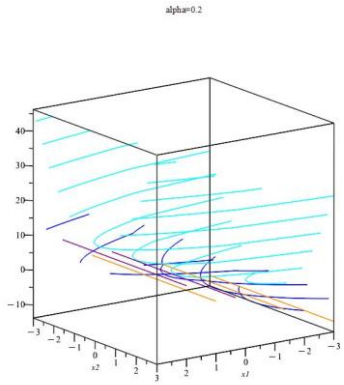

Figure 5 Contour of FVIOP (19) at $\alpha = 0.2$.

The Lagrange multipliers approach can be used to achieve the KKT requirements given in Theorem 3 for problem (23), and the Lagrange function by setting $v = 1$ can be defined as follows:

$$L_\alpha(x, \mu) = \left((12-2\alpha)x_1 + (5-\alpha)x_2^2\right) + \mu(\alpha)\left((x_1-2)^2 + x_2^2 - 4\right) \text{for all } \alpha \in [0,1]. \tag{24}$$

The following are Lagrange function (24) definitions for the KKT requirements stated in Theorem 3:

$$\begin{cases} \dfrac{\partial L_\alpha}{\partial x_1} = 12 - 2\alpha - 2\mu(\alpha) + 4\mu(\alpha)x_1 = 0 \\ \dfrac{\partial L_\alpha}{\partial x_2} = 2\alpha x_2 - 2\mu(\alpha)x_2 = 0 \\ \dfrac{\partial L_\alpha}{\partial \mu(\alpha)} = (x_1 - 2)^2 + x_2^2 - 4 = 0 \end{cases} \tag{25}$$

When system (25) with constraints of SOOP (11) is solved using Maple 2023, the solution is generated based on the value of the α parameter, as shown below. Figure 3 depicts Lagrange function (24) for $\alpha = 0.2$

$$\left\{ \mu(\alpha) = -\frac{\alpha}{2} + 3, x_1 = 0, x_2 = 0 \right\}$$

When these values are put into (23), the value of becomes $Z_a(x_1, x_2) = 0.$ In addition, Figures 4 and 5 show the surface and contour for (problem (19)) the real-valued functions $f_\alpha^L(x)$, $f_\alpha^R(x)$, $g_\alpha^L(x)$, and $g_\alpha^R(x)$ at $\alpha = 0.2.$

After examining the fractional optimization problem obtained following the transformations (21) with the surfaces provided in Figure 1 and Figure 2, it is evident that this problem does not possess a convex structure. Additionally, by employing the Maple 2023 software, the objective function value was found to be $Z_\alpha(x_1, x_2) = 1.417$ for the value $\alpha = 0.2$.

Problem (21) has been transformed into a non-fractional optimization problem (23) using Dinkelbach's method (1967). This transformation, aided by the Lagrange function, has resulted in an unconstrained optimization problem (24). Through the utilization of the Lagrange function, the unconstrained optimization problem (24) obtained a convex region at the point $\alpha = 0.2$, as shown in Figure 3. This indicates that, by employing the first-order optimality condition, global optimal points can be obtained for problem (23).

Subsequently, utilizing the unconstrained problem (24) and the KKT conditions provided in Theorem 3, equation system (25) was derived. This equation system was solved by incorporating the inequality constraint of the problem. The results of this process, calculated for the value $\alpha = 0.2,$ yielded an objective function value of $Z_{\alpha}(x_1, x_2)$ equal to 0 for the non-fractional problem (23).

Furthermore, graphs obtained using the value $\alpha = 0.2$ for FVIOP (19) are presented in Figure 4 and Figure 5, revealing that problem FVIOP (19) is a convex optimization problem.

These findings demonstrate that transforming the fractional and non-linear optimization problem (21) into the non-fractional optimization problem (23) using Dinkelbach's method yields superior results. Moreover, this transformation converts the domain of the fractional problem, which is concave, into a convex region, confirming the accuracy of the information provided in Lemma 1.

Finally, when the values of the parameter α are divided into 10 equally spaced intervals between 0 and 1, it is observed that negligible changes occur in the objective function for all values.

The purchase of such a solution resulted in the acquisition of an optimal solution for problem (23). Furthermore, this solution is Pareto efficient for problem (19). Furthermore, function (22) always fulfills the differentiability and convexity conditions stated by Chalco-Cano et al. (2016) for any real value of v. Another interesting aspect is that v can be a fuzzy valued number while still meeting these constraints.

5. Conclusions

The utilization of the equal weighting method facilitated the conversion of a FVFOP into a non-fractional FOP, thereby transforming it into a single-objective optimization problem. This transformation was carried out by employing Lagrange multipliers and KKT conditions to optimize the desired objectives. An illustrative problem was then solved using Maple 2023 software, and the results were presented graphically to underscore the convexity of the problem and the level of numerical precision achieved.

The solution procedure used in this study can be readily extended to problems with multiple objective functions, known as FVIOP. Furthermore, after obtaining the fractional optimization problem from

FOP using transformations, this problem can be solved using both intelligent and numerical optimization algorithms. It can also be easily converted to an unconstrained optimization problem using penalty methods and the Lagrange function, and solutions can be obtained with various algorithms.

In future research, an attempt will be made to obtain a dynamic system, also referred to as a neural network, for solving FVIOP problems. The changes in decision variables over time for optimization problems with fuzzy and static structures will be investigated.

References

[1]. Agarwal, D., Singh, P., & El Sayed, M. A. (2023). The Karush–Kuhn–Tucker (KKT) optimality conditions for fuzzy-valued fractional optimization problems. Mathematics and Computers in Simulation, 205, 861-877.

[2]. Bede, B., & Stefanini, L. (2013). Generalized differentiability of fuzzy-valued functions. Fuzzy Sets and Systems, 230, 119–141.

[3]. Bellman, R. E., & Zadeh, L. A. (1970). Decision making in a fuzzy environment. Management Science, 17(4), 141–164.

[4]. Chalco-Cano, Y., Rufián-Lizana, A., Román-Flores, H., & Jiménez-Gamero, M. D. (2013a). Calculus for interval-valued functions using generalized Hukuhara derivative and applications. Fuzzy Sets and Systems, 219, 49–67.

[5]. Chalco-Cano, Y., Lodwick, W. A., & Rufián-Lizana, A. (2013b). Optimality conditions of type KKT for optimization problems with interval-valued objective functions via generalized derivative. Fuzzy Optimization and Decision Making, 12(3), 305-322.

[6]. Chalco-Cano, Y., Lodwick, W. A., Osuna-Gómez, R., & Rufián-Lizana, A. (2016). The Karush–Kuhn–Tucker optimality conditions for fuzzy optimization problems. Fuzzy Optimization and Decision Making, 15(1), 57-73.

[7]. Cochocki, A., & Unbehauen, R. (1993). Neural networks for optimization and signal processing. John Wiley & Sons, Inc..

[8]. Dinkelbach, W. (1967). On non-linear fractional programming. Manag. Sci., 13 (7).

[9]. Hukuhara, M. (1967). Integration des applications mesurables dont la valeur est un compact convexe. Funkcialaj Ekvacioj, 10, 205–223.

[10]. Inuiguchi, M., & Ramík, J. (2000). Possibilistic linear programming: A brief review of fuzzy mathematical programming and a comparison with stochastic programming in portfolio selection problem. Fuzzy Sets and Systems, 111, 3–28.

[11]. Jagannathan, R. (1966). On some properties of programming problems in parametric form pertaining to fractional programming. Manag. Sci., 12, 609–615.

[12]. Pop, B., & Stancu-Minasian, I.M. (2008). A method of solving fully fuzzified linear fractional programming problem. J. Appl. Math. Comput., 27, 227–242.

[13]. Słowiński, R. (Ed.). (1998). Fuzzy sets in decision analysis. Operations research and statistics. Kluwer, Boston.

[14]. Słowiński, R., & Teghem, J. (Eds.). (1990). Stochastic versus fuzzy approaches to multiobjective mathematical programming under uncertainty. Kluwer, Boston.

[15]. Stefanini, L., & Bede, B. (2009). Generalized Hukuhara differentiability of interval-valued functions and interval differential equations. Nonlinear Analysis, 71, 1311–1328.

[16]. Stefanini, L. (2010). A generalization of Hukuhara difference and division for interval and fuzzy arithmetic. Fuzzy Sets and Systems, 161, 1564–1584.

[17]. Su, T., & Hang, D. D. (2022). Optimality and duality in nonsmooth multiobjective fractional programming problem with constraints. *4OR*, 1-33.

[18]. Su, T. V., & Hang, D. D. (2023). Second-order optimality conditions in locally Lipschitz multiobjective fractional programming problem with inequality constraints. *Optimization*, *72*(5), 1171-1198.

[19]. Thuy, N. T., & Van Su, T. (2023). Robust optimality conditions and duality for nonsmooth multiobjective fractional semi-infinite programming problems with uncertain data. *Optimization*, *72*(7), 1745-1775.

[20]. Wu, H.-C. (2007). The Karush–Kuhn–Tucker optimality conditions for the optimization problem with fuzzy-valued objective function. Mathematical Methods of Operations Research, 66, 203–224.

[21]. Wu, H.-C. (2009a). The Karush–Kuhn–Tucker optimality conditions for multi-objective programming problems with

fuzzy-valued objective functions. Fuzzy Optimization and Decision Making, 8, 1–28.

[22]. Wu, H.-C. (2009b). The optimality conditions for optimization problems with convex constraints and multiple fuzzy-valued objective functions. Fuzzy Optimization and Decision Making, 8, 295–321.

[23]. Zadeh, L.A. (1965). Fuzzy sets. Inf. Control, 8, 338–353.

[24]. Zimmermann, H.J. (1978). Fuzzy programming and linear programming with several objective functions. Fuzzy Sets Syst., 1, 45–65.

[25]. Zimmermann, H.J. (1991). Fuzzy Set Theory and its Applications, 2nd Ed. Kluwer-Nijhoff.